Spectroscopy of light scattering and nonlinear optics. Nonlinear-optical methods of active spectroscopy of Raman and Rayleigh scattering

S. A. Akhmanov and N. I. Koroteev

Moscow State University
Usp. Fiz. Nauk **123**, 405–471 (November 1977)

PACS numbers: 42.65.Cq, 07.65.–b, 78.45.+h, 78.30.–j

CONTENTS

I. INTRODUCTION. METHODS OF NONLINEAR OPTICS IN LIGHT-SCATTERING SPECTROSCOPY. CLASSIFICATION OF THE METHODS OF ACTIVE SPECTROSCOPY

1. The discovery of nonlinear optical phenomena has changed the face of many branches of physical optics; this fully pertains also to light-scattering spectroscopy. Moreover, we should stress that this is just where the soil for modern nonlinear optics was most ready, especially in inelastic light-scattering spectroscopy. In fact, spontaneous inelastic light scattering itself stems from the breakdown of the superposition principle: the light waves and the optical (or acoustic) vibrations of the medium mutually influence one another. Study of one of the facets of this mutual influence—light modulation by spontaneous (thermal) elementary excitations—is the topic of spontaneous-scattering spectroscopy. The quantum-theoretical and classical patterns of the phenomenon were elucidated in studies of 1929–1930. The classical, "modulation" treatment of Raman scattering of light had already been given in the early studies of Mandel'shtam and Landsberg,[1] who reported the first observations of the effect. The discovery of the reverse action of light on the medium, or optical generation of elementary excitations, lagged by almost 30 years. Yet we should stress that the theoretical interpretation of stimulated Raman scattering, which Woodbury and Ng[2] fortuitously discovered in 1962, actually did not require information on matter beyond the limits of what was known in the spectroscopy of spontaneous Raman scattering. Hence a quantum theory of stimulated Raman scattering was given even in the same year 1962,[3,4] and a detailed classical theory in 1963–1964.[5–8] we shall discuss below the relationship between spontaneous and stimulated scattering on the basis of the classical theory of stimulated Raman scattering developed by R. V. Khokhlov.

The classical description of the interaction of light with intramolecular motions is based on accounting for the relationship of the electronic polarizability α of the molecules to the nuclear configuration as fixed by the coordinates Q_i of the nuclei. In the simplest one-dimensional case[9] we have

$$\alpha(Q)=\alpha_0+\left(\frac{\partial\alpha}{\partial Q}\right)_0 Q+\ldots \qquad (\text{I}.1)$$

The term $(\partial\alpha/\partial Q)_0\, Q$ describes the modulation of the light by the molecular vibrations: new frequency components arise in the induced polarization of the molecule that are shifted by the frequency of the vibrations of the nuclei:

$$p=\alpha(Q)\,E=\alpha_0 E+\left(\frac{\partial\alpha}{\partial Q}\right)_0 QE+\ldots \qquad (\text{I}.2)$$

Whenever Q is governed by the thermal movements in the medium, (I.2) describes spontaneous Raman scattering.

The relationship $\alpha=\alpha(Q)$ at the same time engenders the reaction of the light waves on the molecular vibrations. Actually, the energy of interaction of the molecule with the light wave is expressed by using (I.2) in the form $\mathcal{H}=pE=-\alpha(Q)E^2$. Hence, when $\partial\alpha/\partial Q\neq 0$, the following force acting on the molecular vibrations arises in the light field:

$$F_Q=-\frac{\partial\mathcal{H}}{\partial Q}=\frac{\partial\alpha}{\partial Q}E^2, \qquad (\text{I}.3)$$

Evidently, this force can lead to resonance pumping of them if the field contains two spectral components of frequencies ω_1 and ω_2 whose difference is close to the intrinsic frequency Ω of the molecular vibrations: $\omega_1-\omega_2\approx\Omega$.

Under these conditions, a regular forced vibration is

 0038-5670/77/2011-0899$01.10

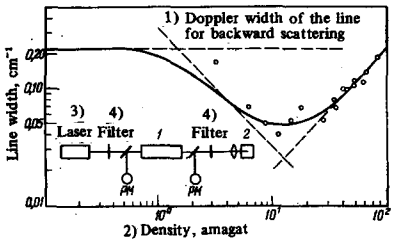

FIG. 1. Pressure-dependence of the width of the vibrational–rotational line Q_{01} (1) of gaseous hydrogen in the region of collision-induced narrowing.[15] This curve was obtained by measurements of stimulated Raman scattering of the Stokes ray obtained in another (generator) cuvette containing hydrogen (2) in which the pressure was varied in order to scan the frequency of the Stokes ray.

imposed on the chaotic intramolecular movement, which is fluctuational in type. The phases of the forced vibration in different molecules are determined by the phases of the components of the light wave (phasing of molecular vibrations).

As we have stated, the reaction of the light on the molecular vibrations was first experimentally discovered in 1962.[2,3] It was identified as the cause of the onset of instability of an intense monochromatic wave in a Raman-active medium. Here the second component of the light doublet, which is necessary for phasing the oscillations, stemmed from the spontaneous Raman scattering of the intense wave; the effect itself was called stimulated Raman scattering.

Stimulated Raman scattering is a threshold effect: instability arises if the intensity of the monochromatic wave (of frequency ω_1) is higher than some threshold value, $I_1 \geq I_{thr}$. Under this condition, the low-frequency (Stokes) wave at the frequency $\omega_2 \approx \omega_1 - \Omega$ grows exponentially inside the medium; when $I_2 \ll I_1$, we have

$$I_2 = I_{20} e^{gI_1 z}, \tag{I.4}$$

while the gain

$$g = \frac{16\pi^2 c^2}{\hbar \omega_2^3 n^2 \Gamma} N \frac{d\sigma}{d\Omega} g'(\omega_1 - \omega_2) \tag{I.5}$$

is expressed directly in terms of the parameters of the spontaneous-scattering line: the scattering cross-section $d\sigma/d\Omega$, the line width Γ, the density N of the molecules, and the form factor $g'(\omega_1 - \omega_2)$ of the line.

When $gI_1 z \gg 1$, the original wave of frequency ω_1 is depleted and the waves efficiently exchange energy. The theory of the other types of stimulated scattering is based on an analogous scheme.

As for the state of the medium, phasing of the molecular oscillators arises throughout the volume occupied by the field during stimulated Raman scattering, and the population difference of their vibrational levels is altered.

2. Stimulated scattering is one of the most important causes of instability of a high-power light wave and of nonlinear dissipation of its energy in a medium. This aspect of the phenomenon is being intensively studied even up to the present (see, e.g., the reviews[10–14]). Yet the topic of the present review is another, spectroscopic, aspect of stimulated processes in light scattering. Although these problems attracted the attention of the authors of the first studies dating to 1963–1966, we must say that the spectroscopic potentialities of stimulated processes have been realized only in the past 4–5 years after efficient tunable generators in the visible and infrared ranges had been invented.

3. The spectroscopic potentialities of stimulated scattering proper, which arises when $I_1 > I_{thr}$, are restricted. Thus, the strong competition between different lines that arises under instability conditions and the substantial role of the competing nonlinear processes (especially those like self-focusing and self-modulation) all often destroy the spectroscopic information obtainable from stimulated Raman spectra. This was clearly understood even in the first stage of study of stimulated Raman scattering. Hence, over a long period, investigators have directed their efforts toward seeking a method that would occupy an intermediate position between the methods of spontaneous and stimulated Raman scattering, while combining the broad spectroscopic potentialities of the former and such merits of the latter as the phasing of the Raman-active vibrations over a large volume, the attainment of large filling numbers of the phonon modes, high scattering efficiency, etc.

In 1966–1967, Bloembergen and his associates[15] developed a method for measuring the contour of a Raman gain line. Here, in a Raman-active medium, one studies the amplification of the radiation of a tunable laser of frequency ω_2 in the field of an intense wave of frequency ω_1. In contrast to stimulated Raman scattering, one can control the amplification process. The authors of Ref. 15 studied in detail the contour of the gain line $g = g(\omega_1 - \omega_2)$ in compressed hydrogen. They used the obtained data for determining the Raman cross section $d\sigma/d\Omega$ (see Eq. (I.5)) and the pressure dependence of the width of the spontaneous-scattering line (Fig. 1). Although a set of subsequent studies[16–19] has applied this method to solids and liquids, it has not become widespread. Exact measurements of small amplifications are difficult, while problems arise at large amplifications that are characteristic of the stimulated Raman scattering regime.[1)]

The abovesaid can also pertain to the technique of measuring the attenuation of the anti-Stokes wave in an intense pump field (inverse Raman scattering), though a number of successful experimental studies exist here.[74,78]

4. Another approach in using the methods of nonlinear optics for studying Raman-active transitions in molecules, which allows one to eliminate uncontrollable instabilities, has been used by Maker and Terhune[20] (see also Ref. 139). They studied a four-frequency process of the following type in the field of a biharmonic light

[1)]Reports of successful development of this technique have appeared only very recently.[202]

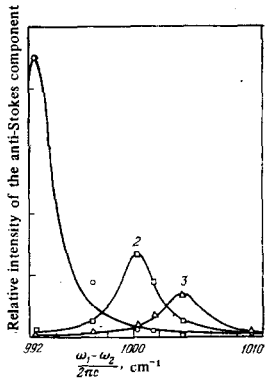

FIG. 2. Results of the first experiments of Maker and Terhune[20] on coherent ARS. They studied the relationship of the intensity of the anti-Stokes signal at the frequency $\omega_a = 2\omega_1 - \omega_2$ to the frequency difference of the pump waves, $\Delta = \omega_1 - \omega_2$. They used discrete sets of line pairs ω_1 and ω_2. 1—benzene (C_6H_6), 2—bromobenzene (C_6H_5Br), 3—toluene ($C_6H_5CH_3$). Solid lines—Lorentzian curves that best fit the obtained experimental points (the line shape of the ARS signal is discussed in more detail in Sec. 1c of Chap. II).

wave (of frequencies ω_1 and ω_2) at intensities below the stimulated Raman threshold:

$$\omega_a = \omega_1 + \omega_1 - \omega_2 = 2\omega_1 - \omega_2. \qquad (I.6)$$

When they selected the frequencies ω_1 and ω_2 of the waves to give $\omega_1 - \omega_2 = \Omega$ (Ω is the natural vibration frequency of the molecule), the intensity I_a of the signal at the anti-Stokes frequency ω_a sharply rose. Figure 2 shows the results of Maker and Terhune's first experiments.

Lack of a tunable-frequency laser compelled the authors of Ref. 20 to restrict the measurements only to certain fixed points.

They interpreted the results in terms of a phenomenological theory. The curves in Fig. 2 show the dispersion of the susceptibility that describes the process of (I.9); the intensity of the signal at the frequency ω_a is

$$I_a \sim |\chi^{(3)}(\omega_a; \omega_1, \omega_1, -\omega_2)|^2 I_1^2 I_2 \frac{\sin^2(\Delta kL)/2}{\Delta k^2}. \qquad (I.7)$$

One can give a classical microscopic picture of the phenomenon in terms of phasing of the molecular vibrations in a biharmonic pump field having the form of (I.6) with $\omega_1 - \omega_2 \approx \Omega$, while the "probe" wave is subsequently scattered coherently by them (here it is one of the exciting waves (ω_1); see also Fig. 3 and its legend).

Giordmaine and Kaiser[22] have introduced concepts of the phasing of coherent molecular vibrations and scattering of a probe wave by them (see also[21]). They observed efficient Stokes and anti-Stokes scattering of the relatively weak second optical harmonic of a ruby laser by coherent vibrations of a calcite crystal that had been excited by the stimulated Raman scattering of the main laser radiation. We should stress that the efficient scattering of the probe ray in this experiment, just as in practically all the subsequent experiments on coherent scattering, stems primarily from the phasing of the stimulated molecular vibrations, rather than from their large amplitude. The estimates[22] show that the amplitudes of the stimulated vibrations of the molecules remain 2–3 orders of magnitude smaller, even in the strongest light fields, than the mean-square deviations of their nuclei from the equilibrium positions arising from thermal movement at $T \approx 300$ °K.

The further studies along this line that date to 1966–1972[23–27,55] have mainly amounted to demonstrations of the principles that were proposed in the first studies. Some exceptions are the studies of Bloembergen, Wynne *et al.*,[26,27] who estimated the dispersion of the nonlinear susceptibility of semiconductors placed in a magnetic field by a wave-mixing method of the type of (I.6).

5. We should note some studies performed[28–31] at about the same time, where static diffraction gratings induced by light in transparent or absorbing media were observed. These gratings were produced in the field of high-power standing light waves owing to spatial modulation of, say the light-intensity-dependent refractive index:

$$n = n_0 + n_2 I(x, y, z). \qquad (I.8)$$

One can also produce light-induced diffraction gratings by spatial modulation of other parameters of the medium (absorption coefficient, etc.); see Fig. 3b.

It was subsequently found that studies of generation and resorption of these light-induced gratings by recording of the diffraction of a probe light ray by them are of considerable spectroscopic interest—actually the theme is that of new possibilities of getting information that had previously been extracted from spontaneous elastic light scattering.

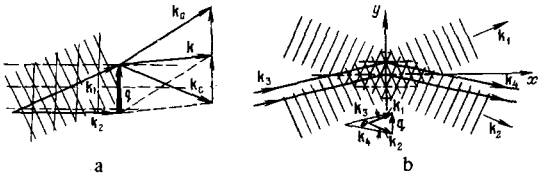

FIG. 3. Active spectroscopy of elastic and inelastic light scattering; optical induction of running and standing diffraction gratings. Figure 3a illustrates the principle of active Raman spectroscopy of light; the waves $\mathbf{E}^{(1)}$ and $\mathbf{E}^{(2)}$, whose frequency difference is close to the frequency of an optical phonon, induce the running polarizability wave $\alpha(\omega_1 - \omega_2) = \alpha_0 \exp[-i(\omega_1 - \omega_2)t + i\mathbf{q}\cdot\mathbf{r}]$, where $\mathbf{q} = \mathbf{k}_1 - \mathbf{k}_2$; the probe wave $\mathbf{E}(t, r) = \mathbf{E} = \mathbf{E}\exp(-i\omega t + i\mathbf{k}\cdot\mathbf{r})$ gives two components, the Stokes component (at frequency $\omega_s = \omega - (\omega_1 - \omega_2)$) and the anti-Stokes (at frequency $\omega_a = \omega + (\omega_1 - \omega_2)$), which are coherently scattered when the Bragg condition $\mathbf{k} - \mathbf{k}_s = \mathbf{k}_a - \mathbf{k} = \mathbf{q} = \mathbf{k}_1 - \mathbf{k}_2$ is satisfied. In particular, one can use as the probe wave one of the waves that induces the running grating (self-diffraction). Figure 3b illustrates the principle of active spectroscopy of elastic light scattering: two crossed waves at the same frequency induce a standing grating, owing to nonlinearity of the refractive index; diffraction of the probe wave by it or self-diffraction of one of the waves $\mathbf{E}^{(1)}$ or $\mathbf{E}^{(2)}$ can be used for static or dynamic measurements of optically induced changes in the refractive index.

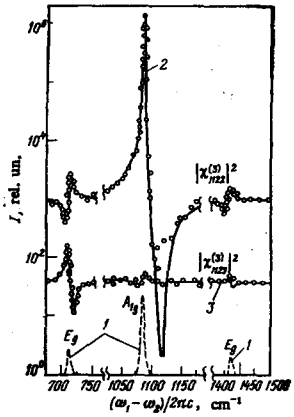

FIG. 4. Raman spectra of a calcite crystal ($CaCO_3$) obtained by using different methods. Curve 1—spontaneous Raman spectroscopy, curves 2, 3—active spectroscopy. The latter curves were obtained at different orientations of the polarization vectors of the interacting waves. [36,38]

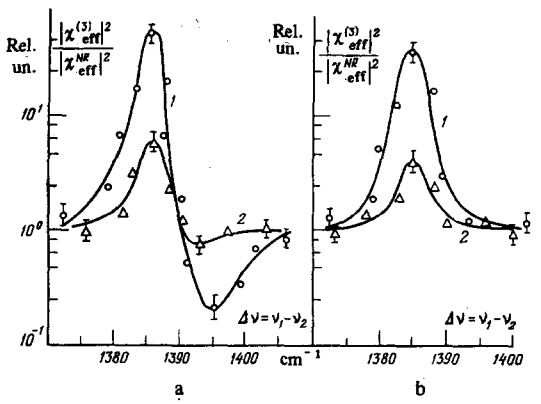

FIG. 6. Determination of the concentration of a carbon dioxide admixture in a nitrogen atmosphere by using ARS. [40] Removal of the nondispersing pedestal in the spectrum of the ARS signal (it arises from the molecules of the buffer gas) by using specially chosen polarization conditions (curves 1 and 2 in Fig. 6b) yields a considerable increase in the sensitivity of the gas analysis. a) Shape of the ARS signal from the gas mixture without using polarization measurements; the relative concentration of CO_2 molecules $n = 10^{-2}$ (1) and 10^{-3} (2); b) the same, but using the polarization method, $n = 10^{-3}$ (1), 10^{-4} (2). The total pressure of the mixture $P = 22$ atm.

In closing this brief review of the early studies on spectroscopic applications of stimulated processes in scattering, we point out the 1966 study of De Martini and Ducuing, [32] in which the technique of stimulated scattering was used to measure the vibrational relaxation time of Raman-active transitions. The idea consists in using the scattering of the probe beam to trace the time course of the population differences of a vibrational transition that has been excited by stimulated Raman scattering. We must say that this method has proved highly convenient; it is being used even now.

6. The nonlinear-optics methods described in Secs. 4 and 5 in the spectroscopy of Raman (inelastic) and Rayleigh (elastic) light scattering can be combined within the framework of the concept of active light-scattering spectroscopy. The distinctive feature of the latter is the shift from studying light scattering by elementary excitations of the medium, which have an equilibrium fluctuational nature, to studying light scattering in a specially "prepared" medium, in which the studied internal motions have been selectively excited in advance to some extent by using supplementary light sources. Depending on whether one exploits the coherence of the stimulated elementary excitations that lead to scattering of the probe light, we can speak of coherent or incoherent active scattering spectroscopy. One can distinguish in each of these two variants of active spectroscopy problems involving either steady-state excitation of the studied internal motions, or conversely, non-steady-state excitations, in which transition and relaxation processes are essential. Correspondingly, one can speak of steady-state or non-steady-state active spectroscopy in its coherent or incoherent variant. As for the active spectroscopy of Raman scattering, coherent spectroscopy has been especially intensively developed in recent years.

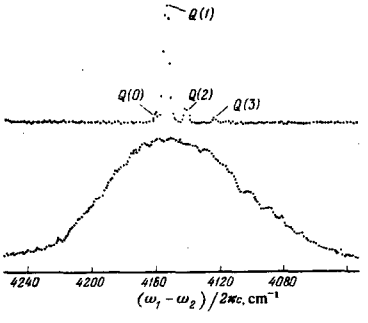

FIG. 5. Rapid analysis using ARS. The complete spectrum of the Q-band of gaseous hydrogen was obtained in a time equal to the duration of a pulse of a Q-switched laser ($\tau_u \approx 10^{-8}$ sec). [37] The spectrum is shown below of the broad-band component of the pump doublet (for more details, see Sec. 6c of Chap. II).

Several studies were reported in 1972 at the International Conference on Quantum Electronics that used tunable parametric light generators[33] and dye lasers[34] (see also Ref. 35) for exciting molecular vibrations. Now one can clearly formulate the important merits of the method that have attracted the attention of various research groups to it. There are the lack of an intensity threshold, and consequently, the possibility of detecting a signal at moderate powers of the pumping waves; the possibility of studying the complete Raman spectrum of the medium; signal detection in a frequency range free from stray exciting radiation and parasitic luminescence-type effects; the possibility of ultrahigh spectral resolution of Raman transitions; etc.

7. We can judge the new possibilities in physical and analytical applications of light scattering that are opened up by the active-spectroscopy method upon turning to Figs. 4–8 (see below). Figure 4 shows Raman spectra[36] of a $CaCO_3$ crystal in the range from 600 to 1500 cm^{-1}. Curve 1 shows the spontaneous scattering spectrum, and curves 2 and 3 correspond to spectra measured by the active-spectroscopy method. The new information obtained from these measurements is discussed in Sec. 3d of Chap. II of this review. Here we shall note only the sharp enhancement of the signal intensity and the new possibilities of measuring the different tensor components of the cubic susceptibility.

Figure 5 shows the spectrum[37] of the Q-branch of the Raman band of hydrogen obtained in a time of $\sim 10^{-8}$ sec by the active-spectroscopy method with noise excitation (see Refs. 36 and 38 and Sec. 6c of this review). We see that the entire Q-band is well resolved in an unprecedentedly short observation time. This method is the basis of the application of active spectroscopy to the analysis of the dynamics of Raman spectra; the possibilities that open up here are of considerable interest for non-steady-state media (explosions, flames, jets, etc.) and for biophysics (e.g., for studying the dynamics of the visual process[39]). The large signal/noise ratios that one can get in the active-spectroscopy method allow one to increase substantially the sensitivity of determining impurities by using Raman spectroscopy. Figure 6 illustrates these possibilities with the example of detecting an admixture of CO_2 in N_2.[40] One can reliably detect by this method a $1:10^6$ concentration of CO_2 in a time of $\sim 10^{-8}$ sec.

The coherent nature of active spectroscopy opens up completely new possibilities of studying resonance scattering; in contrast to spontaneous-scattering spectroscopy, the different resonance contributions to the susceptibility interfere. This is illustrated by Figs. 7 and 8. Figure 7 shows "active" spectra of toluene measured in a mixture with the dye rhodamine 6G whose absorption line coincides with one of the frequencies, ω_1 or ω_2. We see that under *double-resonance* conditions ($\omega_1 - \omega_2 \approx \Omega$ is a vibrational frequency of toluene, while $\omega_2 \approx \omega_{0,e}$ is an electronic transition frequency in rhodamine) the spectrum is substantially distorted. The distortion can be used to measure new spectroscopic parameters, such as the sign of the susceptibilities, as well as for resolving lines and increasing the signal/noise ratio.

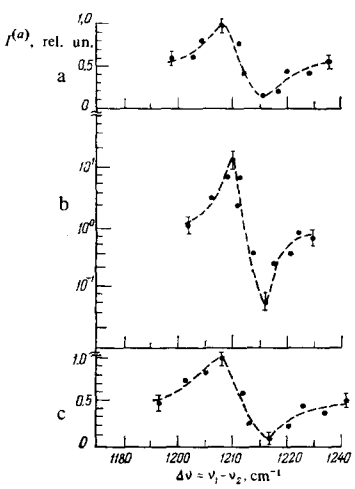

FIG. 7. Deformation of the contour of a spectral line obtained by ARS in toluene upon adding various amounts of the dye rhodamine 6G, which absorbs one of the pump waves.[41] The deformation arises from the interference inherent in ARS of the nonlinear optical susceptibilities of the different components of the solution; its manifestation does not require intermolecular interaction—actually the things that interfere are the "imprints" left by the different molecules of the mixture on the coherent wave of the scattered light. N_2 is the density of the molecules of rhodamine 6G. a) $N_2 = 0$, b) $N_2 = 0.45 \times 10^{16}$ cm^{-3}, c) $N_2 = 1.7 \times 10^{16}$ cm^{-3}.

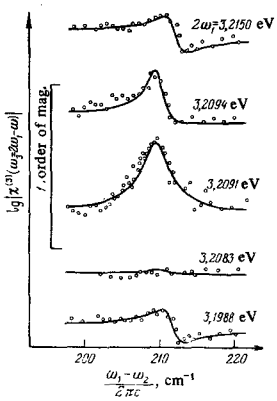

FIG. 8. Interference phenomena in the spectrum of the anti-Stokes ARS signal (ω_a) obtained in a CuCl crystal under double exciton–phonon resonance conditions. Here we have $\omega_a = 2\omega_1 - \omega_2$, with $\omega_1 - \omega_2 \approx \Omega_{background}$, $2\omega_1 \approx \Omega_{exc}$[42]; $\Omega_{exc} = 3.208$ eV.

Figure 8 shows the "active spectrum" obtained by Bloembergen and his associates[42] in CuCl under double-resonance conditions in which $\omega_1 - \omega_2 \approx \Omega_{background}$ is the frequency of an optical phonon, and $2\omega_1 \approx \Omega_{exc}$ is the exciton frequency (for more details, see Secs. 12*b*, *c* of Chap. III).

Essentially the experiments made it possible to measure correctly for the first time a nonlinear susceptibility involving excitation of excitons. The experiment of Bloembergen and his associates fully illustrates one of the interesting possibilities opened up by the method of active spectroscopy, that of studying resonance processes under conditions in which both the frequencies of the probe rays and the frequency of the radiation to be detected lie in a region of transparency. We present below and discuss in detail also other physical and analytical applications of the method of active spectroscopy. Recently its use has permitted people, in particular, to detect second sound optically.[43] It is also of interest to apply the method of active spectroscopy to plasma diagnostics.[44] Yet in closing this short introduction, we note still another aspect of active spectroscopy—the possibility of obtaining strongly nonequilibrium states in the phonon subsystem. This problem has been discussed for a long time (see Refs. 45 and 46, the review[47] and the collected volume[48]). However, attempts to detect anharmonic effects from optical phonons excited by a high-power laser doublet have failed. Interest in phenomena of this type continues even now. Apparently the most promising approach here is to study coherent intermode interactions in molecules in the absence of collisions. Estimates show that the intensity of current lasers suffices for observing such processes in a set of triatomic and polyatomic molecules.[49]

8. This review turns its major attention to steady-state coherent active spectroscopy and its applications for studying elementary excitations in gases, liquids, and solids. Many results have been obtained here in the past 3–4 years that require generalization and analysis. Coherent active Raman spectroscopy (CARS) is becoming one of the best-developed methods of nonlinear laser spectroscopy.[2)][50,51] The materials on non-

[2)]Besides "coherent anti-Stokes Raman scattering," the abbreviation CARS is used also for three- or four-wave mixing spectroscopy and is especially widespread in the American literature.

steady-state active spectroscopy are more readily compilations of data; a number of reviews[52,53] has been published here in recent years.

II. ACTIVE RAMAN SPECTROSCOPY (ARS)

1. A simple classical model of electron-phonon coupling. General properties of "active" spectra

a) The propagation of light in an isotropic nonlinear medium is described by the wave equation for the field $\mathbf{E}$:

$$\nabla^2\mathbf{E}-\frac{n^2}{c^2}\frac{\partial^2\mathbf{E}}{\partial t^2}=\frac{4\pi}{c^2}\frac{\partial^2\mathbf{p}^{(NL)}}{\partial t^2},$$

Here $\mathbf{P}^{(NL)}$ is the polarization, which depends nonlinearly on the field of the light wave, and n is the refractive index. To start we shall assume that all waves that participate in the interaction are plane and monochromatic:

$$\mathbf{E}(\mathbf{r},\ t)=\mathrm{Re}\,(\mathbf{E}^{(1)}e^{-i\omega_1 t+i\mathbf{k}_1\mathbf{r}}+\mathbf{E}^{(2)}e^{-i\omega_2 t+i\mathbf{k}_2\mathbf{r}}+\mathbf{E}e^{-i\omega t+i\mathbf{k}\mathbf{r}}+\mathbf{E}^{(a)}e^{-i\omega_a t+i\mathbf{k}_a\mathbf{r}}). \tag{1.1}$$

The amplitudes are assumed everywhere to be bounded by slowly varying functions of $\mathbf{r}$ and t, and $\omega_a=\omega+(\omega_1-\omega_2)$, where ω is the frequency of the probe wave. Then the nonlinear polarization $\mathbf{P}^{(NL)}(\mathbf{r},t)$ is also a superposition of plane waves. The abbreviated equation for the amplitude of the scattered anti-Stokes component of the probe wave that propagates along the z axis has the form

$$\frac{n(\omega_a)}{c}\frac{\partial\mathbf{E}^{(a)}}{\partial t}+\frac{\partial\mathbf{E}^{(a)}}{\partial z}=i\frac{2\pi\omega_a}{cn(\omega_a)}\mathbf{P}^{(NL)}(\omega_a)e^{-ik_a z}; \tag{1.2}$$

Here $\mathbf{P}^{(NL)}(\omega_a)$ is the spectral component of the nonlinear polarization at the frequency ω_a. We shall assume henceforth that the waves $\mathbf{E}^{(1,2)}$ are given; this case is of special interest in spectroscopy.

Let us examine a simple model of a rarefied medium of noninteracting molecules having a single non-degenerate Raman-active vibration of frequency Ω. In a classical model the Hamiltonian of the molecule in the presence of the field of the light wave has the following form (we omit the vector and tensor indices for the present):

$$\mathcal{H}=\mathcal{H}_0-pE=\mathcal{H}_0-\tfrac{1}{2}\alpha(x)EE; \tag{1.3}$$

Here $\mathcal{H}_0=T+\Phi(x)$ is the Hamiltonian of an unperturbed molecule having the kinetic energy T and the potential energy $\Phi(x)$ of the nuclei in the field of the electrons; $\alpha(x)$ is the electronic polarizability, which depends parametrically on the nuclear configuration x; and p is the induced dipole moment:

$$p=-\frac{\partial\mathcal{H}}{\partial E}. \tag{1.4}$$

The light field exerts a perturbing influence on the positions of the nuclei that displaces them from their equilibrium positions. If these displacements are small, we can represent them in a power series in the normal coordinate Q. Then the Hamiltonian of (1.3) acquires the following form (we restrict the treatment to only the first terms of the expansion):

$$\mathcal{H}=T+\tfrac{1}{2}M\Omega^2Q^2-\tfrac{1}{2}\alpha_0E^2-\tfrac{1}{2}\left(\frac{\partial\alpha}{\partial Q}\right)_0QE^2; \tag{1.5}$$

Here M is the reduced mass, and we have $\alpha_0=\alpha(0)$ as the purely electronic polarizability in the equilibrium position of the nuclei; the derivative $(\partial\alpha/\partial Q)_0$ is also taken at $Q=0$. The last term in (1.5) describes the electron-phonon coupling. We can easily derive the following equation for Q from (1.5):

$$M\ddot{Q}=-\frac{\partial\mathcal{H}}{\partial Q}. \tag{1.6}$$

If we phenomenologically introduce into this equation a term to describe damping we get as a result

$$\ddot{Q}+2\Gamma\dot{Q}+\Omega^2Q=\frac{1}{2M}\left(\frac{\partial\alpha}{\partial Q}\right)_0E^2. \tag{1.7}$$

The "stimulated" solution of (1.7) has a resonance at $\omega_1-\omega_2\approx\Omega$ (people say in this case that the molecular vibrations are coherently pumped in the biharmonic light field).

In the steady-state case we have

$$Q=\frac{1}{2M}\left(\frac{\partial\alpha}{\partial Q}\right)_0E^{(1)}E^{(2)*}\frac{\exp[i(\mathbf{k}_1-\mathbf{k}_2)\mathbf{r}-i(\omega_1-\omega_2)t]}{\Omega^2-(\omega_1-\omega_2)^2-2i\Gamma(\omega_1-\omega_2)}. \tag{1.8}$$

We shall calculate from (1.4) and (1.8) an expression for the induced dipole moment at the frequency $\omega_a=\omega+(\omega_1-\omega_2)$. By multiplying it by the density N of molecules, we get the macroscopic polarization, which is cubic in the amplitude of the light field:

$$P^{(NL)}(\mathbf{r},\ t)=P^{(3)}(\omega_a)e^{-i\omega_a t+i\mathbf{k}_p\mathbf{r}}=\frac{N}{4M}\left(\frac{\partial\alpha}{\partial Q}\right)_0^2\frac{EE^{(1)}E^{(2)*}}{D(\Omega,\ \omega_1-\omega_2)}e^{i(-\omega_a t+\mathbf{k}_p\mathbf{r})}, \tag{1.9}$$

$$D(\Omega,\ \omega_1-\omega_2)=\Omega^2-(\omega_1-\omega_2)^2-2i\Gamma(\omega_1-\omega_2), \tag{1.10}$$

$$\mathbf{k}_p=\mathbf{k}+\mathbf{k}_1-\mathbf{k}_2.$$

Substitution of (1.9) into Eq. (1.3) in the steady-state case $(\partial/\partial t=0)$ gives

$$\frac{\partial E^{(a)}}{\partial z}=i\frac{\pi\omega_aN}{2cn(\omega_a)M}\left(\frac{\partial\alpha}{\partial Q}\right)_0^2\frac{EE^{(1)}E^{(2)*}e^{-i\Delta kz}}{D(\Omega,\ \omega_1-\omega_2)}; \tag{1.11}$$

Here $\Delta k=k_{az}-k_z-k_{1z}-k_{2z}$ is the phase mismatch. The solution of (1.11) with null boundary conditions for $z=0$ has the form

$$E^{(a)}(z)=i\frac{\pi\omega_aN}{cn(\omega_a)M}\left(\frac{\partial\alpha}{\partial Q}\right)_0^2D^{-1}(\Omega,\ \omega_1-\omega_2)\frac{\sin(\Delta kz/2)}{\Delta k}e^{-i\Delta kz/2}EE^{(1)}E^{(2)*}. \tag{1.12}$$

Hence we see that the increment in the field $\mathbf{E}^{(a)}$ starts at zero, while the most rapid increase is observed in the direction of phase synchronization $\Delta\mathbf{k}=0$. However, the requirements on the arrangement of the beams prove in many cases to be not too severe. In gases the coherent-interaction lengths with parallel propagation of the beams amount to $l_{coh}=\pi/\Delta k\sim10$–$100$ cm. One can easily attain a value $l_{coh}\geq1$ cm in strongly dispersive media by divergence of the interacting beams by small angles (~1–$3°$). Finally, one can compensate the wave mismatch by using strong focusing of the collinear interacting beams into a focal volume having the length l_{foc}

$\ll l_{coh}$ (for more details, see Sec. 6d of Chap. II). Of course, the possibility remains in all cases of using exact synchronization.

b) Let us estimate the efficiency of scattering of the probe beam in a coherent ARS system as compared with its efficiency of spontaneous scattering. The latter is characterized by the Raman cross section, which involves the molecular parameters by the following formula[3] for a "forward" scattering system:

$$\frac{d\sigma}{do}=\frac{\omega_c^2}{c^4}\left(\frac{\partial\alpha}{\partial Q}\right)_0^2\frac{\hbar}{2M\Omega}. \tag{1.13}$$

The power of the probe radiation scattered into the solid angle δo (Stokes component) is given by the expression

$$P_{spont}^{c}=\frac{d\sigma}{do}lNP\delta o; \tag{1.14}$$

Here N is the density of the molecules, l is the length of the illuminated specimen, and P is the power of the probe beam.

We can find the total power of the coherently scattered radiation from (1.12) with account for (1.13) by assuming the transverse distribution of all the interacting beams to be Gaussian with the same radius w (as before, we assume the phase fronts of all the waves to be planar):

$$P_{ARS}^{(a)}\approx\left(lN\frac{d\sigma}{do}\right)^2\cdot\frac{2^6\pi^2c^4}{\omega_c^2(\hbar\Gamma)^2n^4}\operatorname{sinc}^2\left(\frac{\Delta kl}{2}\right)\frac{PP_1P_2}{w^4}; \tag{1.15}$$

Here $\operatorname{sinc}x=\sin x/x$, and P, P_1, and P_2 are the total powers of the beams at frequencies ω, ω_1, and ω_2, respectively.

Upon comparing (1.15) and (1.14), we get the following expression for the power enhancement of the anti-Stokes scattering signal of the beam in an ASRS system over the level of spontaneous scattering of the same probe beam:

$$\eta=\frac{P_{ARS}^{(a)}}{P_{spont}^{(c)}}\approx lN\frac{d\sigma}{do}\operatorname{sinc}^2\left(\frac{\Delta kl}{2}\right)\cdot\frac{2^6\pi^2c^4}{\omega_c^2\hbar^2\Gamma^2n^6}\frac{P_1P_2}{w^4}\frac{1}{\delta o}. \tag{1.16}$$

Estimates by Eq. (1.16), which are confirmed by many experiments[33,36,54] (see also Ref. 96), show that when $\Delta k=0$ one can easily get a value of $\eta\sim10^3$–10^6 in condensed media for well marked Raman lines by using, as as needed, focused pump beams of power $P_{1,2}\sim$ 10–100 kW. One can get an analogous enhancement in gaseous media by using pump beams of power $P_{1,2}\sim$ 1–10 MW.

This circumstance occasions the considerable advantage of coherent ARS over spontaneous Raman spectroscopy in terms of the signal/noise ratio.

We note from (1.16) that a potentiality can be seen for absolute measurement of the Raman cross-section $d\sigma/do$ by measuring the relative increase in the scattering power of the probe beam when the coherent "pump" is turned on (see Refs. 33 and 36).

c) Scanning of the difference of pumping frequencies $\omega_1-\omega_2$ near Ω makes it possible to study the shape of the molecular resonance line. However, the shape of the spectral line strongly differs from that of the spontaneous scattering line.[35,36]

The most essential point here is that the ARS signal does not vanish when $|\omega_1-\omega_2|\gg\Gamma$, even in the case of a an isolated line, in contrast to the spontaneous-scattering case. Actually, under these conditions we have

$$P^{(3)}(\omega_a)=\chi^{(3)E}EE^{(1)}E^{(2)*}. \tag{1.17}$$

Here $\chi^{(3)E}$ is the non-resonance cubic susceptibility that arises from the electronic contribution. Upon introducing the resonance cubic susceptibility by using (1.9) and formulas like (1.17), we have

$$\chi^{(3)R}=\frac{N}{4M}\left(\frac{\partial\alpha}{\partial Q}\right)^2D^{-1}(\Omega,\ \omega_1-\omega_2)\approx\frac{\bar{\chi}^{(3)R}}{-i-\Delta},$$

where

$$\bar{\chi}^{(3)R}=\frac{N}{8M\Omega\Gamma}\left(\frac{\partial\alpha}{\partial Q}\right)_0^2,\quad\Delta=\frac{-\Omega+(\omega_1-\omega_2)}{\Gamma},$$

and we have the following expression for $P^{(3)}$ for arbitrary $\omega_1-\omega_2$:

$$P^{(3)}=(\chi^{(3)R}+\chi^{(3)E})EE^{(1)}E^{(2)*}, \tag{1.18}$$

and the *dispersion of the intensity* of the anti-Stokes signal under resonance conditions is determined by the expression

$$I_a(\omega)\sim|\chi^{(3)R}+\chi^{(3)E}|^2II_1I_2. \tag{1.19}$$

Figure 9 shows the shapes of the corresponding resonance curves. If we measure the ratio I_{max}/I_{min} upon scanning $\omega_1-\omega_2$, together with the frequency that corresponds to the signal minimum, and the width of the resonance, we can measure all the parameters that are defined in spontaneous Raman spectroscopy. We note that the potentiality arises of ultrahigh spectral resolution of Raman transitions that is governed only by the

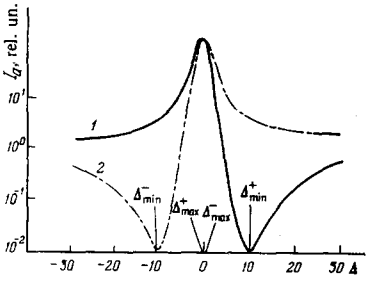

FIG. 9. Overall shape of the frequency-dependence of the intensity of the anti-Stokes ARS signal calculated by Eq. (1.19). The values of the parameters are as follows: $\alpha=|\bar{\chi}^{(3)R}|/|\chi^{(3)E}|=10$, sign $\bar{\chi}^{(3)R}=$ sign $\chi^{(3)E}$ (curve 1), sign $\bar{\chi}^{(3)E}$ (curve 2); $\Delta^{\pm}_{max}=(\alpha/2)\pm\sqrt{1+(\alpha/2)^2}$, $\Delta^{\pm}_{min}=(\alpha/2)\pm\sqrt{1+(\alpha/2)^2}$.

[3]A more exact expression that accounts for the features of the molecular Raman tensor and for averaging over orientations is given in Sec. 2*d* of Chap. II as Eq. (2.21).

widths of the lines ω_1 and ω_2 that are used[111–114] when one employs narrow-band tunable lasers in active spectroscopy (the generation line width of the best specimens of continuous-wave lasers does not exceed 10 kHz).[115,116]

The spectrum of $|\chi^{(3)}(\omega_a;\ \omega_1,\ \omega_1-\omega_2)|^2$ can also be obtained in one laser pulse without scanning the frequencies ω_1 and ω_2: in order to do this, the line ω_2 must have as much broader a spectrum as possible that overlaps the entire Raman line.[36,38] Then the form of the Raman resonance is obtained by normalizing the spectrum $I_a(\omega_a)$ to the spectrum of the broad-band pump component (ω_2) (for further details, see Sec. 6*c* of Chap. II, Fig. 5).

Moreover, one can also get additional information from the spectrum of the intensity, including the sign of the susceptibilities. On the other hand, the existence of a non-resonance pedestal can be used as a standard for absolute measurements.

Of course, the intensity spectrum bears only part of the information on the scattering medium. It is substantially supplemented by the data on the dispersion of the polarization and the dispersion of the phase advance (see below, Sec. 3). Hence, actually three types of active spectroscopy are developing rapidly now:

1) *Amplitude active spectroscopy, which operates with the dispersion of the intensity of the scattered signal.*

2) *Polarization active spectroscopy, which operates with the dispersion of the polarization of the scattered signal.*

3) *Phase active spectroscopy, which operates with the phase advance of the scattered signal.*

The classical pattern, whose simplest variant is described in this section, suffices to describe practically all the effects of coherent ARS. We shall introduce the quantum equations that account for the movement of the populations only in Sec. 5 (see also Ref. 100).

2. Coherent steady-state ARS in terms of the nonlinear susceptibilities

As we have seen in Sec. 1, the processes that occur in coherent ARS in a centrosymmetric medium can be described within the framework of the phenomenological expansion of the nonlinear polarizability by a term that is cubic in the field. In this section we shall turn in somewhat greater detail, first to the phenomenological description of ARS, and then we shall discuss some problems involving the microscopic calculation of the 4th-order tensor of the cubic susceptibility. Also we shall discuss the limitations imposed by the symmetry of the medium. Later we shall treat the correspondence between the components of this tensor and the parameters that figure in the theory of spontaneous Raman scattering.

a) The phenomenological approach. We can represent in the following form the electric polarizability (cubic in the electric-field intensity) that is induced in a steady-state homogeneous nonlinear medium by the field of the light wave $\mathbf{E}(\mathbf{r}, t)$:[7] [4)]

$$P_i^{(3)}(\mathbf{r}, t)=\int_{-\infty}^{t}dt'\int_{-\infty}^{t}dt''\int_{-\infty}^{t}dt'''\chi_{ijkl}^{(3)}(\mathbf{r}, t-t', t-t'', t''-t''')\times E_j(\mathbf{r}, t')E_k(\mathbf{r}, t'')E_l(\mathbf{r}, t'''). \tag{2.1}$$

Henceforth we shall use Eq. (2.1) in a Fourier representation. In line with (1.2), the electric field in the medium amounts to a superposition of four plane light waves: the pump waves of frequencies ω_1 and ω_2, the probe wave of frequency ω, and the anti-Stokes[5)] scattered wave of frequency $\omega_a=\omega+\omega_1-\omega_2$. The spectral component $\mathbf{P}^{(3)}$ at the frequency ω_a has the form:

$$\begin{aligned}P_i^{(3)}(\omega_a)=\sum_{j,k,l}(&\chi_{ijkl}^{(3)}(\omega_a;\ \omega,\ \omega_1,\ -\omega_2)E_jE_k^{(1)}E_l^{(2)*}\\&+\chi_{ijkl}^{(3)}(\omega_a;\ \omega,\ -\omega_2,\ \omega_1)E_jE_k^{(2)*}E_l^{(1)}+\chi_{ijkl}^{(3)}(\omega_a;\ \omega_1,\ \omega,\ -\omega_2)E_j^{(1)}E_kE_l^{(2)*}\\&+\chi_{ijkl}^{(3)}(\omega_a;\ \omega_1,\ -\omega_2,\ \omega)E_j^{(1)}E_k^{(2)*}E_l+\chi_{ijkl}^{(3)}(\omega_a;\ -\omega_2,\ \omega,\ \omega_1)E_j^{(2)*}E_kE_l^{(1)}\\&+\chi_{ijkl}^{(3)}(\omega_a;\ -\omega_2,\ \omega_1,\ \omega)E_j^{(2)*}E_k^{(1)}E_l\};\end{aligned} \tag{2.2}$$

Here we have

$$\chi_{ijkl}^{(3)}(\omega_a;\ \omega,\ \omega_1,\ -\omega_2)=\frac{1}{4}\int_0^\infty d\tau'\int_0^\infty d\tau''\int_0^\infty d\tau'''\chi_{ijkl}^{(3)}(\tau',\ \tau'',\ \tau''')\exp[-i(\omega\tau'+\omega_1\tau''-\omega_2\tau''')] \tag{2.3}$$

etc. As usual,[20,58] the factor 1/4 has been introduced in defining the spectral component of the cubic susceptibility tensor of (2.3) in order to eliminate numerical coefficients in Eq. (2.2).

When one of the pump components is used as the probe beam, i.e., when, e.g., $\omega=\omega_1$, then evidently the number of terms within the summation in (2.3) must be diminished twofold.[6)] In line with the definitions (2.1) and (2.3) in the expression for $\chi^{(3)}$, the latter three frequency arguments can change places with simultaneous permutation of the corresponding tensor indices.

Upon using this, we can put Eq. (2.3) into the following form:

$$P_i^{(3)}(\omega_a)=\mathcal{Z}\chi_{ijkl}^{(3)}(\omega_a;\ \omega,\ \omega_1,\ -\omega_2)E_jE_k^{(1)}E_l^{(2)*}; \tag{2.4}$$

here we have the coefficient $\mathcal{Z}=6$ if all the frequencies ω, ω_1, and $-\omega_2$ differ, and $\mathcal{Z}=3$ for twofold degeneracy of one of the frequencies, e.g., when $\omega=\omega_1$ (summation is performed over repeated indices).

Since Eq. (2.4) must remain invariant with respect to the spatially symmetric operations that transform the medium into itself, this imposes additional conditions on the components of the tensor $\chi_{ijkl}^{(3)}$. Thus not

---

[4)] We thus restrict the treatment to the dipole approximation, while neglecting effects involving the quadrupole and magnetic-dipole terms of the expansion, as well as the spatial dispersion.

[5)] For the sake of argument, we shall restrict the treatment only to the case of anti-Stokes scattering, since the case of Stokes scattering ($\omega_s=\omega-(\omega_1-\omega_2)$) can be treated by analogy.

[6)] In Eq. (2.2) we have kept only the terms that describe frequency-mixing processes: $\omega_a=\omega+\omega_1-\omega_2$, that are characteristic of ARS; the other terms that describe stimulated Raman-scattering effects or inverse Raman scattering ($\omega_a=\omega_a+\omega-\omega$) or the optical Kerr effect ($\omega_a=\omega_a+\omega_a-\omega_a$, $\omega_a=\omega_a+\omega_{1,2}-\omega_{1,2}$) have been omitted as inconsequential.

all of its 81 components prove to be independent, while some of the components vanish. References 56 and 57 give a list of the non-zero components of the tensor $\chi^{(3)}_{ijkl}$ for all the crystal classes and for isotropic media.

In particular, 21 components of the tensor $\chi^{(3)}_{ijkl}$ differ from zero in isotropic media, of which only three are independent:

$$\left.\begin{aligned}
&\chi^{(3)}_{1111}=\chi^{(3)}_{2222}=\chi^{(3)}_{3333},\\
&\chi^{(3)}_{1122}=\chi^{(3)}_{1133}=\chi^{(3)}_{2211}=\chi^{(3)}_{2233}=\chi^{(3)}_{3311}=\chi^{(3)}_{3322}=\chi^{(3)}_{2323},\\
&\chi^{(3)}_{1212}=\chi^{(3)}_{1231}=\chi^{(3)}_{1313}=\chi^{(3)}_{1331}=\chi^{(3)}_{2323}=\chi^{(3)}_{2332},\\
&\chi^{(3)}_{1221}=\chi^{(3)}_{1213}=\chi^{(3)}_{1331}=\chi^{(3)}_{2113}=\chi^{(3)}_{2332}=\chi^{(3)}_{2323},\\
&\chi^{(3)}_{1111}=\chi^{(3)}_{1122}+\chi^{(3)}_{1212}+\chi^{(3)}_{1221}.
\end{aligned}\right\} \qquad (2.5)$$

The frequency arguments of all the components are assumed identical. Upon using the last of the relationships, we can write the following expression for the vector $\mathbf{P}^{(3)}(\omega_\sigma)$ in an isotropic medium, which stems from (2.4):

$$\mathbf{P}^{(3)}(\omega_\sigma)=\mathscr{D}\,[\chi^{(3)}_{1122}(\omega_\sigma;\ \omega,\ \omega_1,\ -\omega_2)\,\mathbf{E}\,(\mathbf{E}^{(1)}\mathbf{E}^{(2)*})+\chi^{(3)}_{1212}(\omega_\sigma;\ \omega,\ \omega_1,\ -\omega_2)\,\mathbf{E}^{(1)}\,(\mathbf{E}\mathbf{E}^{(2)*})+\chi^{(3)}_{1221}(\omega_\sigma;\ \omega,\ \omega_1,\ -\omega_2)\,\mathbf{E}^{(2)*}\,(\mathbf{E}\mathbf{E}^{(1)})]. \qquad (2.6)$$

Whenever the propagation of the light waves and their nonlinear interaction do not excite internal motions in the medium (real electronic transitions, pumping of ions, etc.), i.e., in a loss-free medium, there is an additional class of spatial-frequency transformations that leave the components of the tensor $\chi^{(3)}_{ijkl}$ invariant. In these media, the value of $\chi^{(3)}_{ijkl}$ does not change upon permuting pairs of any indices (rather than only the last three) if we simultaneously permute the frequencies to match.[56, 58] If here we can neglect the frequency dispersion in the region of the frequencies ω_σ, ω, ω_1, and $-\omega_2$, then we get simple symmetry relations that are commonly called the Kleinman relationships[8, 59] by analogy with those for the third-order tensor. Under this assumption we can permute any of the tensor indices (while preserving the order of the frequencies) without changing the value of the susceptibility. The Kleinman relationships decrease even further the number of non-zero independent components of $\chi^{(3)}_{ijkl}$. The validity of the Kleinman relationships for fourth-order nonlinear susceptibility tensors has been repeatedly tested in experiments of the third-harmonic-generation type and nonlinear three-wave mixing[60, 61] under conditions in which none of the frequencies ω_1, ω_2, and ω_3 of the waves that participate in the nonlinear interaction nor any of their combinations ($\omega_1\pm\omega_2$; $\omega_1\pm\omega_3$; $2\omega_1$; $\omega_2\pm\omega_3$; $2\omega_2$, etc.) coincide with any resonance of the medium.

Yet precisely the latter requirement is not fulfilled in ARS experiments. Hence one cannot apply the Kleinman relationships to those terms in the expression for $\chi^{(3)}_{ijkl}$ that arise from the contributions of the "resonance" dynamic subsystem of the medium (in this case, the subsystem of vibrating nuclei of the molecules; see Sec. 2*c* below).

With this we close the purely phenomenological treatment of the nonlinear susceptibilities, and proceed to calculate them on the basis of microscopic models.

b) A microscopic model. In homogeneous media made of identical elements (atoms and molecules in gases and liquids, unit cells in crystals), people commonly introduce also the nonlinear polarizabilities of the individual elements, or the hyperpolarizabilities γ_{ijkl}, along with the macroscopic nonlinear susceptibilities $\chi^{(3)}_{ijkl}$. Their mean values are determined by using the relationship

$$\langle\gamma_{ijkl}(\omega_\sigma;\ \omega,\ \omega_1,\ -\omega_2)\rangle=\frac{1}{NL^4}\chi^{(3)}_{ijkl}(\omega_\sigma;\ \omega,\ \omega_1,\ -\omega_2);$$

Here N is the density of the primary elements that form the medium. The angle brackets denote averaging over their orientations. One can omit these brackets for a crystalline medium; and we have $L=(n^2+2)/3$ as the Lorentz correction factor for the internal field.[7] Correspondingly, we can also introduce the mean polarization of such an element (for concreteness we shall speak of a molecule):

$$\langle p_i^{(3)}(\omega_\sigma)\rangle=\mathscr{D}\,\langle\gamma_{ijkl}(\omega_\sigma;\ \omega,\ \omega_1,\ -\omega_2)\rangle\,L^4E_jE_k^{(1)}E_l^{(2)*}. \qquad (2.7)$$

In line with what we have said in Sec. 1*a*, let us represent the Hamiltonian of a molecule lying in the light field as a power series in the field and in the normal vibrational coordinates Q_σ[56]:

$$\begin{aligned}
\mathscr{H}(\mathscr{E},\ \{x\})=\mathscr{H}_0\{x\}&-\mu_i(\{x\})\,\mathscr{E}_i-\frac{1}{2}\,\alpha_{ij}(\{x\})\,\mathscr{E}_i\mathscr{E}_j\\
&-\frac{1}{3}\,\beta_{ijk}(\{x\})\,\mathscr{E}_i\mathscr{E}_j\mathscr{E}_k-\frac{1}{4}\,\gamma_{ijkl}\mathscr{E}_i\mathscr{E}_j\mathscr{E}_k\mathscr{E}_l\ldots=T_i+\frac{1}{2}\,M\Omega_\sigma^2Q_\sigma^2\\
&+\frac{1}{3}\left(\frac{\partial^3\Phi}{\partial Q_\sigma\,\partial Q_{\sigma'}\,\partial Q_{\sigma''}}\right)Q_\sigma Q_{\sigma'}Q_{\sigma''}+\ldots-\mu_{0i}\mathscr{E}_i\\
&-\left(\frac{\partial\mu_i}{\partial Q_\sigma}\right)_0Q_\sigma\mathscr{E}_i-\ldots-\frac{1}{2}\,\alpha^E_{ij}\mathscr{E}_i\mathscr{E}_j-\frac{1}{2}\left(\frac{\partial\alpha_{ij}}{\partial Q_\sigma}\right)_0Q_\sigma\mathscr{E}_i\mathscr{E}_j\\
&-\frac{1}{4}\left(\frac{\partial^2\alpha_{ij}}{\partial Q_\sigma\partial Q_{\sigma'}}\right)_0Q_\sigma Q_{\sigma'}\mathscr{E}_i\mathscr{E}_j-\frac{1}{3}\,\beta^E_{ijk}\mathscr{E}_i\mathscr{E}_j\mathscr{E}_k\\
&-\frac{1}{3}\left(\frac{\partial\beta_{ijk}}{\partial Q_\sigma\partial Q_\sigma}\right)_0Q_\sigma\mathscr{E}_i\mathscr{E}_j\mathscr{E}_k-\frac{1}{4}\,\gamma^E_{ijkl}\mathscr{E}_i\mathscr{E}_j\mathscr{E}_k\mathscr{E}_l\ldots;
\end{aligned} \qquad (2.8)$$

Here $\mu_i(\{x\})$ is the dipole moment of the molecule; $\alpha_{ij}(\{x\})$, $\beta_{ijk}(\{x\})$, and $\gamma_{ijkl}(\{x\})$ are the tensors of the electronic linear, quadratic, and cubic polarizabilities of the molecule for the arbitrary configuration $\{x\}$ of the nuclei; $\mathscr{E}_i$ is the internal field acting on the ions; and α^E_{ij}, β^E_{ijk}, and γ^E_{ijkl} are respectively the 1st-, 2nd-, and 3rd-order purely electronic polarizabilities of the molecule in the equilibrium position of the nuclei, $Q_\sigma=0$. The derivatives are also taken in the equilibrium position $Q_\sigma=0$. In (2.8), summation is implied over the repeated tensor indices i, j, k, and l and over the indices σ, σ', ..., that specify the normal modes.

Upon using (2.8) with the aid of (1.4), we get

$$\begin{aligned}
p_i=-\frac{\partial\mathscr{H}(\mathscr{E}_i,\ \{x\})}{\partial\mathscr{E}_i}&=\mu_{0i}+\left(\frac{\partial\mu}{\partial Q_\sigma}\right)_0Q_\sigma+\alpha^E_{ij}\mathscr{E}_j+\left(\frac{\partial\alpha_{ij}}{\partial Q_\sigma}\right)_0Q_\sigma\mathscr{E}_j\\
&+\frac{1}{2}\left(\frac{\partial^2\alpha_{ij}}{\partial Q_\sigma\,\partial Q_{\sigma'}}\right)_0Q_\sigma Q_{\sigma'}\mathscr{E}_j+\beta^E_{ijk}\mathscr{E}_j\mathscr{E}_k+\left(\frac{\partial\beta_{ijk}}{\partial Q_\sigma}\right)_0\mathscr{E}_j\mathscr{E}_kQ_\sigma+\gamma^E_{ijkl}\mathscr{E}_j\mathscr{E}_k\mathscr{E}_l
\end{aligned} \qquad (2.9)$$

The equations of motion for Q_σ are obtained from (2.8) by using the relationship

$$M\ddot{Q}_\sigma=-\frac{\partial\mathscr{H}}{\partial Q_\sigma}. \qquad (2.10)$$

[7] Strictly speaking, we should write $L_\sigma LL_1L_2$ instead of L^4, where, e.g., $L_\sigma=(n^2(\omega_\sigma)+1)/3$, etc. However, in a medium that is optically transparent at all the frequencies ω, $\omega_{1,2,\sigma}$, it is not essential to allow for this circumstance.

The system of equations (2.9) and (2.10) describes all the effects that are discussed in this study. Yet the analysis of this system in general form is unwieldy and ineffective. Instead, we shall take account only of its individual terms, being governed each time by qualitative physical considerations.

We shall be primarily interested in this section in the term on the right-hand side of (2.10), which is analogous to the right-hand side of (1.7); if we keep only this term, we get

$$\ddot{Q}_\sigma + 2\Gamma\dot{Q}_\sigma + \Omega^2 Q_\sigma = \frac{1}{2M}\left(\frac{\partial\alpha_{kl}}{\partial Q_\sigma}\right)\mathscr{E}_k\mathscr{E}_l. \tag{2.11}$$

Upon substituting the solution of (2.11) into (2.8), we can easily derive an equation for the spectral component of the nonlinear polarizability of a single particle that arises from the resonance contribution of the normal mode Q_σ (this part of the polarization is described in (2.9) by the term proportional to $(\partial\alpha_{ij}/\partial Q_\sigma)$). One can get the corresponding term in the macroscopic polarization by averaging over the orientations:

$$P_i^{(3)R(\sigma)}(\omega_a) = \frac{N}{8M}\left\langle\left(\frac{\partial\alpha_{ij}}{\partial Q_\sigma}\right)_0\left[\left(\frac{\partial\alpha_{kl}}{\partial Q_\sigma}\right)_0 + \left(\frac{\partial\alpha_{lk}}{\partial Q_\sigma}\right)_0\right]\right\rangle \times D^{-1}(\Omega_\sigma,\ \omega_1-\omega_2)\,L^4E_jE_k^{(1)}E_l^{(2)*}. \tag{2.12}$$

$D(\Omega_\sigma,\ \omega_1-\omega_2)$ has been defined in (1.10). In a region of transparency, the Raman-scattering tensor $(\partial\alpha_{ij}/\partial Q)_0$ of the totally symmetric vibrations is always symmetric. However, the non-totally-symmetric vibrations, which "mix" the different electronic states, can be characterized by an appreciable antisymmetric component of the Raman-scattering tensor.[68] Nevertheless, unless stated otherwise, we shall hereinafter consider the Raman-scattering tensor to be symmetric. Thus the total nonlinear macroscopic polarization at the frequency ω_a with account taken of the purely electronic contribution and of the resonance Raman contributions of the ionic subsystem can be written in the form

$$P_i^{(3)}(\omega_a) = P_i^{(3)E}(\omega_a) + P_i^{(3)R}(\omega_a) = \mathscr{D}\chi_{ijkl}^{(3)E}(\omega_a;\ \omega,\ \omega_1,\ -\omega_2)\,E_jE_k^{(1)}E_l^{(2)*} + \sum_\sigma \frac{N}{8M}\cdot 2\left\langle\left(\frac{\partial\alpha_{ij}}{\partial Q_\sigma}\right)_0\left(\frac{\partial\alpha_{kl}}{\partial Q_\sigma}\right)_0\right\rangle D^{-1}(\Omega_\sigma,\ \omega_1-\omega_2)\,L^4E_jE_k^{(1)}E_l^{(2)*} = \mathscr{D}\chi_{ijkl}^{(3)}(\omega_a;\ \omega,\ \omega_1,\ -\omega_2)\,E_jE_k^{(1)}E_l^{(2)*}. \tag{2.13}$$

We have cast the expression (2.13) in a form analogous to the phenomenological representation (2.4) by introducing the nonlinear optical susceptibility tensor of the medium $\chi_{ijkl}^{(3)}(\omega_a;\ \omega,\ \omega_1,\ -\omega_2)$, which accounts for the contributions of the electronic and ionic subsystems of the medium, and which has the symmetry properties of the phenomenologically introduced cubic susceptibility tensor. In order to do this, we must symmetrize the terms that correspond to the resonance ionic contributions of (2.12) with respect to the three latter indices:

$$\chi_{ijkl}^{(3)}(\omega_a;\ \omega,\ \omega_1,\ -\omega_2) = \chi_{ijkl}^{(3)E}(\omega_a;\ \omega,\ \omega_1,\ -\omega_2) + \sum_\sigma \chi_{ijkl}^{(3)R(\sigma)}(\omega_a;\ \omega,\ \omega_1,\ -\omega_2). \tag{2.14}$$

Here we have

$$\chi_{ijkl}^{(3)R(\sigma)}(\omega_a;\ \omega,\ \omega_1,\ -\omega_2) = \frac{NL^4}{24M}\left[\left\langle\left(\frac{\partial\alpha_{ij}}{\partial Q_\sigma}\right)_0\left(\frac{\partial\alpha_{kl}}{\partial Q_\sigma}\right)_0\right\rangle D^{-1}(\Omega_\sigma,\ \omega_1-\omega_2) + \left\langle\left(\frac{\partial\alpha_{ik}}{\partial Q_\sigma}\right)_0\left(\frac{\partial\alpha_{jl}}{\partial Q_\sigma}\right)_0\right\rangle D^{-1}(\Omega_\sigma,\ \omega-\omega_2) + \left\langle\left(\frac{\partial\alpha_{il}}{\partial Q_\sigma}\right)_0\left(\frac{\partial\alpha_{kj}}{\partial Q_\sigma}\right)_0\right\rangle D^{-1}(\Omega_\sigma,\ \omega+\omega_1)\right]. \tag{2.15}$$

c) Isotropic media: averaging over the orientations. In an isotropic medium made of freely oriented molecules (gas or liquid), the tensor (2.15) has only three independent components (see (2.5)). When $\omega=\omega_1$, the additional symmetry condition $\chi_{1122}(\omega_a;\ \omega_1,\ \omega_1,\ -\omega_2) = \chi_{1212}(\omega_a;\ \omega_1,\ \omega_1,\ -\omega_2)$ reduces the number of independent components to two, and the condition (2.5) of isotropicity acquires the form

$$\chi_{1111}^{(3)R(\sigma)}(\omega_a;\ \omega_1,\ \omega_1,\ -\omega_2) = 2\chi_{1122}^{(3)R(\sigma)}(\omega_a;\ \omega_1,\ \omega_1,\ -\omega_2) + \chi_{1221}^{(3)R(\sigma)}(\omega_2;\ \omega_1,\ \omega_1,\ -\omega_2). \tag{2.16}$$

The Kleinman relationships for the case of an isotropic medium are reduced to the equality

$$\chi_{1111}^{(3)E}(\omega_a;\ \omega,\ \omega_1,\ -\omega_2) = 3\chi_{1122}^{(3)E}(\omega_a;\ \omega,\ \omega_1,\ -\omega_2). \tag{2.17}$$

We can express the products $\langle(\partial\alpha_{ij}/\partial Q_\sigma)_0\,(\partial\alpha_{kl}/\partial Q_\sigma)_0\rangle$ averaged over the orientations in terms of the invariants of the tensor $(\partial\alpha_{ij}/\partial Q_\sigma)_0$. Further,

$$b_\sigma = \frac{1}{3}\mathrm{Sp}\left[\left(\frac{\partial\alpha_{ik}}{\partial Q_\sigma}\right)_0\right] = \frac{1}{3}(\alpha_{1,\sigma}+\alpha_{2,\sigma}+\alpha_{3,\sigma})$$

is the mean polarizability, which governs the scalar (isotropic) Raman scattering, and

$$g_\sigma^2 = \frac{3}{2}\left[\mathrm{Sp}\left(\frac{\partial\alpha_{ik}}{\partial Q_\sigma}\right)_0^2 - 3b_\sigma^2\right] = \frac{1}{2}\left[(\alpha_{1,\sigma}-\alpha_{2,\sigma})^2+(\alpha_{1,\sigma}-\alpha_{3,\sigma})^2+(\alpha_{2,\sigma}-\alpha_{3,\sigma})^2\right]$$

is the anisotropy, which is involved in quadrupole (anisotropic) Raman scattering. Here $\alpha_{1,\sigma}$, $\alpha_{2,\sigma}$, and $\alpha_{3,\sigma}$ are the principal values of the tensor $(\partial\alpha_{ij}/\partial Q_\sigma)_0$. Upon averaging, we get[5,36]

$$\left\langle\left(\frac{\partial\alpha_{11}}{\partial Q_\sigma}\right)_0\left(\frac{\partial\alpha_{11}}{\partial Q_\sigma}\right)_0\right\rangle = b_\sigma^2 + \frac{4}{45}g_\sigma^2, \tag{2.18}$$

$$\left\langle\left(\frac{\partial\alpha_{11}}{\partial Q_\sigma}\right)_0\left(\frac{\partial\alpha_{22}}{\partial Q_\sigma}\right)_0\right\rangle = b_\sigma^2 - \frac{2}{45}g_\sigma^2, \tag{2.19}$$

$$\left\langle\left(\frac{\partial\alpha_{12}}{\partial Q_\sigma}\right)_0\left(\frac{\partial\alpha_{12}}{\partial Q_\sigma}\right)_0\right\rangle = \left\langle\left(\frac{\partial\alpha_{12}}{\partial Q_\sigma}\right)_0\left(\frac{\partial\alpha_{21}}{\partial Q_\sigma}\right)_0\right\rangle = b_\sigma^2 + \frac{1}{15}g_\sigma^2. \tag{2.20}$$

We should bear in mind the fact that one can express also the differential spontaneous Raman-scattering cross section $d\sigma/do$ and the degree of depolarization ρ of the scattered radiation by using the invariants b^2 and g^2 of the Raman tensor. In particular, the following relations hold for forward scattering excited by linearly polarized radiation under the assumption that the Raman tensor is symmetric:

$$\frac{d\sigma}{do} = \frac{\hbar\omega_1^4}{2M\Omega c^4}\left(b^2+\frac{7}{45}g^2\right), \qquad \rho = \frac{3g^2}{45b^2+4g^2}. \tag{2.21}$$

Table I presents in explicit form the nonzero components of the tensor $\chi_{ijkl}^{(3)}$ for an isotropic medium that has an isolated Raman resonance at the frequency $\Omega\approx\omega_1$

$-\omega_2$, together with expressions that present in vector form the relation between the amplitudes of the interacting fields and the nonlinear polarization. We see in particular from Table I that

$$\rho=\frac{\chi^{(3)R}_{1221}(\omega_a;\ \omega_1,\ \omega_1,\ -\omega_2)}{\chi^{(3)R}_{1111}(\omega_a;\ \omega_1,\ \omega_1,\ -\omega_2)}. \tag{2.22}$$

3. Polarization effects in active spectroscopy

Polarization measurements in spontaneous Raman spectra give rich information on the studied medium (see, e.g., Refs. 62–64). The possibility of making such measurements stems from the tensor nature of spontaneous scattering. The order of the tensor $\chi^{(3)}_{ijkl}$ that one measures in ARS is twice as great as the order of the Raman-scattering tensor. Therefore the possibilities for polarization measurements are generally broader here.

The coherence of the scattering process in ARS engenders several effects that have no analog in spontaneous Raman scattering, such as the dispersion of the plane of polarization of the scattered signal upon scanning $\omega_1-\omega_2$ through a Raman resonance region[60] or the effect of removal of the coherent background.[66]

a) Isotropic media: dispersion of the plane of polarization of the ARS *signal.* The relationship of the intensity of the ARS signal to the polarization of the interacting light waves is given for an isotropic medium by Eq. (2.13), which defines the nonlinear source in Eq. (1.3) for the coherently scattered signal (see also Table I).

For the sake of argument, we shall restrict the treatment to the case of ARS with degenerate frequencies $(\omega=\omega_1)$.

TABLE I.

ARS scheme with a probe beam—nondegenerate frequencies $\omega_a=\omega+\omega_1-\omega_2$	
$\chi^{(3)R}_{1111}(\omega_a;\ \omega,\ \omega_1,\ -\omega_2)$	$\frac{NL^4}{48M\Omega\Gamma}\,\frac{b^2+(4/45)\,g^2}{-i-\Delta}$
$\chi^{(3)R}_{1122}(\omega_a;\ \omega,\ \omega_1,\ -\omega_2)$	$\frac{NL^4}{48M\Omega\Gamma}\,\frac{b^2-(2/45)\,g^2}{-i-\Delta}=(1-2\rho)\,\chi^{(3)R}_{1111}$
$\chi^{(3)R}_{1221}(\omega_a;\ \omega,\ \omega_1,\ -\omega_2)=\chi^{(3)R}_{1212}(\omega_a;\ \omega,\ \omega_1,\ -\omega_2)$	$\frac{NL^4}{48M\Gamma\Omega}\,\frac{(1/15)\,g^2}{-i-\Delta}=\rho\chi^{(3)R}_{1111}$
$\mathbf{P}^{(3)}(\omega_a)=2\chi^{(3)E}_{1111}[\mathbf{E}(\mathbf{E}^{(1)}\mathbf{E}^{(2)*})+\mathbf{E}^{(1)}(\mathbf{E}\mathbf{E}^{(2)*})+\mathbf{E}^{(2)*}(\mathbf{E}\mathbf{E}^{(1)})]$ $+6\,[\chi^{(3)R}_{1122}\mathbf{E}(\mathbf{E}^{(1)}\mathbf{E}^{(2)*})+\chi^{(3)R}_{1212}\mathbf{E}^{(1)}(\mathbf{E}\mathbf{E}^{(2)*})+\chi^{(3)R}_{1221}\mathbf{E}^{(2)*}(\mathbf{E}\mathbf{E}^{(1)})]$ *)	
ARS scheme with degenerate frequencies $\omega_a=2\omega_1-\omega_2\ \ (\omega=\omega_1)$	
$\chi^{(3)R}_{1111}(\omega_a;\ \omega_1,\ \omega_1,\ -\omega_2)$	$\frac{NL^4}{24M\Omega\Gamma}\,\frac{b^2+(4/45)\,g^2}{-i-\Delta}$
$\chi^{(3)R}_{1122}(\omega_a;\ \omega_1,\ \omega_1,\ -\omega_2)=\chi^{(3)R}_{1212}(\omega_a;\ \omega_1,\ \omega_1,\ -\omega_2)$	$\frac{NL^4}{24M\Omega\Gamma}\,\frac{(1/2)\,b^2+(1/90)\,g^2}{-i-\Delta}=\frac{1-\rho}{2}\,\chi^{(3)R}_{1111}$
$\chi^{(3)R}_{1221}(\omega_a;\ \omega_1,\ \omega_1,\ -\omega_2)$	$\frac{NL^4}{24M\Omega\Gamma}\,\frac{(1/15)\,g^2}{-i-\Delta}=\rho\chi^{(3)R}_{1111}$
$\mathbf{P}^{(3)}(\omega_a)=\chi^{(3)E}_{1111}[2\mathbf{E}^{(1)}(\mathbf{E}^{(1)}\mathbf{E}^{(2)*})+\mathbf{E}^{(2)*}(\mathbf{E}^{(1)}\mathbf{E}^{(1)})]+$ $+3\,[2\chi^{(3)R}_{1122}\mathbf{E}^{(1)}(\mathbf{E}^{(1)}\mathbf{E}^{(2)*})+\chi^{(3)R}_{1221}\mathbf{E}^{(2)*}(\mathbf{E}^{(1)}\mathbf{E}^{(1)})]$ *), $\Delta=\frac{\omega_1-\omega_2-\Omega}{\Gamma}$	

*The components $\chi^{(3)E}_{ijkl}$ are assumed to obey the Kleinman relationships.

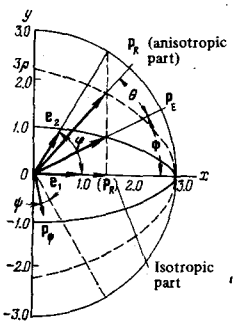

FIG. 10. Mutual arrangement of the polarization unit vectors of the pump waves ($\mathbf{e}_1$, $\mathbf{e}_2$), the resonance ($\mathbf{P}_R$) and non-resonance electronic ($\mathbf{P}_E$) components of the nonlinear source, and the vector $\mathbf{P}_\psi$, which fixes the plane of the oscillations transmitted by the analyzer.

By using the data of Table I together with Eqs. (2.17) and (2.22), we can write the following expression for the nonlinear source at the frequency $\omega_a=2\omega_1-\omega_2$:

$$\frac{\mathbf{P}^{(3)}(\omega_a)}{(E^{(1)})^2E^{(2)*}}=\chi^{(3)E}_{1111}\mathbf{P}_E+\chi^{(3)R}_{1111}\mathbf{P}_R, \tag{3.1}$$

where

$$\mathbf{P}_E=2\mathbf{e}_1(\mathbf{e}_1\mathbf{e}_2^*)+\mathbf{e}_2^*(\mathbf{e}_1\mathbf{e}_1), \tag{3.2}$$

$$\mathbf{P}_R=3(1-\rho)\,\mathbf{e}_1(\mathbf{e}_1\mathbf{e}_2^*)+3\rho\mathbf{e}_2^*(\mathbf{e}_1\mathbf{e}_1), \tag{3.3}$$

while $\mathbf{e}_1$ and $\mathbf{e}_2$ are the polarization unit vectors of the pump waves; they are real in the case of plane-polarized pump waves. Figure 10 shows the mutual arrangement of these vectors in the plane defined by the real unit vectors $\mathbf{e}_1$ and $\mathbf{e}_2$ with collinear propagation of all the waves. The solid line in Fig. 10 shows the geometric locus of the ends of the vector $\mathbf{P}_E$ as the angle φ between the vectors $\mathbf{e}_1$ and $\mathbf{e}_2$ is varied. It is an ellipse with semiaxes of 3 and 1. The polarization state of the coherently scattered wave far from a Raman resonance ($|\omega_1-\omega_2|\neq\Omega$) is determined by the vector $\mathbf{P}_E$. In line with (3.1), the ARS signal in this case is linearly polarized. The angle Φ between $\mathbf{e}_1$ and $\mathbf{P}_E$ is $\Phi=\arctan\times[(1/3)\tan\phi]$.[8)] The projection of the real vector $\mathbf{P}_R$ on the coordinate axes are given by the expressions

$$(\mathbf{P}_R)_x=3\cos\varphi,\quad (\mathbf{P}_R)_y=3\rho\sin\varphi, \tag{3.4}$$

so that

$$|\mathbf{P}_R|^2=9\,[\cos^2\varphi+\rho^2\sin^2\varphi]. \tag{3.5}$$

Again this is the equation of an ellipse; its semiaxes are 3 and 3ρ. It is shown in Fig. 10 by the dotted line for the case of a depolarized Raman line ($\rho=3/4$). When the studied line is fully polarized ($\rho=0$), this ellipse degenerates into a straight line parallel to $\mathbf{e}_1$. The angle θ between the vectors $\mathbf{P}_R$ and $\mathbf{P}_E$ can be determined by the formula

$$\operatorname{tg}(\theta)=\frac{(-1+3\rho)\sin 2\varphi}{(3+\rho)+(3-\rho)\cos 2\varphi}, \tag{3.6}$$

[8)]Whenever the real components of $\chi^{(3)E}_{ijkl}$ are not connected by the Kleinman relationships (2.17), we have

$$\Phi=\operatorname{arctg}\left\{\left[\frac{\chi^{(3)E}_{1221}}{(2\chi^{(3)E}_{1122}+\chi^{(3)E}_{1221})}\right]\operatorname{tg}\varphi\right\}.$$

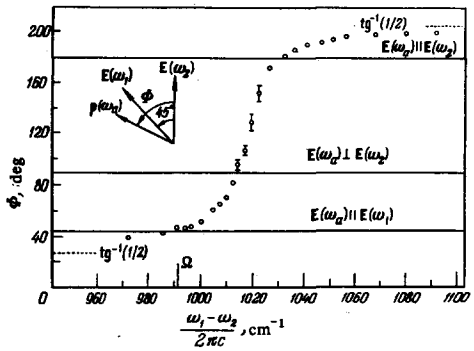

FIG. 11. Rotation of the plane of polarization of the wave of the anti-Stokes component (ω_a) generated in benzene upon scanning the frequency difference $\omega_1-\omega_2$ of the pump waves through the region of the Raman resonance with the totally symmetric vibration of its molecule (angle Φ') ($\Omega/2\pi c = 992$ cm^{-1})[60] (the angle Φ' is denoted by Φ in the diagram).

Here we have adopted the angle θ as positive when the vector $\mathbf{P}_E$ is rotated in a direction counterclockwise to $\mathbf{P}_R$. We can easily see that the angle θ is at a maximum when $\varphi=\varphi_m$, where

$$\cos 2\varphi_m = -\frac{3-\rho}{3+\rho}. \tag{3.7}$$

In particular, when $\rho=3/4$, $\varphi_m=\arccos(\sqrt{5/5})\approx 63°25'$ and $\theta_{max}=\arctan(5/12)\approx 22°40'$.

The values given in Table I of the non-zero components of the tensor $\chi^{(3)}_{ijkl}$ of an isotropic medium are expressed in terms of linear combinations of squares of the invariants of the molecular Raman tensor, and do not contain their cross-products. This indicates that one can resolve the tensor $\chi^{(3)R}_{ijkl}$ into irreducible tensor sets of order 0 (scalar component) and 2 (quadrupole component). One can show this also by direct calculation.[9)][67] Correspondingly, one can resolve the vector $\mathbf{P}^{(3)R}(\omega_a)$ into components that correspond to scalar and quadrupole scattering:[10)]

$$\mathbf{P}^{(3)R}(\omega_a) = [\mathbf{P}_R(\omega_a)]^{[0]} + [\mathbf{P}_R(\omega_a)]^{[2]}, \tag{3.8}$$

where

$$[\mathbf{P}_R(\omega_a)]^{[0]} = b^2\,[3\mathbf{e}_1(\mathbf{e}_1\mathbf{e}_2^*)]\frac{NL^4}{24M\Omega\Gamma}\frac{(E^{(1)})^2E^{(3)*}}{-i-\Delta}, \tag{3.9}$$

$$[\mathbf{P}_R(\omega_a)]^{[2]} = \frac{4g^2}{45}\left[\frac{3}{4}\mathbf{e}_1(\mathbf{e}_1\mathbf{e}_2^*)+\frac{9}{4}\mathbf{e}_2^*(\mathbf{e}_1\mathbf{e}_1)\right]\frac{NL^4(E^{(1)})^2E^{(3)*}}{24M\Omega\Gamma(-i-\Delta)}. \tag{3.10}$$

We see from (3.9) that the polarization of the scalar (isotropic) component of the nonlinear source $\mathbf{P}^{(3)R}(\omega_a)$ coincides in direction with $\mathbf{e}_1$, while the polarization of the quadrupole (anisotropic) component of $\mathbf{P}^{(3)R}(\omega_a)$ in the diagram of Fig. 10 is parallel to the vector $\mathbf{P}_R(\rho=3/4)$.

When $\omega_1-\omega_2\approx\Omega$, the polarization vector of the source $\mathbf{P}^{(3)}(\omega_a)$ has an appreciable imaginary component. Correspondingly, the scattered radiation is elliptically polarized. However, when $|\chi^{(3)R}|\gg\chi^{(3)E}$, the ellipticity will be insignificant practically throughout the entire dispersion region. Thus one can always distinguish a direction of preferential polarization (see Sec. 3c). Since the vectors $\mathbf{P}_E$ and $\mathbf{P}_R$ are generally noncollinear when $\mathbf{e}_1$ and $\mathbf{e}_2$ are noncollinear, the plane of polarization of the scattered wave will suffer dispersion as $\omega_1-\omega_2$ is scanned through a resonance region. The dispersion will become more appreciable the more the ratio $\max|\chi^{(3)R}|/\chi^{(3)E}$ differs from unity. Figure 11 shows the experimental relationship of the angle Φ' between $\mathbf{P}^{(3)}$ and $\mathbf{e}_2$ for the coherent anti-Stokes ARS signal of benzene upon scanning $\omega_1-\omega_2$ near the intense Raman line at 992 cm^{-1}.[60] The angle between the vectors $\mathbf{e}_1$ and $\mathbf{e}_2$ is $\pi/4$.

b) Isotropic media: removal of the nondispersing pedestal in spectra obtained in ARS. As we have stated in Sec. 1, the existence of a relatively high pedestal caused by coherent non-resonance processes in the dispersion curves of $|\chi^{(3)}(\omega_a;\omega_1,\omega_1,-\omega_2)|^2$ is the major factor that impedes application of ARS for resolving weak scattering lines of the first, and especially of higher orders, as well as for analyzing mixtures of molecules.

The dispersion of the plane of polarization of the anti-Stokes signal permits one to suppress strongly the coherent background by detecting specially polarized components of the scattered radiation. For media that are characterized by not too strong an optical Kerr effect in two-photon absorption, this method is apparently the most universal of all the known methods for removing the nondispersing pedestal of "active" spectra (see also Secs. 3*d* and 4*b*).

One achieves this effect by using linearly polarized pump rays whose planes of polarization are rotated with respect to one another by the particular angle φ (see Fig. 10). One introduces an analyzer into the coherently scattered anti-Stokes ray. Then let $\mathbf{P}_\psi$ be the unit vector that fixes the plane of the vibrations that it transmits, the angle ψ being measured from the normal to the vector $\mathbf{P}_E$. The projection of the polarization vector of the nonlinear source of (3.1) on the plane of the vibrations that is given by the vector $\mathbf{P}_\psi$ has the form

---

9)In calculating the angular dependence of the anti-Stokes signal that arises from the quadrupole part of the tensor $\chi^{(3)R}_{ijkl}$, the authors of Ref. 67 have apparently erred; cf. Eq. (3.10) of this paper.

10)Whenever the Raman-scattering tensor is asymmetric, one must add the term $[\mathbf{P}_R(\omega)_a]^{[1]}$ to the resolution of (3.8). This term corresponds to antisymmetric (magnetic-dipole) scattering. By using the table of nonlinear coupling coefficients of four-wave interaction for an isotropic medium from Ref. 36, p. 1313, one can show that the expression for $[\mathbf{P}_R(\omega_a)]^{[1]}$ in terms of the invariant of the antisymmetric part of the Raman-scattering tensor

$$g_a^2 = -\frac{1}{4}\mathrm{Sp}\left[\left(\frac{\partial\alpha_{ik}}{\partial Q}\right)_0-\left(\frac{\partial\alpha_{ki}}{\partial Q}\right)_0\right]^2 = \frac{1}{2}\left\{\left[\left(\frac{\partial\alpha_{12}}{\partial Q}\right)_0-\left(\frac{\partial\alpha_{21}}{\partial Q}\right)_0\right]^2+\left[\left(\frac{\partial\alpha_{13}}{\partial Q}\right)_0-\left(\frac{\partial\alpha_{31}}{\partial Q}\right)_0\right]^2+\left[\left(\frac{\partial\alpha_{23}}{\partial Q}\right)_0-\left(\frac{\partial\alpha_{32}}{\partial Q}\right)_0\right]^2\right\} \tag{3.11}$$

has the following form:

$$[\mathbf{P}_R(\omega_a)]^{[1]} = \frac{g_a^2}{2}\{\mathbf{e}_1(\mathbf{e}_1\mathbf{e}_2^*)-\mathbf{e}_2^*(\mathbf{e}_1\mathbf{e}_1)\}\frac{NL^4(E^{(1)})^2E^{(3)*}}{24M\Omega\Gamma}. \tag{3.11a}$$

Thus the vector $[\mathbf{P}_R(\omega_a)]^{[1]}$ is perpendicular to the vector $\mathbf{e}_1$.

$$\frac{\mathbf{P}^{(3)}(\omega_a)\,\mathbf{P}_\psi}{(E^{(1)})^2 E^{(2)*}} = \chi_{1111}^{(3)E}\sin\psi\sqrt{8\cos^2\varphi+1} + \frac{3\chi_{1111}^{(3)R}}{2\sqrt{8\cos^2\varphi+1}} \times\{(1-3\rho)\sin 2\varphi\cos\psi + [(3+\rho)+(3-\rho)\cos 2\varphi]\sin\psi\}. \quad (3.12)$$

Equation (3.12) implies that the component arising from the component $\mathbf{P}_E$ of the nonlinear source $\mathbf{P}^{(3)}(\omega_a)$ is lacking in the anti-Stokes radiation transmitted by the analyzer at $\psi=0$. Here we find

$$\frac{\mathbf{P}^{(3)}(\omega_a)\,\mathbf{P}_{\psi=0}}{(E^{(1)})^2 E^{(2)*}} = \frac{3\sin 2\varphi}{\sqrt{8\cos^2\varphi+1}}[\chi_{1122}^{(3)R}(\omega_a;\omega_1,\omega_1,-\omega_2) - \chi_{1221}^{(3)R}(\omega_a;\omega_1,\omega_1,-\omega_2)]. \quad (3.13)$$

(We recall that the relationship between the components of the tensor $\hat{\chi}^{(3)}$ and the degree of depolarization ρ is given in Table I.)

We can easily convince ourselves that the modulus of the projection is a maximum for $\varphi=\pi/3$: in this case we have

$$\max\left|\frac{\mathbf{P}^{(3)}(\omega_a)\,\mathbf{P}_{\psi=0}}{(E^{(1)})^2 E^{(2)*}}\right| = \frac{3}{2}\left|\chi_{1122}^{(3)R} - \chi_{1221}^{(3)R}\right| = \frac{NL^4}{16M\Omega\Gamma}\left|\frac{(1/2)\,b^2-(1/18)\,g^2}{-i-\Delta}\right|. \quad (3.14)$$

Both polarized ($g^2=0$) and depolarized ($b^2=0$) Raman lines will be represented in spectra obtained by the described method. However, the lines whose degree of depolarization is $\rho=1/3$ will be missing.

The processes that interfere with complete removal of the nondispersing pedestal of ARS spectra prove to be those that depolarize the pump waves and the scattered component. They include, first, the optical Kerr effect, which causes the field at the frequency ω_2 to induce birefringence at the frequency ω_1 and vice versa; second, stresses in the windows of the cuvettes containing the studied liquid or gas; and third, two-photon absorption of one of the pump waves (or both together), which gives rise to an imaginary component of $\chi_{ijkl}^{(3)R}$, etc.

One can get a picture of the efficiency of the described method of suppressing the coherent "background" from Figs. 12, 13, and 6, which are taken from Ref. 66. Just like the dispersion curves of $|\chi_{1111}^{(3)}|^2$ that are given for comparison, all the dispersion curves of $|\chi_{1122}^{(3)}-\chi_{1221}^{(3)}|^2$ are normalized to their values on the wings, far from the Raman resonance. We should bear it in mind that the level of the non-dispersing ARS signal on the wings of the $|\chi_{1122}^{(3)}-\chi_{1221}^{(3)}|^2$ curves is 10^3–10^4 times lower than the signal level on the wings of the corresponding $|\chi_{1111}^{(3)}|^2$ curves, other conditions being the same. The incomplete "subtraction" of the coherent background involves the partial depolarization of the radiation, which is apparently caused by the optical Kerr effect.

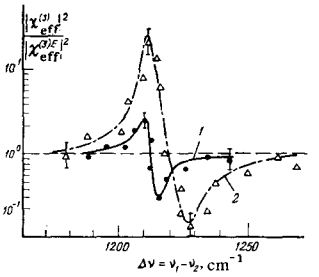

FIG. 12. Dispersion curves of $|\chi_{1111}^{(3)}(\omega_a)|^2$ and $|\chi_{1122}^{(3)}-\chi_{1221}^{(3)}|^2$ of toluene (1 and 2, respectively) in the region of the Raman resonance with the A_1 vibration at $\nu_{A_1}=1209$ cm^{-1}.

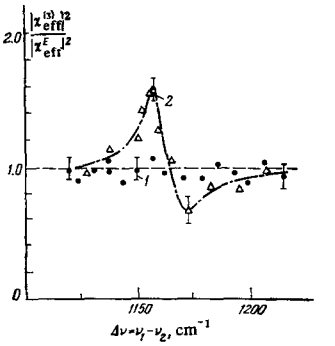

FIG. 13. Dispersion curves of $|\chi_{1111}^{(3)}(\omega_a;\omega_1,\omega_1,-\omega_2)|^2$ and $|\chi_{1122}^{(3)}(\omega_a)-\chi_{1221}^{(3)}(\omega_a)|^2$ (1 and 2, respectively) of mesitylene (1, 3, 5-trimethylbenzene) in the region of the Raman resonance with the weak line of symmetry E_g ($\nu_{E_g}=1164$ cm^{-1}). [66]

The Raman resonance at $\nu=1164$ cm^{-1} in mesitylene is characterized by a small spontaneous Raman cross section that differs by a factor of more than 100 from the cross section of the totally symmetric Raman line at $\nu=999$ cm^{-1}.[73] The former is not visible in the $|\chi_{1111}^{(3)}|^2$ spectrum, and it becomes noticeable only upon applying a polarization technique, i.e., in the $|\chi_{1111}^{(3)}-\chi_{1221}^{(3)}|^2$ spectrum (see Fig. 13).

Finally we shall point out an interesting possibility of shaping the contour of an ARS signal by choosing the angle ψ that defines the orientation of an analyzer introduced into the coherently scattered anti-Stokes ray.

We can easily convince ourselves that when $0\leq\psi\leq|\theta|$ (θ is defined in (3.6)), the sign of the ratio of the resonance and non-resonance terms in (3.12) is opposite to the sign of this ratio at ψ values lying outside the stated interval. In the spectrum, this situation is manifested in the fact that the minima in the relationship of the intensity of the anti-Stokes signal to the frequency mismatch $\omega_1-\omega_2$ lie on opposite sides of the maximum in these two cases. In particular, this situation can be used to resolve partially overlapping lines of different symmetry.[11)]

When one uses in ARS a scheme with nondegenerate frequencies, $\omega_a=\omega+\omega_1-\omega_2$, one can remove the pedestal of the "active" spectrum by adopting orthogonal polarization of the waves ω and ω_1; here the polarization vector $\mathbf{e}_2$ of the wave ω_2 must form an angle of ~45° with each of the vectors $\mathbf{e}$ and $\mathbf{e}_1$.[71] In this scheme one can compensate not only the real part of the nondispersing component of the nonlinear source, but also the imaginary part that arises from the resonance electronic transitions. In order to do this, one must use elliptically po-

[11)] We have used this situation for resolving the nonuniformly broadened Raman band $\Omega/2\pi c\approx 1305$ cm^{-1} in nitric acid.[203] We note in general that the stated method allows one to resolve by the ARS technique lines of differing symmetry, however closely spaced.

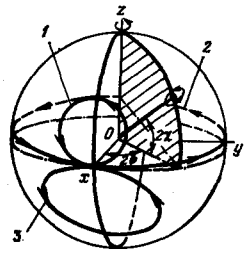

FIG. 14. A picture using the Poincare sphere of the polarization state of the "active" signal upon scanning $\omega_1 - \omega_2$ through the region of an isolated Raman resonance. 1—$\alpha \sin\theta = 0.3$; 2—$\alpha \sin\theta = 10$; 3—$\alpha \sin\theta = -0.45$.

larized beams with specially chosen orientations and eccentricities of the ellipse. However, we shall not account for the effects involving the imaginary component of $\chi^{(3)E}$ in the treatment below, apart from Secs. 4*a* and *b*, while assuming it to be zero.

c) Determination of the polarization ellipse of coherently scattered radiation (coherent ellipsometry of Raman scattering). We have already noted in Sec. 3*a* that the ARS signal generally becomes elliptically polarized when one tunes the frequency difference of the linearly polarized pumping waves to a Raman-active resonance. This requires that the polarization vectors of the pump waves should be noncollinear. Here we wish to call attention to the fact that accurate measurement of the dispersion of the polarization parameters of the coherently scattered radiation upon tuning $\omega_1 - \omega_2$ can substantially supplement the measurement of the dispersion of its intensity. This situation, which has no analog in spontaneous Raman scattering, is of great practical interest besides its purely theoretical interest: since the intensity of the ARS signal is a nonlinear function of the intensity of the pump waves (see (1.15)), it fluctuates strongly even when the pump intensity fluctuations are relatively small. This restricts considerably the accuracy of measurement of the contour of the dispersion curve of $|\chi^{(3)}|^2$. On the other hand, the fluctuations in the polarization of the coherently scattered ARS signal, which are determined only by the polarization fluctuations of the pump waves, can be made as small as one wishes, since the polarization can be reliably controlled. Moreover, the existing methods of ellipsometry are distinguished by extremely high accuracy. Therefore the possibility of measuring the parameters of the Raman lines by ellipsometry at the high level of the detected signal that is characteristic of ARS is highly attractive.

It is convenient to analyze the polarization state of monochromatic waves by using the so-called Poincaré sphere[65] (see Fig. 14). Each wave having an elliptical polarization given by the orientation angle ψ of the long axis of the ellipse and a degree of ellipticity $\chi = \pm \arctan(b/a)$ (b and a are respectively the minor and major semiaxes of the polarization ellipse) is matched with a point on the Poincaré sphere having the coordinates 2ψ and 2χ; values $\chi > 0$ are ascribed to an ellipse having rotation to the right, and $\chi < 0$ to an ellipse with rotation to the left.

If we locate the origin of the spherical coordinates ($2\psi = 0$, $2\chi = 0$) at a point corresponding to the orientation of the polarization vector $\mathbf{P}_E$ of the nondispersing component of the nonlinear source (see Sec. 3*a*), then the polarization ellipse of the anti-Stokes ARS signal near an isolated Raman resonance can be given by the equations

$$\sin 2\chi = \frac{2\alpha \sin\theta}{\Delta^2 - 2\Delta\alpha\cos\theta + 1 + \alpha^2}, \tag{3.15}$$

$$\operatorname{tg} 2\psi = 2\alpha \sin\theta \frac{\alpha\cos\theta - \Delta}{\Delta^2 - 2\Delta\alpha\cos\theta + 1 + \alpha^2\cos^2 2\zeta}, \tag{3.16}$$

here we have $\alpha = |\bar{\chi}^{(3)R}_{1111}/\chi^{(3)E}_{1111}|\,|\mathbf{P}_R|/|\mathbf{P}_E|$; the angle θ is defined by (3.6); $\Delta = (\omega_1 - \omega_2 - \Omega)/\Gamma$, $\chi^{(3)R}_{1111} = \chi^{(3)R}_{1111}(\Delta = 0)$.

If we eliminate from (3.15) and (3.16) the parameter Δ and transform the system of spherical coordinates by rotation about the axis by the angle $\gamma = (\pi/2) - \chi_{max}$, where

$$\sin 2\chi_{max} = \frac{2\alpha \sin\theta}{1 + \alpha^2 \sin^2\theta}, \tag{3.17}$$

we can easily verify that the relationships (3.15) and (3.16) define a circle on the Poincaré sphere tangent to the "equator," which has its center at a point with the coordinates

$$2\chi = \chi_{max}, \quad 2\psi = 0.$$

In Fig. 14 which illustrates the sphere, the line 1 shows this circle for the case of a relatively weak Raman resonance having $\alpha \sin\theta < 1$; the number 2 indicates the same curve for the case $\alpha \sin\theta \gg 1$.

We note that the location of this curve in the "northern" ($\chi > 0$) or "southern" ($\chi < 0$) hemispheres of the Poincaré sphere arises from the sign of the product $\alpha \sin\theta$; this sign differs for the scalar and quadrupole components of the source $\mathbf{P}^{(3)}$. Correspondingly, the rotation directions of the polarization ellipses of these components are opposite. The abovesaid holds as well with regard to the rotation directions of the polarization ellipses of the anti-Stokes components of the coherent scattering in polarized and completely depolarized Raman lines (see Sec. 3*a*).

Equation (3.17) determines the maximum ellipticity of the ARS signal that can be attained when $\Delta = \alpha\cos\theta$; here $2\psi = 0$ or π. If $\alpha \sin\theta \leqslant 1$, then the maximum rotation angle of the long axis of the ellipse $2\psi_{max}$, which is defined by the relationship

$$\pm \sin 2\psi_{max} = \alpha \sin\theta, \tag{3.18}$$

is attained when $\Delta = \alpha\cos\theta \pm \sqrt{1 - \alpha^2 \sin^2\theta}$. When $\alpha \sin\theta > 1$, the long semiaxis of the ellipse performs a complete revolution.

Figure 15 shows for illustration an experimental curve[196] that shows the course of the dispersion of the ellipticity parameters of the anti-Stokes ARS signal in concentrated nitric acid in the region of the broad Raman line at the frequency $\Omega/2\pi c = 1304\ \text{cm}^{-1}$.

d) Crystals: measurement of the tensor components. In contrast to gases and liquids, where the intensities

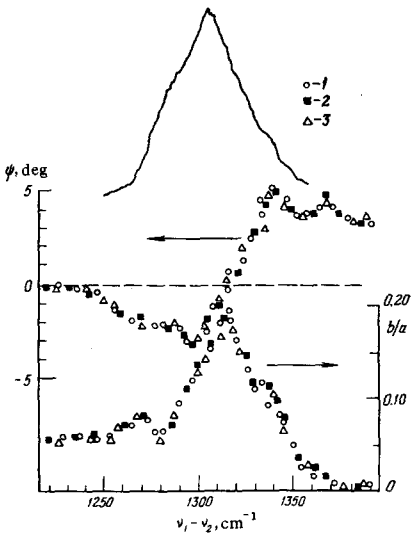

FIG. 15. Dispersion of the elliptical-polarization parameters of the ARS signal of concentrated HNO_3. The symbols 1–3 denote the experimental points obtained in different series of measurements. One can clearly see the fine structure of the line, which is not manifested in the spontaneous Raman spectrum (upper curve). The integral parameters of this Raman line determined from the coherent polarization spectra are: $\rho = 0.08$, $\overline{\chi}^{(3)R}_{1111}/\chi^{(3)E}_{1111} = 0.32$, $2\Gamma/2\pi c = 57$ cm^{-1}.

of the Raman lines depend on the invariants of the scattering tensor, the intensity of the scattered light for crystals depends directly on the components of the Raman-scattering tensor. Correspondingly, the components of the tensor $\chi^{(3)R}_{ijkl}$ also depend on the components of the Raman tensor.

In this case we must omit the angle brackets in Eq. (2.15) that denote averaging over the orientations.

It is expedient to choose a laboratory coordinate system that is associated with the crystal and reflects its symmetry.[75] Whenever vibrations that contribute to $\chi^{(3)R}$ are degenerate and the Raman tensor is correspondingly split, one adds to the right-hand side of (2.15) terms of analogous structure that correspond to each component of the split Raman-scattering tensor.

The classification of Raman-active vibrations and the form of the corresponding Raman tensors for crystals of all classes are well known (see, e.g., Ref. 76). As an example, Table II gives expressions for the nonlinear coupling coefficients for four-photon interactions of different types in a crystal belonging to the point-group symmetry $\bar{3}m$ (calcite):

$$\lambda_{R,\,E} = \sum_{ijkl} \chi^{(3)R,\,E}_{ijkl} e_i^{(a)} e_j e_k^{(1)} e_l^{(2)};$$

Here $e_i^{(a)}$, e_j, etc. are the Cartesian components of the polarization unit vectors of the interacting waves.

The explicit form of the Raman tensors for the totally symmetric A_{1g} vibrations is as follows:

$$\left(\frac{\partial\alpha_{ij}}{\partial Q}\right)_{A_{1g}} = \begin{pmatrix} a & 0 & 0 \\ 0 & a & 0 \\ 0 & 0 & b \end{pmatrix};$$

For the doubly degenerate E_g vibrations we have:

$$\left(\frac{\partial\alpha_{ij}}{\partial Q}\right)'_{E_g} = \begin{pmatrix} 0 & -c & -d \\ -c & 0 & 0 \\ -d & 0 & 0 \end{pmatrix}, \quad \left(\frac{\partial\alpha_{ij}}{\partial Q}\right)''_{E_g} = \begin{pmatrix} c & 0 & 0 \\ 0 & -c & d \\ 0 & d & 0 \end{pmatrix}.$$

The polarization of the interacting rays can correspond to either the ordinary (o) or the extraordinary (e) waves; θ and φ are the polar angle and the azimuth that fix the direction of the collinear wave vectors. The values of the non-zero components of the tensor $\chi^{(3)E}_{ijkl}$ are taken from Ref. 77. We see from Table II that one can measure the different components of the Raman tensor by a suitable choice of polarizations of the interacting waves by comparing $\chi^{(3)R}_{ijkl}$ with the values of the corresponding components of the tensor for the electronic cubic susceptibility $\chi^{(3)E}_{ijkl}$.[36,38] The values and signs of several components of χ^{E}_{ijkl} have been accurately measured in the calcite crystal.[173] Together with the use of the ARS data for the relative values of λ_R/λ_E,[36,38] this permits one to estimate the values and signs of the corresponding components of the Raman-scattering tensors (see Table III).

e) Raman spectra obtained by using the optical Kerr effect. One can obtain the dispersion curves of $|\chi^{(3)}|^2$ in a Raman-resonance region not only from the coherent-scattering spectra, but also by measuring the polarization state of radiation transmitted through an optically excited medium without change of frequency. This phenomenon has been called the optical Kerr effect induced by a Raman resonance (Raman-induced Kerr effect).[72]

TABLE II. Form of the nonlinear coupling coefficients of a four-wave process in crystals of the class $\bar{3}m$.

Form of the nonlinear coupling coefficient \ Polarization of the interacting waves	$o_1o_2o \to o_a$	$o_1o_2o \to e_a$ $o_1o_2e \to o_a$
Totally symmetric vibrations A_{1g}, $\lambda_R / \frac{NL^4}{48M\Omega\Gamma}$	a^2	0
Doubly degenerate vibrations E_g, $\lambda_R / \frac{NL^4}{48M\Omega\Gamma}$	c^2	$cd \sin\theta \cos 3\varphi$
λ_E	$\chi^{(3)R}_{1111}$	$\chi^{(3)E}_{1123} \sin\theta \cos 3\varphi$
Form of the nonlinear coupling coefficient \ Polarization of the interacting waves	$o_1o_2e \to e_a$ $e_1e_2o \to o_a$	$e_1e_2o \to e_a$ $e_1e_2e \to o_a$
Totally symmetric vibrations A_{1g}, $\lambda_R / \frac{NL^4}{48M\Omega\Gamma}$	$a^2 \cos^2\theta + ab \sin^2\theta$	0
Doubly degenerate vibrations E_g, $\lambda_R / \frac{NL^4}{48M\Omega\Gamma}$	$-c^2 \cos^2\theta + cd \sin 2\theta \sin 3\varphi$	$-3\,cd \sin\theta \times \cos^2\theta \cos 3\varphi$
λ_E	$\chi^{(3)E}_{1122} \cos^2\theta + \chi^{(3)E}_{1133} \sin^2\theta + \chi^{(3)E}_{1123} \sin 2\theta \sin 3\varphi$	$-3\chi^{(3)E}_{1123} \sin\theta \times \cos^2\theta \cos 3\varphi$

TABLE III. Experimental values of some components of the Raman susceptibility tensor of calcite measured by ARS from the known values from other experiments of the tensor $\chi^{(3)E}_{ijkl}$.

Type of normal vibration, its frequency	$o_1o_2e \to e_a$, λ_R/λ_E	$o_1o_2e \to o_a$, λ_R/λ_E	$\chi^{(3)R}_{1122}$ *), 10^{-14} cm^3/erg	$\chi^{(3)R}_{1123}$ **), 10^{-15} cm^3/erg	c/d for the E_g lines
E_g, 712 cm^{-1}	−0.5	+1.5	−0.2	−0.9	2.2
A_{1g}, 1086 cm^{-1}	36	−0.2	13.1	+0.12	—
E_g, 1436 cm^{-1}	$\leqslant 0.1$	+0.8	$\leqslant 0.04$	−0.72	$\leqslant 0.5$

*) $\chi^{(3)E}_{1122} = 0.25 \cdot 10^{-14}$ cm^3/erg, $\chi^{(3)E}_{1133} = 0.5 \cdot 10^{-14}$ cm^3/erg.[173]
**) $\chi^{(3)E}_{1123} = -0.4 \cdot 10^{-15}$ cm^3/erg.[173]

In order to observe the effect, one directs into the medium two rays of frequencies ω_1 and ω_2, whose difference can be scanned about the frequency Ω of a Raman-active molecular vibration. One records the polarization state of the weak probe wave at the frequency ω_1, which is perturbed by the nonlinear source.

$$P_i^{(3)}(\omega_1) = 6\chi^{(3)}_{ijkl}(\omega_1; \omega_2, \omega_1, -\omega_2) E_j^{(2)} E_k^{(1)} E_l^{(2)*}. \qquad (3.19)$$

This nonlinear increment undergoes a resonance-type variation when $|\omega_1 - \omega_2| \approx \Omega$. Owing to the anisotropy of the increment, this alters the polarization state of the wave at the frequency ω_1, as can be detected by placing an analyzer at output from the medium that is crossed with the plane of polarization of the unperturbed probe ray.

The frequency-dependence of the intensity of the signal at the output of the analyzer as a function of $\omega_1 - \omega_2$ coincides with the dispersion curve of $|\chi^{(3)}(\omega_1; \omega_2, \omega_1, -\omega_2)|^2$, and it reflects the Raman spectrum of the medium.

The resonance behavior of the nonlinear susceptibility $\chi^{(3)}(\omega_1; \omega_2, \omega_1, -\omega_2)$ has the same nature as that of the susceptibility $\chi^{(3)}(\omega_a; \omega, \omega_1, -\omega_2)$ that we have been treating thus far, as $\omega_1 - \omega_2$ is scanned about Raman resonances. The analogy becomes complete if we take $\omega = \omega_2$ as one of the frequency arguments of the latter susceptibility. Hence we can cast the expression (3.19) for the nonlinear source in an isotropic medium (gas or liquid) into the form of (2.6).

An important merit of the described system of measuring the dispersion of the quantities $|\chi^{(3)}|^2$ is that one need not take special measures for ensuring phase synchronization (the condition $\mathbf{k}_1 = \mathbf{k}_1 + \mathbf{k}_2 - \mathbf{k}_2$ is satisfied identically). Therefore the direction of propagation of the probe radiation with respect to the pump radiation can be arbitrary, e.g., opposite to it.

Like any other four-wave parametric process, the effect has no intensity threshold. In order to observe it with a good signal/noise ratio, one must use focused beams from pulsed Q-switched lasers. Here the required intensities still prove to be considerably below the thresholds for stimulated Raman scattering and self-focusing.

Here, just as in coherent ARS, one can use as the probe ray either monochromatic radiation or broad-band "noise" radiation (see Sec. 6*c* and Fig. 16).

Use of circularly polarized pump radiation allows one to eliminate the "background" transmission of the analyzer caused by the ordinary optical Kerr effect, including also the electronic nonlinearity.[72, 79]

Beyond the analyzer, which is crossed with the plane of polarization of the probe ray, the intensity $I^{(1)}$ of the signal at the frequency ω_1 as a function of the frequency difference is given here by the expression

$$I^{(1)}(\omega_1 - \omega_2) \sim \frac{|E^{(2)}|^2}{4} |\chi^{(3)}_{1122}(\omega_1; \omega_2, -\omega_2, \omega_1) - \chi^{(3)}_{1212}(\omega_1; \omega_2, -\omega_2, \omega_2)|^2. \qquad (3.20)$$

Figure 16 shows the experimental system of R. Hellwarth *et al.*[72] for observing the optical Kerr effect induced by a Raman resonance, while Fig. 17 shows specimens of spectra obtained by using it.

The use of the described system for measuring the parameters of Raman resonances of isotropic media can be especially fruitful in cases when the linear dispersion of the medium interferes with obtaining appreciable coherence lengths $l_{coh} = \pi/\Delta k$ in an ordinary ARS system, e.g., in a plasma (see Sec. 8*d*). We should include among the defects of this system the rather high level of the incoherent background (arising mainly from stray light at the frequency of the detected signal ω_1) and the need of working with a pump beam that is strictly circularly polarized. Otherwise the "background" transmission of the analyzer arising from the ordinary optical Kerr effect can yield too high a pedestal that masks the dispersion of the Raman component of the nonlinear susceptibility. The latter situation restricts the combinations of the components of the tensor χ^R_{ijkl} accessible to measurement by this method to a single one (see (3.20)). This technique has been recently used to study Raman-active modes in crystals.[201]

f) Phase active spectroscopy. The optical Kerr effect induced by a Raman resonance closely borders on the effect discovered by Owyoung of focusing and defocusing of a weak probe ray (of frequency ω_1) in the presence of an intense pump (frequency ω_2) upon tuning the difference $\omega_1 - \omega_2$ at the frequency Ω of a Raman-active molecular vibration.[80] Here the pump induces a change in the refractive index at the frequency ω_1 caused by the nonlinear polarization of (3.19)[81]:

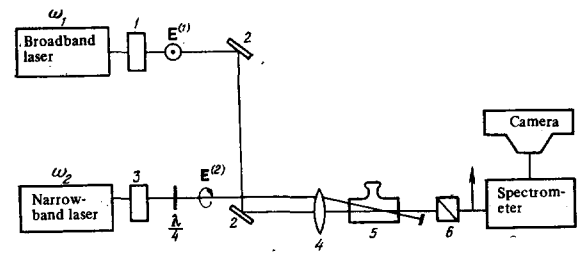

FIG. 16. Diagram of the experiment of Hellwarth *et al.*[72] to observe the Kerr effect induced by a Raman resonance. 1, 3—polarizers, 2—mirrors, $\lambda/4$—quarter-wave plate, 4—lens, 5—cuvette containing the studied liquid, 6—analyzer crossed with the polarizer 1.

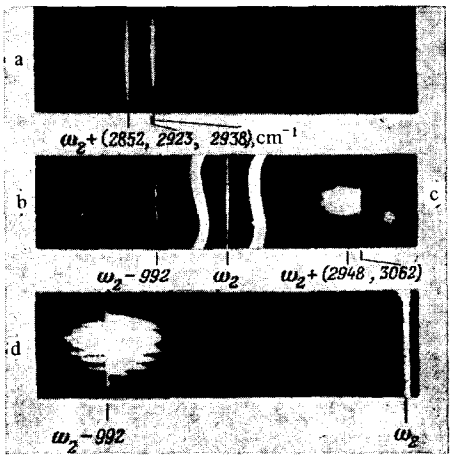

FIG. 17. Spectrograms obtained by using the Kerr effect induced by a Raman resonance. a) Cyclohexane (the analyzer is completely crossed with the plane of polarization of the probe ray); b, c) benzene (spectrograms in the Stokes and anti-Stokes regions, respectively); d) spectrogram in the case in which the analyzer is not completely crossed with the plane of polarization of the probe ray (Stokes region, benzene).

$$n(\omega_1) = n_0 + n_2 |E^{(2)}|^2, \tag{3.21}$$

where

$$n_2 = \frac{4\pi}{n_0} \operatorname{Re} \chi^{(3)}_{1111}(\omega_1; \omega_2, -\omega_2, \omega_1),$$

and n_0 is the unperturbed value of the refractive index.

The value and the sign of the nonlinear increment to the refractive index of (3.20) are functions of $\omega_1 - \omega_2$ when this difference is tuned about Ω. Estimates[80] show that in benzene n_2 varies from the value $n_2' = 4.32 \times 10^{-12}$ cgs esu for $(\omega_1 - \omega_2 - \Omega)/2\pi c = -1.9$ cm^{-1} to the value $n_2'' = -0.81 \times 10^{-12}$ cgs esu at $(\omega_1 - \omega_2 - \Omega)/2\pi c = +1.9$ cm^{-1} ($\Omega/2\pi c = 992$ cm^{-1} is the frequency of the most intense Raman line).

The nonlinear increment to the refractive index n (at ω_1) can be measured either from the change in divergence of the probe beam, (according to (3.21), the pump beam induces a focusing or defocusing lens), or interferometrically.

An experiment[80] performed in a 10-cm cuvette containing benzene using the fundamental radiation of a ruby laser as the pump and the radiation of a tunable dye laser as the probe ray has shown a change in the divergence of the latter beam of more than 30% upon scanning $\omega_1 - \omega_2$ by 3.8 cm^{-1} in the resonance region. Here the amplification of the probe ray caused by stimulated Raman scattering was kept at a moderate level (less than $e^{2.7}$ at the center of the line).

Use of a classical two-beam interferometer (of the Jamin type) to measure the nonlinear increment to the refractive index of (3.12) allows one to make an absolute calibration of $\chi^{(3)}_{1111}$ from the reliably measured value of the Kerr constant in a low-frequency electric field.[82,197] It has been possible by this method, which is one of the most exact methods for absolute measurement of the nonlinear optical susceptibility, to measure $\chi^{(3)}_{1111}$ of benzene and CS_2 with an accuracy better than 20%.

4. Interference phenomena in active spectroscopy

The shape of the spectra that are obtained in coherent ARS substantially differs from that of spontaneous Raman spectra. As was shown in Sec. 1, this difference is explained in the language of nonlinear susceptibilities by the fact that one measures the dispersion of

$$|\chi^{(3)}(\omega_1 - \omega_2)|^2 = [\operatorname{Re}\chi^{(3)}(\omega_1 - \omega_2)]^2 + [\operatorname{Im}\chi^{(3)}(\omega_1 - \omega_2)]^2,$$

upon scanning $\omega_1 - \omega_2$ in coherent ARS, whereas one measures the spectrum of $\operatorname{Im}\chi^{(3)}(\omega_1 - \omega_2)$ in spontaneous Raman scattering.

In line with (2.15) and Table I, the structure of $\chi^{(3)}$ near an isolated Raman resonance of frequency Ω has the shape

$$\chi^{(3)}(\omega_a; \omega, \omega_1, -\omega_2) = \chi^{(3)E} + \frac{\bar{\chi}^{(3)R}}{-i - \Delta}, \tag{4.1}$$

where, e.g.,

$$\bar{\chi}^{(3)R}_{1111} = \frac{NL^4}{24M\Omega\Gamma}\left(b^2 + \frac{4}{45}g^2\right), \quad \Delta = \frac{\omega_1 - \omega_2 - \Omega}{\Gamma}.$$

It is convenient to analyze the interference effects in ARS by using a geometric representation of the cubic susceptibility $\chi^{(3)} = \operatorname{Re}\chi^{(3)} + i\operatorname{Im}\chi^{(3)}$ in the complex plane.[41,84,204]

Figure 18 shows separately the contributions that correspond to the different terms in (4.1). The case in which $\operatorname{Im}\chi^{(3)E} = 0$ corresponds to the solid curve. As Δ is scanned from $-\infty$ to $+\infty$, the complex vector $\chi^{(3)}$ describes the circle drawn as the solid line. One can easily show that

$$|\chi^{(3)}_{\max}| \, |\chi^{(3)}_{\min}| = (\bar{\chi}^{(3)E})^2. \tag{4.2}$$

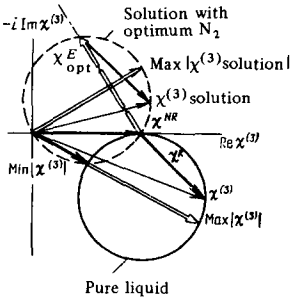

FIG. 18. Representation of the cubic susceptibility of the medium $\chi^{(3)}(\omega_a; \omega_1, \omega_1, -\omega_2) = \chi^{(3)NR} + \chi^{(3)R}$ in the complex plane. As we scan $\omega_1 - \omega_2$ through the region of the Raman resonance, the end of the complex vector $\chi^{(3)}$ of a medium that has a pure real electronic susceptibility $\chi^{(3)NR}$ describes the circle shown by the solid line. When the electronic susceptibility acquires a complex component χ^E, the circle as a whole is translated by this complex vector (dotted circle).[84]

This equation and (4.1) lead to an expression that relates the frequency spacing between the points of maximum and minimum values of $|\chi^{(3)}|$ (ω_{max} and ω_{min}, respectively) to the relative values of the nuclear and electronic contributions $\bar{\chi}^{(3)R}/\chi^{(3)E}$:

$$|\omega_{max}-\omega_{min}|=2\Gamma\sqrt{1+\left(\frac{\bar{\chi}^{(3)R}}{2\chi^{(3)E}}\right)^2}. \quad (4.3)$$

Moreover, measurement of the positions of the points of mutual compensation of the electronic and nuclear contributions allows one to determine the signs of these contributions:

$$\operatorname{sign}\frac{\bar{\chi}^{(3)R}}{\chi^{(3)E}}=\pm\operatorname{sign}(\omega_{min}-\omega_{max}); \quad (4.4)$$

Here the upper sign refers to the case of measuring the anti-Stokes signal ($\omega_a=2\omega_1-\omega_2$), and the lower to the Stokes signal ($\omega_s=2\omega_2-\omega_1$).

The "constant" k of the dispersion curve $|\chi^{(3)}(\omega_a)|^2$, i.e., the ratio of the maximum anti-Stokes signal $I^{(a)}_{max}$ to the minimum $I^{(a)}_{min}$ can be determined by the formula

$$k=\frac{I^{(a)}_{max}}{I^{(a)}_{min}}=\frac{|\chi^{(3)}_{max}|^2}{|\chi^{(3)}_{min}|^2}=\left[\left(\frac{\chi^{(3)R}}{2\chi^{(3)E}}\right)+\sqrt{1+\left(\frac{\bar{\chi}^{(3)R}}{2\chi^{(3)E}}\right)^2}\right]^4. \quad (4.5)$$

a) Measurement of the two-photon absorption cross section by using active spectroscopy. Thus far we have been treating the situation in which the electronic component of the cubic susceptibility $\chi^{(3)E}(\omega_a;\ \omega_1,\ \omega_1,\ -\omega_2)$ has been a purely real quantity. Actually it can also have an imaginary component, e.g., whenever a two-photon electronic resonance occurs: $2\omega_1\approx\Omega_E$, where Ω_E is the frequency of the resonance transition.

As is well known, this situation is manifested in the effect of two-photon absorption (TPA). Its cross-section per unit element of the medium (molecule, unit cell) can be expressed by the following formula[85]:

$$d\sigma^{TPA}_{11}(2\omega_1)=\frac{1}{N}\frac{24\pi\omega_1}{cn_1}\operatorname{Im}\chi^{(3)E}_{1111}(\omega_a;\ \omega_1,\ \omega_1,\ -\omega_2), \quad (4.6)$$

Here N is the density of the elements, and $n_1=n(\omega_1)$ is the refractive index.

The existence of the imaginary part of $\chi^{(3)E}(\omega_a;\ \omega_1,\ \omega_1,\ -\omega_2)$ also affects the form of the spectrum of $|\chi^{(3)}(\omega_a;\ \omega_1,\ \omega_1,\ -\omega_2)|^2$. We can understand the nature of the deformation by turning again to Fig. 18. When $\chi^{(3)E''}=\operatorname{Im}\chi^{(3)E}(\omega_a)\neq 0$, the real axis is no longer tangent to the circle (the geometric locus of the ends of the complex vectors $\chi^{(3)}$) as Δ is scanned (ω_1 is assumed fixed). This circle is shown in Fig. 18 by the dotted line. The relationship (4.2) is altered, and it acquires the form

$$|\chi^{(3)}_{max}||\chi^{(3)}_{min}|=|\chi^{(3)E}|^2\left(1+\frac{\chi^{(3)R''}_0}{|\chi^{(3)E}|}\operatorname{sign}\gamma\right); \quad (4.7)$$

Here $\gamma=\arctan(\chi^{(3)E''}/\chi^{(3)E'})$, and $\chi^{(3)R''}_0=\operatorname{Im}\chi^{(3)R}$ when $\Delta=0$.

The expression for the contrast of the dispersion curve of $|\chi^{(3)}|^2$ is also modified:

$$k=\frac{|\chi^{(3)}_{max}|^2}{|\chi^{(3)}_{min}|^2}=\left(\frac{1+\delta}{1-\delta}\right)^2, \quad (4.8)$$

Here we have

$$\delta=\frac{\bar{\chi}^{(3)R}}{2}\left[\sqrt{\left(\chi^{(3)E''}-\frac{\chi^{(3)R''}_0}{2}\right)^2+(\chi^{(3)E'})^2}\right]^{-1}.$$

When $\gamma\ll 1$, one can use the following formula to determine $\chi^{E''}$:

$$\chi^{(3)E''}\approx\frac{|\chi^{(3)E}|^2-|\chi^{(3)}_{max}||\chi^{(3)}_{min}|}{\bar{\chi}^{(3)R}} \quad (4.9)$$

When $|\chi^{(3)E''}|\ll|\chi^{(3)E'}|$, the part of the dispersion curve $|\chi^{(3)}(\omega_1-\omega_2)|^2$ that is most sensitive to the value of $\chi^{(3)E''}$ is the region near the minimum, since $\operatorname{Re}\chi^{(3)}\approx 0$ in this region. The appearance of an imaginary part of $\chi^{(3)E}$ leads to a frequency shift in the position of the gap in the $|\chi^{(3)}|^2$ curve and makes it shallower (when $\operatorname{sign}\chi^{(3)R''}_0=\operatorname{sign}\chi^{(3)E''}$). Conversely, it becomes deeper when $\operatorname{sign}\chi^{(3)E''}=-\operatorname{sign}\chi^{(3)R''}_0$). One can reverse the sign of $\chi^{(3)E''}/\chi^{(3)R''}_0$ by shifting from measuring the anti-Stokes ARS signal at the frequency $\omega_a=2\omega_1-\omega_2$ to measuring the signal in the Stokes region, $\omega_s=2\omega_2-\omega_1$. Here the sign of $\chi^{(3)E''}$ does not change, while $\chi^{(3)R''}_0$ is multiplied by (-1) because one must keep the term of the type $(\partial\alpha/\partial Q)_0E^{(2)}Q^*$ in the expression (2.9) for the nonlinear source at the frequency $\omega_s=2\omega_2-\omega_1=\omega_2-(\omega_1-\omega_2)$. Then, just as in the expression for $P^{(3)}(\omega_a)$, the analogous term has the form $(\partial\alpha/\partial Q)_0E^{(1)}Q$. This situation permits one to observe in the same given experiment both the "constructive" (deepening the "gap") and "destructive" interference (decreasing the depth of the "gap") of the imaginary parts of the different resonance contrinutions to the total nonlinear susceptibility $\chi^{(3)}$ of the medium.[87]

Measurement of the two-photon absorption parameters from coherent ARS spectra (see also Sec. 4*b*) has a number of advantages over the traditional methods of studying this phenomenon. In particular, here the determination of the TPA cross section does not require exact knowledge of the time and space distribution of the laser radiation that is employed, whereas inaccuracy in determining the latter is the main source of errors in measuring this parameter by direct observation of nonlinear absorption or measurement of luminescence or of the light flux that arises in TPA.[88] The ARS are calibrated absolutely either by the size of the Raman cross section, which can be measured with an accuracy of better than 15%,[89-91] or by the value of $\chi^{(3)E'}$, which is known in a number of cases with an accuracy of 20%.[92]

b) Interference of the complex nonlinear susceptibilities of different molecules. Owing to the coherence of the scattering process in active spectroscopy, the contributions from different molecules of the medium to the intensity of the scattered signal do not add, but interfere. This is expressed in the fact that the macroscopic nonlinear susceptibility of a medium made of different molecules is composed of the nonlinear susceptibilities of each type of molecule:

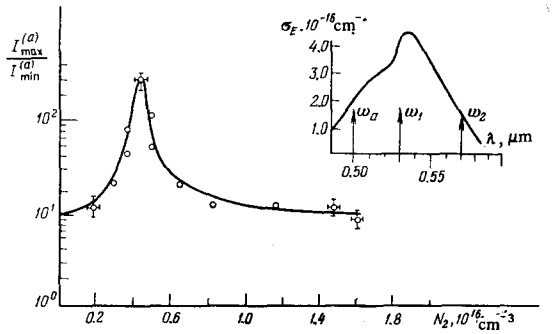

FIG. 19. Experimental relationship of the contrast of the "active" spectrum of toluene $k = I^{(a)}_{max}/I^{(a)}_{min}$ of the Raman line $\nu = 1209$ cm^{-1} to the concentration of rhodamine 6G molecules. The upper right graph shows the contour of the absorption line of the rhodamine 6G molecule in toluene and the mutual arrangement of the pump lines and the coherently scattered anti-Stokes signal. [41]

$$\chi^{(3)}(\omega_a;\ \omega_1,\ \omega_1,\ -\omega_2) = L^4 [N_1 \langle \gamma_1(\omega_a;\ \omega_1,\ \omega_1,\ -\omega_2)\rangle + N_2 \langle \gamma_2(\omega_a;\ \omega_1,\ \omega_1,\ -\omega_2)\rangle + \ldots]; \tag{4.10}$$

Here N_1, N_2, ... are the densities of the molecules possessing the hyperpolarizabilities γ_1, γ_2, ..., respectively; and $L = (\varepsilon + 2)/3$ is the Lorentz correction factor for the internal field. The measurable parameter in ARS is $|\chi^{(3)}|^2$. Therefore the interference of the ARS signals of molecules of different types will be described by cross terms like $2N_1\langle\gamma_1\rangle N_2\langle\gamma_2\rangle$, etc. In particular, the existence in the solution of components that absorb the pump radiation (e.g., the frequency ω_1) deforms the contour of the coherent scattering line of the transparent component of the solution. [41,69] This circumstance can be used, on the one hand, to model the processes that occur in resonance Raman scattering (when the one-photon electronic and Raman resonances are localized in the same molecule), and in particular, to enhance the contrast of the dispersion curves of $|\chi^{(3)}|^2$ in a region of relatively weak scattering lines. On the other hand, it can be used to measure the resonance complex hyperpolarizabilities of the molecules of the absorbing component. [41]

We can represent the cubic susceptibility of a medium made of noninteracting molecules of the stated two types in the following form:

$$\chi^{(3)}_{1111}(\omega_a;\omega_1,\omega_1,-\omega_2) = L^4\left(N_1\langle\bar{\gamma}^{NR}_{1111}\rangle + N_2\langle\bar{\gamma}^{NR}_{1111}\rangle + \frac{N_1\langle\bar{\gamma}^{R}_{1111}\rangle}{-i-\Delta} + N_2\langle\gamma^{E'}_{1111}\rangle + iN_2\langle\gamma^{E''}_{1111}\rangle\right); \tag{4.11}$$

Here N_1 and N_2 are respectively the densities of the Raman-active molecules of the transparent component and of the dye molecules that absorb the pumping radiation; $\langle\bar{\gamma}^{NR}_{1111}\rangle$ and $\langle\bar{\gamma}^{NR}_{1111}\rangle$ are their nonresonance (electronic) polarizabilities; $\langle\bar{\gamma}^{R}_{1111}\rangle = [b^2 + (4/45)g^2]/24M\Omega\Gamma$ (see Table I); and $\langle\gamma^{E'}_{1111}\rangle$ and $\langle\gamma^{E''}_{1111}\rangle$ are the real and imaginary parts of the resonance hyperpolarizability of the molecules of the absorbing component of the solution, which are connected by the Kramers-Kronig relationship. [8]

In order to calculate the contrast of the dispersion curve of $|\chi^{(3)}|^2$ in the region of a Raman resonance ($\Delta \approx 0$), one can use the relationship (4.8), where we must put

$$\bar{\chi}^{(3)R} = L^4 N_1 \langle\bar{\gamma}^{R}_{1111}\rangle, \quad \chi^{(3)E'} = L^4 N_2 \langle\gamma^{E'}_{1111}\rangle, \quad \chi^{(3)E''} = L^4 N_2 \langle\gamma^{E''}_{1111}\rangle.$$

The contrast is maximal when $\delta = 1$ ($k \to \infty$), or equivalently, when the following condition is satisfied:

$$-\bar{\chi}^{(3)R}_{1111}\chi^{(3)E''}_{1111} = (\chi^{(3)E''}_{1111})^2 + (\chi^{(3)E'}_{1111} + \chi^{(3)NR}_{1111})^2, \tag{4.12}$$

where

$$\chi^{(3)NR}_{1111} = L^4 (N_1\langle\gamma^{NR}_{1111}\rangle + N_2\langle\gamma^{NR}_{1111}\rangle).$$

This condition can be satisfied by selecting the concentration N_2 of the dye molecules if $\chi^{(3)R}_{1111}$ and $\chi^{E''}_{1111} \leq 0$. Otherwise the value of k is maximal for maximal δ, which again can be achieved by choice of N_2. Figures 7 and 19 give the results of an experiment to measure the contrast of the dispersion $|\chi^{(3)}|^2$ of toluene near the Raman line at the frequency $\nu = 1209$ cm^{-1} when the dye rhodamine 6G is dissolved in it; this dye absorbs the radiation of the second harmonic of an Nd:YAG laser, while the latter serves as one of the pump waves in ARS. [12] Again we can use Fig. 18 for interpreting these results. Upon scanning ω_2, the end of the complex vector $\chi^{(3)}$ of the pure liquid describes the circle drawn as a solid line. Addition of the dye has the result that the circle is translated as a whole by the complex vector $\chi^{(3)E} = L^4 N_2(\langle\gamma^{E'}\rangle + i\langle\gamma^{E''}\rangle)$ (the length of the translation vector is proportional to N_2). The circle shown by the dotted line corresponds to the optimally chosen dye concentration, so that in this case $k \to \infty$. We can establish by using this diagram and Fig. 19 that, when $N_2 \approx 0.45 \times 10^{16}$ cm^{-3}, $|\chi^{(3)E}_{1111}| = \chi^{(3)NR}_{1111} = 1.5 \times 10^{-14}$ cm^3/erg, [41] so that $\langle\gamma^{E'}_{1111}\rangle + i\langle\gamma^{E''}_{1111}\rangle = (0.3 - i\,0.7) \times 10^{-30}$ cm^6/erg.

Another possibility of enhancing the contrast of coherent scattering spectra is to compensate the nonresonance electronic susceptibility of the Raman-active molecules of a liquid or gas by mixing with it molecules that have a negative real component of $\langle\gamma^{E''}_{1111}\rangle$ when $\langle\gamma^{E''}_{1111}\rangle = 0$. [41]

Whenever both components of the mixture are transparent, while the molecules of each of them have Raman lines at the frequencies Ω_{R1} and Ω_{R2}, respectively, one can observe interference in ARS of their Raman susceptibilities if one uses a scheme with a probe beam. That is, one detects a process that follows the scheme $\omega_a = \omega + \omega_1 - \omega_2$. [93,94]

Interference in the ARS spectrum arises as $\omega_1 - \omega_2$ is tuned to a Raman resonance of the molecules of one component of the solution, $\omega_1 - \omega_2 \approx \Omega_{R1}$, while the difference $\omega - \omega_2$ is tuned to a Raman molecular resonance of the other component, $\omega - \omega_2 \approx \Omega_{R2}$.

---

[12] Recently experiments of this type have been performed under conditions in which both resonances at the frequencies ω_1 and $\omega_1 - \omega_2$ occur in a single molecule. [198-200] Thus the situation is a complete analog of resonance spontaneous scattering in ARS.

The interpretation of the stated experiments to fully analogous with that given above (see also Refs. 70 and 205 and Sec. 8*b* of this chapter).

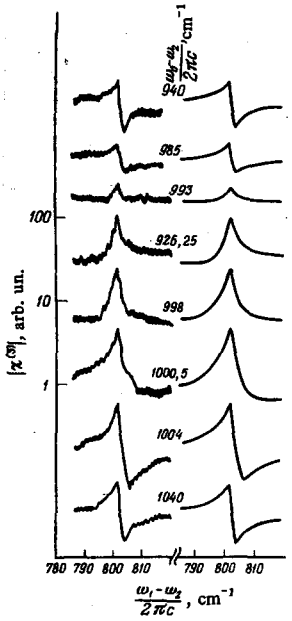

FIG. 20. Experimental results (left) and calculated curves (right) showing the effect of interference of the Raman susceptibilities of the two components of a mixture of benzene with cyclohexane. The variation of $|\chi^{(3)}(\omega_a; \omega_0, \omega_1, -\omega_2)|$ is shown upon scanning $\omega_1-\omega_2$ in the region of the resonance $\nu_{R_1}=802$ cm^{-1} of cyclohexane while $\omega_0-\omega_2$ is tuned about the line $\nu_{R_2}=992$ cm^{-1} of benzene.[93,94]

Figure 20 shows the deformation of the dispersion curve of $|\chi^{(3)}|^2$ of a solution of cyclohexane in benzene in the region of the Raman resonance $\nu_{R1}=802$ cm^{-1} of cyclohexane ($\omega_1-\omega_2$ is being scanned) as the frequency difference $\omega-\omega_2$ is tuned in the vicinity of the Raman line $\nu_{R2}=992$ cm^{-1} of benzene.[94] We see that by choice of $\omega-\omega_2$ one can get either a considerable increase in the contrast of the dispersion curve of $|\chi^{(3)}|^2$ of the solution, or a decline.

The interference phenomenon can also be used to calibrate the intensity of one type of resonance from the known intensity of another.

The absolute calibration of the two-photon absorption parameters of molecules existing in a solution from the value of the spontaneous Raman cross-section of the solvent molecules is especially convenient on the experimental level (see also Sec. 4*a*). Since the cross sections of the most intense Raman lines of such solvents as benzene, carbon disulfide, and chloroform are known to good accuracy (better than 20%), while the interference method possesses high sensitivity and contains no additional sources of error, one can measure the absolute TPA cross-sections here with an accuracy no worse than 30%.[86]

c) Interference of the real components of the nonlinear susceptibilities. The existence of a nondispersing pedestal in the spectrum of the "active" signal gives a general reference level for all the Raman lines. This permits one to compare the intensities of different lines, and in particular, to use the non-resonance signal from a gas mixture as the reference signal in measuring the concentration of one of the components of the mixture from the intensity of the characteristic Raman lines of its molecules in the "active" spectrum.

At relatively high concentrations of the component to be measured ($\max N_1|\langle\gamma^R\rangle| > (N_1\langle\bar{\gamma}^E\rangle + N_2\langle\bar{\bar{\gamma}}^E\rangle)$), the intensity of the anti-Stokes signal $I^{(a)}$ at the center of the Raman line depends quadratically on the density N_1 of the molecules of the component to be measured, since from (4.10) we have

$$I^{(a)} \propto |\chi^{(3)}|^2 = N_1^2|\langle\gamma^R\rangle|^2 + (N_1\langle\bar{\gamma}^{NR}\rangle + N_2\langle\bar{\bar{\gamma}}^{NR}\rangle)^2 + 2N_1\langle\gamma^{R'}\rangle(N_1\langle\bar{\gamma}^{NR}\rangle + N_2\langle\bar{\bar{\gamma}}^{NR}\rangle) \quad (4.13)$$

At exact resonance ($\omega_1-\omega_2=\Omega$) we have $\langle\gamma^{R'}\rangle=0$. At low concentrations N_1 ($\max N_1|\langle\gamma^R\rangle| \lesssim N_2\langle\bar{\bar{\gamma}}^{NR}\rangle$), it is more advantageous for increasing the sensitivity to tune away from the center of the line by the half-width of the latter: $\omega_1-\omega_2=\Omega\pm\Gamma$, since then we can neglect the first term on the right-hand side of (4.13), and the relationship of the intensity of the ARS signal to N_1 becomes linear.[54] The order of magnitude of the minimum concentration $N_{1,\min}$ of the molecules of the impurity that can still be reliably measured by this method is determined by the relationship

$$\frac{N_{1\min}}{N_2} \approx \frac{\langle\bar{\bar{\gamma}}^{NR}\rangle}{\langle\bar{\gamma}^R\rangle} \approx \frac{24M\Omega\Gamma\langle\bar{\bar{\gamma}}^{NR}\rangle}{b^2}. \quad (4.14)$$

For ordinary buffer gases such as nitrogen, methane, air, etc., $\langle\bar{\bar{\gamma}}^{NR}\rangle$ is of the order of 10^{-37} cm^6/erg.[127] The value of b^2 for most simple molecules is approximately constant, and is of the order of 10^{-32} cm^4. Therefore the estimate (4.14) is minimal for the lines that have the minimum line width Γ. In the region of relatively low pressures of the buffer gas, at which the effect of collision broadening is insignificant, the value of Γ for purely vibrational transitions (Q-lines) is mainly determined by vibrational-rotational interaction, and it lies in the range from 10^{-1} to 1 cm^{-1}. Thus we get the following estimate for the minimum detectable concentration[95]:

$$\frac{N_1^{\min}}{N_2^{\text{buf}}} \approx 10^{-5}-10^{-3},$$

Here the lower value pertains only to the Q_{01} (1) line of hydrogen, which has an anomalously narrow width, $\Gamma/2\pi c \approx 1.5\times10^{-2}$ cm^{-1}.

One can further increase the sensitivity by reducing the non-resonance pedestal of the lines in active spectroscopy (see Secs. 3*b* and 4*b*), or by going to measurement of the purely rotational components, which simultaneously have large Raman cross sections and small line widths.[83]

Interference of the real parts of $\chi^{(3)E}$ in ARS is also used for measuring the electronic component of the nonlinear increment to the refractive index n_2 (see (3.21)) under the condition that we can neglect its frequency dispersion, that is, we can assume that

$$\chi^{(3)E}(\omega_a;\ \omega_1,\ \omega_1,\ -\omega_2) = \chi^{(3)E}(\omega_1;\ \omega_1,\ \omega_2,\ -\omega_2).$$

As a rule, this condition is satisfied accurately enough in a region of transparency.

The method of "composite samples," which has been proposed by M. Levenson,[97] consists in comparing $\chi^{(3)E}(\omega_a)$ of the sample to be measured with the peak value of the Raman susceptibility $\chi^{(3)R}(\omega_a;\ \omega_1,\ \omega_1,\ -\omega_2)$ of

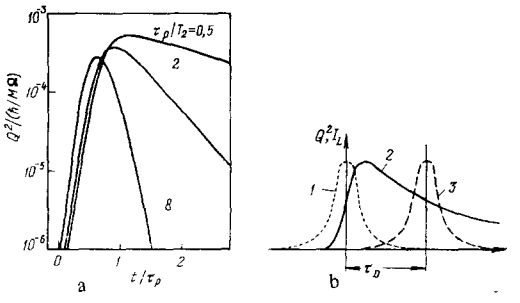

FIG. 21. a) Variation of the intensity of the coherent molecular vibrations excited in stimulated Raman scattering of a brief laser pulse (of duration τ_p; this variation was calculated by using Eqs. (5.1) and (5.2); the parameter of the curves is the ratio τ_p/T_2; $\tau_p/T_2 = 2$ for the second curve from the top); b) a diagram explaining the principle of non-steady-state ARS (1—pump pulse, 2—pulse of the stimulated molecular vibrations, 3—pulse of the probe radiation lagging by the time τ_D). [52]

a standard specimen that has an isolated, rather intense Raman line (calcite with a Ramn line at $\nu = 1086$ cm^{-1}, or benzene with a Raman line at $\nu = 992$ cm^{-1}). In principle the method is applicable to either liquid or gaseous or solid transparent substances.[13] In the latter case, a thin plate (0.1–0.3 mm) of the studied specimen is pressed onto the thin standard specimen (calcite), whereupon one takes the active spectrum in the region of a strong Raman resonance of the standard substance. The dispersion of the intensity of the ARS signal is described by the relationship

$$I^{(a)}(\omega_a) \propto |\chi_1^{(3)}(\omega_a; \omega_1, \omega_1, -\omega_2) l_1 + \chi_2^{(3)}(\omega_a; \omega_1, \omega_1, -\omega_2) l_2|^2 = |\chi_{\text{eff}}^{(3)E}|^2 l_1^2 \left[1 + \frac{(\bar{\chi}_1^{(3)R}/\chi_{\text{eff}}^{(3)E})^2}{1+\Delta^2} - \frac{2\bar{\chi}_1^{(3)R}/\chi_{\text{eff}}^{(3)E}}{1+\Delta^2}\Delta\right], \quad (4.15)$$

Here l_1 and l_2 are respectively the lengths of the standard and the studied specimens, and $\chi_1^{(3)}$ and $\chi_2^{(3)}$ are their cubic susceptibilities. The representation (4.1) holds for $\chi_1^{(3)}$, while we have the following expression for $\chi_{\text{eff}}^{(3)E}$:

$$\chi_{\text{eff}}^{(3)E} = \chi_1^{(3)E} + \chi_2^{(3)E}\frac{l_2}{l_1}. \quad (4.16)$$

We see from (4.15) that the effect of the studied specimen on the "active" spectrum of the standard consists in an effective change in its nondispersing component. The value of $\chi_{\text{eff}}^{(3)E}$ is calibrated against the known value of $\bar{\chi}_1^{(3)R}$, and then one calculates $\chi_2^{(3)E}$ by Eq. (4.16). The interference of the ARS signals of the two specimens that is described by the relationship (4.15) exists only when the process in both media is synchronous. This is achieved by noncollinear propagation of the pump beams and by using small values of the lengths l_1 and l_2 (of the order of several hundred μm).

5. Non-steady-state ARS

The theory of ARS based on the nonlinear susceptibilities that has been developed in the preceding sections is quite adequate for cases in which one uses continuous-wave lasers. Of course, it is also applicable when one employs in ARS pulsed lasers whose pulse duration considerably exceeds all the characteristic rise and relaxation times in the studied system. In particular, the formulas written in the preceding sections continue to hold for condensed media for pulses of duration down to 10^{-8}–10^{-9} sec.

Moreover, since about 1970, people have performed ARS experiments with pulses whose duration τ_p does not exceed the "longitudinal" (T_1) and "transverse" (T_2) relaxation times. These experiments open up the possibility of directly measuring the times T_1 and T_2 (see Sec. 7*b*).

Naturally, the theory developed in Secs. 1–4 is not a applicable here, and we must turn directly to the microscopic equations.

In the simple case of light fields that are not too strong, the point is to use Eq. (1.7) for the molecular vibrations. However, if the field intensities of the light waves are high enough, the classical approach, which operates only with the amplitudes Q (the nondiagonal element of the density matrix) is inapplicable: we must account also for the movement of the populations of the vibrational levels.

We briefly present below the results of such an analysis, which permits us to provide a theory of non-steady-state phenomena in ARS using ultrashort pulses[98,99] (see also the reviews[50,52,53]).

We shall first treat the case in which the vibrational transition is excited by a doublet of applied pump pulses $E^{(1)}(t)$ and $E^{(2)}(t)$.

For a two-level system, the abbreviated equations for the amplitude of the nondiagonal element of the density matrix Q and the difference of the populations n have the following form[52,98,99]:

$$\frac{\partial Q}{\partial t} + \frac{Q}{2T_2} = \frac{i}{4M\Omega}\left(\frac{\partial\alpha}{\partial Q}\right)_0 E^{(1)}(t)\, E^{(2)*}(t)\,(1-2n)\, e^{i(k_1-k_2)z}, \quad (5.1)$$

$$\frac{\partial n}{\partial t} + \frac{n}{T_1} = \frac{i}{8\hbar}\left(\frac{\partial\alpha}{\partial Q}\right)_0 (E^{(1)}E^{(2)*}Q^* - E^{(1)*}E^{(2)}Q). \quad (5.2)$$

We should add to these equations another one for the amplitude of the anti-Stokes wave:

$$\frac{\partial E^{(a)}}{\partial z} + \frac{1}{v_a}\frac{\partial E^{(a)}}{\partial t} = \frac{i\pi\omega_a^2 N}{c^2 k_a}\left(\frac{\partial\alpha}{\partial Q}\right)_0 QEe^{i\Delta kz}, \quad (5.3)$$

Here v_a is the group velocity. By using these equations, we can treat two variants of non-steady-state ARS.

a) Coherent non-steady-state ARS. In this variant, the phase mismatch Δk plays the governing role. Figure 21a shows the time course of the square of the amplitude Q^2 as calculated by (5.1) and (5.2) in the case in which the molecular vibrations are excited by a doublet of pulses of Gaussian shape having the same duration τ_p. From the spectroscopic standpoint, the regions of the curves of greatest interest are those that are not rising, but decaying with the time T_2. In full agreement with the abovesaid, one can probe these regions by using delayed pulses of the probe radiation (Fig. 21*b*), which

[13] This method has been applied to liquid crystals in Ref. 206.

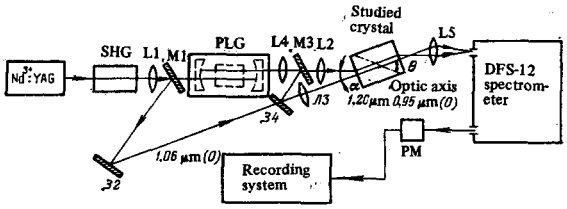

FIG. 22. Block diagram of an ARS spectrometer based on a parametric light generator (PLG). One records the Stokes scattering of the probe ray ($\lambda = 0.53$ μm) by the coherently excited vibrations of the crystal in the biharmonic pump field ($\lambda \approx 0.95$ μm (tunable/PLG radiation), $\lambda \approx 1.06$ μm). SHG—second-harmonic generator based on an $LiNbO_3$ crystal, Li—L5—focusing lenses, M1—M4—mirrors, PM—photomultiplier. [33]

is scattered with change of frequency along the synchronization direction $\Delta k = 0$.

b) Incoherent non-steady-state ARS. The population difference n also varies appreciably in strong fields, and here the increase in n can evolve in a time considerably shorter than T_1 (evidently an analogous situation also occurs during establishment of Q: see Fig. 21a).

The decline in n after cessation of the perturbation occurs in times $\sim T_1$. The probing of $n(t)$ is based on a process identical with that of spontaneous anti-Stokes scattering. This implies that the spontaneous anti-Stokes scattering of the probe pulse by the optically induced population changes is practically isotropic. One can caluclate the intensity of the anti-Stokes signal by using the formulas that describe the anti-Stokes scattering in the ordinary, spontaneous variant of Raman scattering. However, in contrast to the case of spontaneous Raman scattering, we are dealing here with a regular time course of $n(t)$ that can be established by using delay lines introduced into the channel of the probe pulse.

We stress that incoherent ARS has $I_a \sim z^2$, as in the coherent variant. Here it is actually difficult to create large changes in n (in condensed media $\Delta n = (N_2 - N_1)/(N_2 + N_1) \leq 10^{-3}$, where N_1 and N_2 are respectively the populations of the lower and upper levels).[14)] These circumstances yield a considerably lower signal level in incoherent ARS than in the coherent variant.

Given sufficiently strong lines, stimulated Raman scattering is often used in experiments for direct measurement of T_1 and T_2, together with exciting the vibrational transition with a doublet. Here, in contrast with steady-state spectroscopy, the use of stimulated Raman scattering is not undesirable. Of course, the technique involving a doublet of tunable lines retains all the advantages of scanning the complete spectrum of vibrational modes (see Sec. 6*d*).

c) Coherent effects. Thus far, in discussing the propagation in a Raman-active medium of two ultrashort pulses of frequencies ω_1 and ω_2 ($\omega_1 - \omega_2 \approx \Omega$), we have assumed a fixed light field with conversion of a small fraction of the energy of the waves into the energy of the molecular vibrations, which is then transformed into heat. Actually, this is precisely the situation in all experiments to measure T_1 and T_2. However, if we have the duration of the two pulses τ_{p1}, $\tau_{p2} \ll T_2$, while their intensities satisfy certain relationships, a strong coherent interaction of these pulses with the molecular system can occur.[101,102] It is analogous to the effect that occurs in self-induced transparency.[104] The reason for the effect is that the energy gained by the molecular system is given up by it without feedback into the optical field.[101] We can expect that the technique of studying coherent effects in Raman transitions will have the same applications as the effect of self-induced transparency for one-photon transitions.[103,104]

6. Experimental technique of ARS

a) Spectrometers for steady-state and quasi-steady-state ARS: The coherent scattering process that ARS is based on is essentially a nonlinear optical process. Hence laser-type light sources of high spectral brilliance, monochromaticity, and spatial coherence and intensity are required to achieve it.

A tunable laser must tune over a rather broad interval to ensure that it will overlap all the spectral range containing the Raman lines of interest to the experimenter when paired with the fixed-frequency line.

The first ARS experiments were performed with a discrete set of line pairs from Q-switched lasers and the stimulated-Raman-scattering components in various organic liquids.[20,23,24] A parametric light generator (PLG) pumped by the second harmonic of an Nd:YAG frequency laser was the first smoothly tunable source applied in ARS.[33] The radiation of this PLG is tuned over a broad range in the near infrared (from 0.7 to 2.5 μm and beyond). Together with the fundamental harmonic of the reference laser ($\lambda = 1.06$ μm), this gives the pair of pump waves in ARS (Fig. 22). Important merits of the PLG are the extremely broad tuning range that involves no resonances of the material, together with the high peak power (up to tens of megawatts), and the possibility of working at a very high frequency of repetition of generation pulses (up to 10 kHz when pumped by nonosecond pulses).[105] The pump radiation of the PLG that is not converted into the tunable lines is used as the probe ray so that the spectra can be recorded in the visible.

From the standpoint of getting large coherent interaction distances with collinear propagation of the waves, a system that is more convenient and is currently widely applied is that in which the two ARS pump lines lie in the visible, while one detects either the anti-Stokes coherent scattering ($\omega_a = 2\omega_1 - \omega_2$) or the Stokes scattering ($\omega_s = 2\omega_2 - \omega_1$) of one of them.

One can use as sources of the line pairs the second harmonic of a Nd:YAG frequency laser and a dye laser excited by it[35,54,66,72] (see Fig. 23), or two dye lasers

[14)] To be sure, in gases and cryogenic liquids (such as liquified N_2, O_2, etc.), at intensities I_1, $I_2 \sim 10^2$ MW/cm^2, the value of Δn can be as much as several dozen percent.

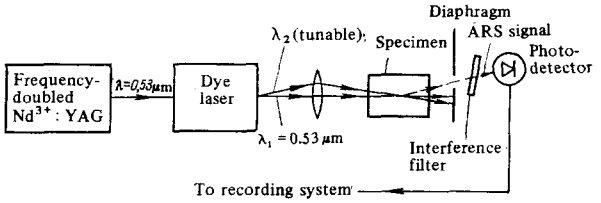

FIG. 23. Block diagram of a spectrometer based on a tunable dye laser. The well-collimated ARS signal is discriminated from the pump radiation by using an opaque screen containing a diaphragm that transmits only the ray of the useful signal. One need not employ a monochromator. [54]

excited by the same nitrogen laser. [60, 97, 93] Other combinations of sources are also possible. [106–109]

Whenever one need not obtain intensities as large as possible of the scattered component, but one must resolve the fine structure of lines, measure exactly the frequency of molecular vibrations, [209] or shift the Raman spectrum into a region free of stray light and ordinary luminescence, one can apply continuous lasers as the pump source in coherent ARS [110–114, 207, 208] (Fig. 24). Then the spectral resolution is determined by the width of the line of the tunable laser [15] (the best continuous dye lasers have a line width less than 10 kHz [115]). As a rule, in order to get an anti-Stokes signal comparable in intensity with the Stokes signal of spontaneous Raman scattering, one must use strongly focused beams at a power of the order of hundreds of milliwatts. [111] One gets good results in analyzing gaseous media by ARS using continuous lasers by placing the studied samples inside the resonator of the pump laser. [114]

b) Requirements on the spectroscopic apparatus. In recording the ARS signals from large concentrations of materials that have well marked Raman lines when the powers of the pump lines lie in the range 50–100 kW, one can completely forgo a monochromator, while limiting the system only to spatial discrimination with a screen that transmits the collimated radiation of the scattered component and blocks the direct pump rays. In order to prevent the incoherently scattered pump light from reaching the photodetector, people usually employ in addition an interference filter tuned to the frequency of the anti-Stokes component (see Fig. 23).

If one uses two tunable lines for pumping in ARS, and the rate of tuning of the low-frequency component of the doublet (ω_2) is twice the rate of tuning of the other component (ω_1), then the frequency of the ARS signal $\omega_a = 2\omega_1 - \omega_2$ remains constant, so that one can avoid tuning the interference filter while scanning $\omega_1 - \omega_2$.

In the remaining cases, one must use a single or double monochromator, especially when employing continuous-wave lasers for pumping. The fundamental characteristic that determines the suitability of a monochromator for use in ARS is a low level of stray light at the exit slit of the instrument; as a rule, a level of discrimination of 10^{-9}–10^{-10} suffices.

Since the ray of the ARS signal is collimated and spatially coherent, the spectral apparatus used need not have a high aperture, while the light-sensitive layer of the photodetector can have a small area.

The function and operating regime of the spectral apparatus in an ARS system can differ, depending on which of the two modifications of this method one uses—ARS with narrow-band excitation or ARS with broad-band pumping.

c) Schemes involving noise pumping. In the variant of ARS with a broad-band pump, [36, 38] the beating of the different spectral components of the broad-band (noise) tunable source with the monochromatic fixed-frequency line simultaneously excites molecular vibrations in a broad spectral range. The "active" spectrum is recorded upon scanning the monochromator, just as in spontaneous Raman spectroscopy:

$$|\chi^{(3)}(\omega_a; \omega_1, \omega_1, -\omega_2)|^2 \propto \frac{S^{(a)}(\omega_a)}{S^{(2)}(\omega_2)};$$

Here $S^{(a)}(\omega_a)$ is the spectral density of the anti-Stokes signal at the frequency $\omega_a = 2\omega_1 - 2\omega_1 - \omega_2$, $S^{(2)}(\omega_2)$ is the spectral density of the broad-band pumping component, and ω_1 is the frequency of the fixed line.

An important merit of this modification of ARS is that one can get the dispersion curve of $|\chi^{(3)}|^2$ over a broad region of the spectrum during one laser flash in times of 10^{-8}–10^{-11} sec (see Fig. 5). In this case the image of the spectrum of the coherently scattered component produced by the spectral apparatus should be either photographed or recorded with a strobed multichannel receiver based on an electron-optical converter and/or a television camera (see, e.g., Ref. 117).

It seems especially promising to use this modification of ARS for quick analysis of fast chemical reactions and explosive processes, and also for non-steady-state plasma diagnostics.

d) Choice of the optimal focusing of the pump radiation; distortions of "active" spectra. In order to get

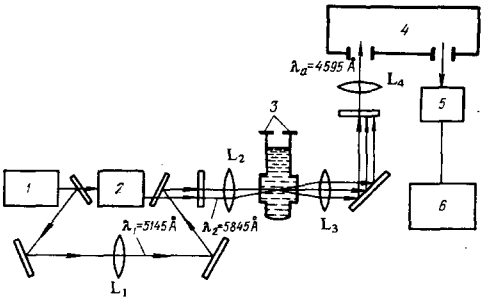

FIG. 24. Block diagram of an ARS experiment in the field of continuous-wave lasers. 1—single-mode ionized-argon laser ($P_1 \approx 2$W). 2—tunable dye laser ($P_2 \approx 150$ mW), 3—liquid-nitrogen Dewar, 4—DFS-24 monochromator, 5—photomultiplier, 6—amplifier and recorder, L_1–L_4—lenses. [111]

[15] The fixed-frequency line width can without difficulty be made considerably narrower than the line of the tunable laser. [116]

as high as possible a power of the ARS signal for given powers of the pump rays, people usually focus the latter within the studied specimen by using a system of achromatic lenses. A theory of four-wave nonlinear interactions in focused beams has been developed.[118–120] One can easily show from the results of these calculations that there is no optimal degree of focusing of Gaussian pump beams in isotropic media in ARS-type frequency-shift processes that would maximize the power of the ARS signal. Under conditions of phase synchronization, $\Delta k = 0$, the total power of the ARS signal increases with increasing degree of focusing only until the so-called "confrontal" parameter of the focused beams $b = kw_0^2$ ($k = 2\pi/\lambda$ is the wave vector, and w_0 is the radius of the focal spot) is comparable with the length of the studied specimen. With further increase in the degree of focusing (decreasing b), the power of the ARS signal saturates and completely ceases to depend on b. In this case one can calculate the power of the ARS signal by the formula[120]

$$P_a = \frac{2^6\pi^4\omega_1^4}{c^6} |3\chi^{(3)}_{1111}|^2 P_1^2 P_2. \qquad (6.1)$$

Here P_1 and P_2 are the powers of the pump beams; the latter are assumed to have a Gaussian intensity profile (cf. (1.15)). However, the application of extremely "strong" focusing is justified whenever for any reasons one cannot ensure strict fulfillment of the phase-synchronization condition throughout the length of the specimen, i.e., when $\Delta k \neq 0$. The fundamental contribution to the ARS signal comes from the region near the focus of the pump beams, which has a characteristic size of the order of b; hence, if we choose $b \ll l_{coh} = \pi/\Delta k$, we can effectively "compensate" the phase mismatch Δk. That is, we can get just as intense an ARS signal as in the case of exact phase synchronization. In this case the total power of the anti-Stokes ARS signal again can be calculated by Eq. (6.1). The natural limit for increase in the energy flux density of the pump waves by focusing is imposed by optical breakdown and other processes that damage the studied medium. Moreover, in order to avoid distorting spectra obtained by ARS, one must maintain the intensities of the pump waves at a level that does not exceed the threshold values for excitation of stimulated Raman scattering and other nonlinear-optical processes.[204] In particular, Ref. 121 discusses distortions of "active" spectra that arise under the action of inverse Raman scattering of the pump lines.

It proves very effective in increasing the intensity of the recorded signal in ARS to use optical fibers[211] or (in studying gases at low pressures) thin hollow dielectric waveguides.[212]

e) Technique of non-steady-state ARS; generation of tunable ultrashort pulses. The fundamental element of a non-steady-state ARS spectrometer is the reference generator of hypershort pulses. If one is studying the optical modes of a medium under non-steady-state excitation arising from stimulated Raman scattering, then the need for hypershort pulses of smoothly tunable frequency in the second generator drops out. Most experiments on non-steady-state ARS have been performed up to now precisely by using the technique of stimulated Raman scattering.

One usually uses as the reference generator a longitudinal mode-locked neodymium-glass laser; one isolates a single pulse from the train of generation peaks by using a fast-acting cell. This pulse is amplified, and part of it is converted into the second harmonic. Stimulated Raman scattering is excited by the pulse at the fundamental frequency, while the excited optical mode is probed by the pulse of the second harmonic, which is applied to the studied medium with a suitable time delay.

In addition to the described scheme, which has been applied by W. Kaiser and his associates, there is a non-steady-state ARS scheme that employs coherent one- and two-photon excitation of the studied optical modes by using tunable ultrashort-pulse generators. One can use as the latter tunable dye lasers[122] or parametric light generators.[123,124] Both types of tunable lasers are excited by ultrashort pulses of the radiation of mode-locked lasers or of their harmonics. There is a possibility of locking the modes of a tunable dye laser by using a saturating filter placed inside the laser resonator.[125] The most convenient scheme of a parametric generator of ultrashort pulses is a two-crystal scheme: one excites in the first (generator) crystal a broad-band parametric superluminescence, which is amplified in the second amplifier crystal. In order to narrow the spectrum of the radiation, one puts a diaphragm between the generator and amplifier crystals that blocks the parametric superluminescence radiation that stems from the noncollinear interactions. One can get an analogous effect by placing the amplifier crystal far enough from the generator crystal.

A recent study[126] has used a two-crystal scheme based on $LiNbO_3$ crystals to build a generator of picosecond pulses that are tunable in a range up to 4.6 μm. Use of a special, so-called 47° crystal allowed them to get an efficiency of conversion into tunable radiation of up to 10% upon pumping with a picosecond YAG laser ($\lambda \approx 1.06$ μm).

7. Physical applications of ARS

a) Active spectroscopy and traditional spectroscopic methods. The set of applications of ARS is determined in many ways by the broad potentialities possessed by the phenomenon of Raman scattering of light that it is based on. We should expect the greatest impact from applying ARS wherever the theoretical potentialities of spontaneous scattering cannot be realized fully owing to weakness of the signal or to a high background level caused by more efficient processes (e.g., luminescence).

In these cases the success of application of ARS arises from such merits as a signal level elevated by many orders of magnitude and the possibility of recording it in the anti-Stokes region free of the background stray light of luminescence, high spectral resolution, and exactly defined geometric conditions.

However, as we have seen above, the spectroscopic information obtainable by ARS is richer; polarization measurements in ARS are also highly informative.

This allows us to pose and solve completely new physical problems. We point out among them the above-discussed interference effects in ARS (see Sec. 4), which allow one not only to measure the relative efficiencies of different physical processes such as Raman scattering, the optical Kerr effect, and one- and two-photon absorption (which are often manifested even in different molecules), but also to establish the relative phases of their complex contributions to the experimentally measured absolute value of the nonlinear optical susceptibility $|\chi^{(3)}|^2$. A new potentiality offered by ARS is that of directly tracing the interaction of the electron shell and the nuclei of a molecule while its environment, temperature, external fields, etc. are varied. This is especially important in studying complicated biological molecules like chlorophyll or a protein.

Application of ARS in a system with a probe beam for measuring the vibrational spectra of colored and strongly luminescent media permits one in principle to distinguish the effects of resonance Raman scattering proper and resonance fluorescence, since one-photon resonance can occur in one of the pump waves ω_1 and ω_2, while the frequencies of the probing and the scattered radiation can lie in a region of transparency of the medium.[69] We shall take up below in somewhat greater detail the points that have been discussed in insufficient detail (or not at all) in the preceding text.

b) Direct measurements of relaxation times. The direct measurements of transition and relaxation processes in atoms, molecules, and condensed media that have become possible within the framework of non-steady-state ARS (Sec. 5) primarily give information on the relaxation times that was previously either completely unattainable (especially in liquids), or obtainable by indirect methods.

TABLE IV. Measured dephasing times T_2 and lifetimes T_1 of excited states.[14]

Substance	T (K)	$\Omega/2\pi c$, cm^{-1}	T_2, ps	$\Delta\Omega/2\pi c$, cm^{-1}	$(T_2)_{calc}$, ps*	T_1, ps	T_1/T_2	References
N_2 (liq.)	77	2326	75±8	0.067	79±8	$1.5\cdot10^{12}$	$2\cdot10^{10}$	134, 135
						$(56\pm10)\cdot10^{12}$	$7.5\cdot10^{11}$	136
C_2H_5OH	300	2928		20	0.26	20±5	77	130, 142, 135
		1440				40		135
CH_3CCl_3	300	2939	1.3±0.6	4.9	1.1	5.2±0.8	4	131, 143
		1450				4		143
n-heptane	293	2900	6			11.0±1.5	1.83	147
	248	2900				14.0		147
	203	2900				16.0		147
Isodecane	293	2900	11			10.8		147
	248					21.0		147
n-Tridecane	293	2900	15		1.40	21.0		147
1,6-Heptadiene	293	2900				60.0		147
CCl_4	300	459	4.0±0.5			3.8		130, 137
$SnBr_4$		221	3.0±0.3					137
$SiCl_4$		425	3.0±0.5			~2.8		137
CD_3OD	293	2200					25±10	143
$CaCO_3$	295	1086	4.4±0.3	1.1—1.4		3.8—4.8		143
	297	1086	8.5±0.2					132
	90	1086	8.7±0.7	0.68		7.8±0.9		143
	100	1086	19.1±4					132
Diamond	295	1332	2.9±0.3	1.65—2.2		3.2—2.4		130
	77	1332	3.4±0.3	1.48		3.6		130
GaP	300	361	5.5±0.5					143
C_6H_6	300	992	5±1.4	2.3		4.7±0.2		133
C_6D_6	300	945	8±1.4	1.8		7.0±0.2		133

*The T_2 values given in this column were calculated for uniformly broadened lines by the formula $T_2 = 1/\Delta\Omega$.

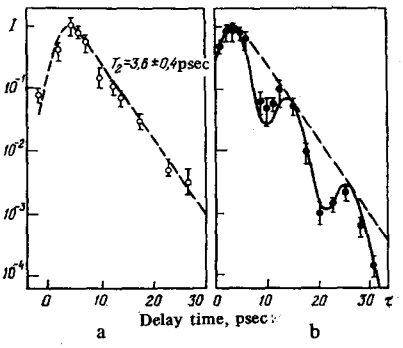

FIG. 25. Result of the experiments of Kaiser *et al.*[137] on non-steady-state ARS of an inhomogeneously broadened Raman line in the CCl_4 molecule. a) Curve characterizing the decline in the coherent anti-Stokes Raman scattering of the probe pulse with lag time with respect to the exciting pulse; conditions are adopted for recording the signal from the $C^{37}Cl_4$ molecule; b) the same, when CCl_4 molecules containing all the naturally occurring isotopes of chlorine contribute to the scattered signal.

Experiments to measure the "longitudinal" relaxation time were first performed in 1966 by DeMartini and Ducuing in gaseous hydrogen. The first excited state of the latter was populated via stimulated Raman scattering of a high-power pump pulse.[32] Experiments on gases have subsequently been continued.[128,129]

Experiments in condensed media were first peformed in 1971–1972 by W. Kaiser and his associates.[130] They showed, first, that the dephasing times of the molecular vibrations that are manifested in the stimulated Raman spectra coincide with the indirect estimates from measuring the widths of the corresponding lines, and second, that these same media as a rule have $T_2/T_1 \leq 1$, whereby liquid show[16] $T_2/T_1 \approx 10^{-1}-10^{-2}$ (see also Refs: 14 and 52 and Table IV): In principle, coherent non-steady-state ARS allows one to distinguish the contributions to the width of a Raman resonance line from homogeneous and inhomogeneous broadening mechanisms.[137] In this case the technique of non-steady-state ARS can be correlated with that of observing quantum beating in non-steady-state luminescence from several closely spaced levels[138] (Fig. 25).

The methods of measuring relaxation times that are based on non-steady-state ARS are applicable not only to vibrational transitions in molecules, but also to other quantum levels, e.g., to electronic energy levels in isolated atoms. One can excite them either via a Raman process[109] or by direct one- or two-photon absorption.[140,141] In the latter case one records the time course of the lag of the intensity of the coherent or incoherent anti-Stokes component of the probe pulse (ω_2)

[16]We note that the ratio T_2/T_1 is anomalously small in liquefied gases made of dipole-free molecules (see Table IV).

at the frequency $\omega_3 = 2\omega_1 + \omega_2$ (ω_1 is the frequency of the pump pulse).

c) Direct probing of the degree of excitation of different optical modes. It is very promising to apply the methods of non-steady-state ARS to studying the relaxation mechanisms of strongly excited optical modes.

If one measures the scattered probe ray components due to interaction with the normal molecular vibrations that lie at lower frequencies than those excited by pumping, then it proves possible to establish the channels of dissipation of the energy of the molecule from the increase in the anti-Stokes incoherent scattering signal from those levels that amount to remnants of the decayed vibrational excitation.[131,142]

The first experiments of this type, which were performed on ethanol, showed that the energy of the totally symmetric vibration of its molecule (frequency $\nu_{11} = 2928\ cm^{-1}$) is partitioned equally between two internal vibrations of the CH_3 group (frequency $\nu_8 = 1454\ cm^{-1}$) in a time of $\sim 10^{-11}$ sec. Here the anharmonicity of the totally symmetric vibration plays the fundamental role in its decay.[142]

W. Kaiser and his associates[52,143] have employed an analogous method to establish the decisive effect of intermolecular interactions on the relaxation of the totally symmetric vibration of CH_3CCl_3 surrounded by solvent molecules.

Application of the technique of incoherent anti-Stokes scattering of probe pulses by overtones of the fundamental vibrations that are directly excited by a resonance infrared field might allow one directly to observe the dynamics of the stepwise acquisition of energy that precedes collisionless dissociation of the molecule in the field of a strong resonance infrared wave.[144]

In principle, one can also solve this same problem by using coherent ARS; correspondingly, the level of the recorded signal here would be considerably higher than in the case of incoherent anti-Stokes scattering.

The method in based on the fact that the resonance Raman susceptibility $\chi^{R,J}(\omega_a; \omega_1, \omega_1, -\omega_2)$ that involves a definite vibrational-rotational transition at the frequency Ω_J, $\omega_1 - \omega_2 \approx \Omega_J$, is proportional to the number density N_J of the molecules existing in the lower level of the transition (see Sec. 2).[17] Owing to anharmonicity, the lines in the spectrum of $|\chi^{(3)}(\omega_a; \omega_1, \omega_1, -\omega_2)|^2$ that involve transitions between the ground and first excited vibrational levels ($v = 0 \rightarrow v = 1$) generally do not overlap with the lines that correspond to transitions between the higher vibrational levels. The ratio of the intensities of these lines gives a measure of the population of the upper vibrational states.

[17]We assume here, as we do throughout this study, that the population of the upper level of the Raman transition can be neglected in comparison with that of the lower level. This holds true in the case of high-frequency vibrational transitions, while in other cases in which the spacing between the levels is comparable with or less than kT, we must take $N_J - N_J$, instead of N_J, where N_J, is the population of the upper level (see, e.g., Ref. 145).

Such an experiment has already been performed in deuterium with excitation of the first vibrational level ($v_J = 1$) in a discharge by electron impact.[107] They estimated the "vibrational" temperature, $T_v = 1050\,°K$, from the results of the measurements, whereas the "rotational" temperature was considerably lower, $T_r = 400\,°K$.

8. Analytical applications of active spectroscopy

a) Analysis of the composition of gas mixtures and of the atmosphere. Along with the considerable increase in the level of the detected signal, application of coherent ARS in gas analysis (see Sec. 4c) is promising for a number of other reasons. First, the weak linear dispersion of all the atmospheric gases at normal pressure allows one to attain coherent interaction lengths ($l_{coh} = \pi/\Delta k$) in linear propagation of the order of several tens of centimeters and the more.[95] Second, the narrowness of most of the Raman lines that are suitable for identification of impurities greatly elevates the peak values of the Raman susceptibility ($\overline{\gamma}^R$) over the electronic hyperpolarizability (γ^E). This involves the existence of the coherent "background" in the ARS spectra (see Sec. 4c) and it exceeds that for condensed media by 3–5 orders of magnitude. Third, the application here of a polarization methodology (Sec. 3b and Fig. 6) that is not encumbered with the depolarizing effect of the ordinary optical Kerr effect makes it possible to improve the discrimination of the Raman resonances from the coherent "background" by another 2–3 orders of magnitude to ensure a sensitivity of ARS in determining impurities at a level of 10^{-5}–10^{-7} molecules per molecule of the buffer gas.

We should include among the defects of coherent ARS its inapplicability for remote probing by a back-scattering scheme, owing to the impossibility of satisfying the synchronization conditions, together with the difficulty of applying it to paths longer than several tens of meters.

b) Non-steady-state plasma diagnostics using active spectroscopy. Coherent ARS and also the optical Kerr effect induced by a Raman resonance (Sec. 3d) can become useful methods for direct determinations of frequencies, amplitudes, damping, and dispersion constants of the collective excitations in a plasma (primarily plasmons, and possibly ion-sound waves), especially in cases in which the plasma is non-steady-state and is characterized by a large density.[44,150] The small efficiency of the spontaneous process and the high level of the incoherent background have been precisely the fundamental obstacles to the use of spontaneous Raman scattering for plasma diagnostics. While the coherent methods of ARS and of the optical Kerr effect possess the broad spectroscopic potentialities of spontaneous Raman scattering, yet they considerably surpass it in signal-to-noise ratio.

The coherent threshold-free methods of ARS and of the optical Kerr effect can be used also for studying stimulated-scattering processes. As is assumed in

Refs. 148 and 149, the latter play an important role in restricting the efficiency of the laser heating of the plasma. Estimates have shown[144] that it is preferable to use a coherent ARS scheme in the case of a hot and not very dense plasma ($\omega_q/c \geq 0.2\, k_D$, where ω_q is the frequency of a plasmon having the wave vector $q = k_1 - k_2$, and $k_D = \sqrt{4\pi n e^2/kT}$ is the reciprocal of the Debye shielding length). This is because here the linear dispersion of the plasma does not impede one from attaining the synchronous regime $\Delta k = 0$ ($\Delta k = k_a - 2k_1 - k_2$, where $k_1 - k_2 = q$). On the other hand, the effect of the linear dispersion is considerable for a relatively dense cold plasma ($0.2\, k_D \geq 2k_1$), and the synchronization condition $\Delta k = 0$ cannot be satisfied. Here it is more expedient to use the Raman-resonance-induced Kerr effect.

In both cases it suffices to use pump beams of ~10 MW power to get a reliably detectable signal.

In order to take the Raman spectrum of a non-steady-state plasma in the two methods, one can use the variant with broad-band pumping (see Sec. 6c), which increases the speed of action.

An additional advantage of the stated methods is the localization of the information that one gets by using them.

c) Local and rapid analysis using active spectroscopy. Owing to the nonlinearity of the scattering process is coherent ARS, the fundamental contribution to the signal intensity in focused beams comes from the region near the common focus of the pumping beams.

This situation allows one to perform an exact local analysis with coherent ARS by using sharply focused beams, i.e., to determine the spatial distribution of the scattering particles by scanning the intersection point of the pump rays. Here the decrease in the illuminated volume upon focusing the rays does not diminish the intensity of the signal (see Secs. 1 and 6d). The accuracy of measuring the spatial distribution is determined by the dimensions of the focal volume. For example, it is not hard to get a focal volume in the form of a cylinder of 10 μm diameter and length of the order of 100 μm. As we have noted repeatedly, an especially valuable property of ARS is the possibility that it offers of getting the complete Raman spectra of optical media during a single laser pulse (see Fig. 5), i.e., in a time of from 10^{-8} to 10^{-12} sec. One attains this by using the variant of coherent ARS with 2 broad-band pump (see Sec. 6c) at the cost of reducing the spectral resolution. In this case the latter is determined by the resolution of the linear spectral apparatus, rather than the line widths of the lasers used (see Fig. 5).

d) Use of ARS *to study complicated molecules.* Reports have been published very recently on using coherent ARS for studying the vibrational spectra of complicated molecules, including biological ones. Besides the possibility of removing the masking effect of luminescence on the scattering spectra, application of ARS here has also a number of other advantages: it requires an insignificant volume of the studied sample; and one can use pulsed lasers of moderate mean power to get a reliably detectable signal, which reduces the probability of radiation damage to the specimen, etc. It is especially promising to use ARS to obtain resonance scattering spectra in which one or both pump lines lie in the vicinity of an electronic absorption band.[198-200]

The considerable increase in $\overline{\chi}^{(3)R}$ of the studied molecules that occurs under these conditions is equivalent to an effective diminution of the nondispersing coherent "background" caused by the solvent molecules. This allows one to work with very small concentrations of the studied molecules. Active Raman spectra have been obtained[200] of an aqueous solution of vitamin B_{12} at a concentration of 10^{-3} mol/L upon excitation in the absorption band of this vitamin. Here one distinctly observes interference of the resonance electronic and vibrational nonlinear susceptibilities of the vitamin molecules and of the "background" nonresonance susceptibility of the solvent molecules (however, the authors of Ref. 200 give an erroneous interpretation of the interference that they found).

III. ACTIVE SPECTROSCOPY OF RAYLEIGH SCATTERING AND OTHER TYPES OF SCATTERING

9. Active spectroscopy of elastic (Rayleigh) light scattering

a) Optical induction of phase gratings in a medium and coherent scattering by them (diffraction and self-diffraction). The ideas of the method of active spectroscopy can be used successfully also in the spectroscopy of elastic (Rayleigh) molecular light scattering. This form of scattering arises from the relatively slow small scale fluctuations in the refractive index. Naturally, here also one can proceed from fluctuational variations in the refractive index to coherent scattering by phase gratings induced in the medium by using two crossed beams.

These light-induced gratings have already been studied for a long time in holography[28-30] and in laser technology (distributed-feedback lasers).[151,152] Yet we wish to call attention here to the spectroscopic aspects of such experiments.[31,153]

If two pump beams obtained from the same laser intersect at a small angle θ in a weakly absorbing medium (see Fig. 3b), then a standing temperature "wave" δT ($\mathbf{q}$, Ω) is produced that is characterized by the wave vector $\mathbf{q}$ and the amplitude δT:

$$\mathbf{q} = \mathbf{k}_1 - \mathbf{k}_2, \quad \delta T = \frac{2\alpha \sqrt{I_1 I_2}}{\varkappa q^2}; \tag{9.1}$$

Here $\mathbf{k}_1$ and $\mathbf{k}_2$ are the wave vectors of the pump waves, which respectively have the intensities I_1 and I_2; α is the absorption coefficient for the light; and $\varkappa$ is the thermal conductivity. The frequency Ω can be fixed by modulating one of the pump beams. Under ordinary conditions, when the heat propagates diffusely δT ($\mathbf{q}$, Ω) has a maximum at $\Omega = 0$. After the pump pulses have passed, the nonpropagating temperature "wave" attenuates with a relaxation time $\tau_R = c_p/\varkappa q^2$, where c_p is the heat capacity of the medium at constant pressure.

The periodic temperature modulation leads to a modulation of the refractive index, since we have

$$n=n(\rho, T)=n_0+\left(\frac{\partial n}{\partial \rho}\right)_T \delta\rho+\left(\frac{\partial n}{\partial T}\right)_\rho \delta T. \qquad (9.2)$$

One can detect the phase grating described by (9.1) and (9.2) and its decay by using diffraction of a specially introduced probe ray ($\mathbf{k}_3$, ω_3) or diffraction of one of the exciting beams (self-diffraction) (see Fig. 3b); the scattering maximum corresponds to fulfillment of the condition $\Delta\mathbf{k}=0$. One can determine the amplitude of the diffracted wave from the equation

$$\frac{\partial E^{(4)}}{\partial z}=ik_4\left(\frac{1}{n}\frac{\partial n}{\partial T}\right)_{\text{eff}} \delta T\cdot E^{(3)}, \qquad (9.3)$$

Here the factor $(n^{-1}\partial n/\partial T)_{eff}$ describes the relation of the temperature fluctuations to the refractive-index fluctuations.

The parameter to be measured can be either the amplitude of the diffracted wave, which bears information on the variation of the quantity $(\sigma\partial/\partial T)_{eff}$ as we assume the temperature of the specimen to vary, or the characteristics of the temperature wave itself: the dependence of its amplitude δT on $\mathbf{q}$ with varying angle of crossing of the pump rays and on Ω as the modulation frequency is varied, etc.

In addition to the "temperature" grating, other types of gratings can also be formed in the region of intersection of the rays that involve, e.g., generation of free carriers in semiconductors or spatial modulation of the absorption coefficient, etc. In many cases, it may prove convenient to record these gratings by using coherent light scattering from them.

b) Active Rayleigh-scattering spectroscopy in crystals; optical recording of second sound. The employment of induced temperature gratings makes it possible to vary in a controlled way the level of modulation of the temperature (in the experiments described in Ref. 31, they could vary it over wide ranges up to a level that exceeds by a factor of 10^4–10^5 the rms value of the fluctuational inhomogeneities), and also substantially to use the coherence of the created temperature wave for increasing the efficiency of collection of the diffracted light. All of this allows one to elevate the intensity of the detected light signal by several orders of magnitude, and it justifies the application of the term here of active Rayleigh-scattering spectroscopy. [18)]

The experiment of Pohl and his associates[31] by the described method measured the relationship of the intensity of the scattered probe beam in an LiF crystal to the temperature. This permitted them for the first time to confirm for crystals the theory of Landau and Placzek[154] of Rayleigh light scattering. Moreover, they established that contributions to $(\partial n/\partial T)_{eff}$ arise not only from the purely isobaric temperature that involve the fluctuations of n solely via the thermal expansion, but also the explicit temperature-dependence of the refractive index plays a certain role (the second term in (9.2)).

Recently these same authors[155] applied radiofrequency modulation to one of the infrared beams that induced a temperature grating in an NaF crystal at a temperature $T\approx 15$ °K. They were able to measure the relationship of the amplitude δT of the temperature wave to the modulation frequency Ω, and to detect a peak at the frequency $\Omega_0\approx 6.5$ MHz. which corresponds to propagating, weakly damped temperature waves (the so-called "second sound") in the NaF crystal.[156] They established that the condition $\Omega_0=c_{II}|\mathbf{q}|$ (where c_{II} is the velocity of second sound) is satisfied with good accuracy. In spite of the weakness of the optical signal, they noted a broadening and shift of this peak with increasing temperature that corresponded to a change in the mechanism of heat propagation from a "second sound" regime to an ordinary diffusion mechanism. This is the first observation of propagating heat waves in a crystal by optical methods.

c) Active elastic light-scattering spectroscopy in semiconductors and dye solutions. Dynamic holograms obtained by generation of free carriers in semiconductors in crossed laser beams can be used for spectroscopic purposes, in particular, for measuring the diffusion of free carriers, and also for detecting nonlinear many-quantum processes involving free carriers.[153] Just as in the case of the temperature grating, here one can controllably vary the grating parameters (depth of modulation, lattice constant) by simply varying the parameters of the pump beams. In Ref. 153 they measured the efficiency of self-diffraction of one of the rays. As the intensity of the pump rays obtained from a neodymium glass laser was increased, this allowed them to observe a transition from a one-quantum regime of carrier generation in crystalline CdSe to a two-quantum regime. Then, at larger carrier concentrations, a quadratic-recombination mechanism was switched on. The induced change in the refractive index of CdSe amounts to $\Delta n\approx 10^{-5}$ at an intensity of the pump waves $I_{1,2}\approx 10$ MW/cm^2. The use of weak probe pulses applied with a certain time lag allowed them to measure the diffusion time of free carriers and to elucidate the role of nonlinear recombination in the "resorption" of the phase grating.

Important results that closely border on those obtained by using non-steady-state ARS (see Sec. 6) have been obtained by using picosecond pulses for inducing diffraction gratings in solutions of rhodamine 6G in different solvents.[157] In contrast to the experiments described above, here the induced grating was an amplitude grating: the absorption coefficient of the probe beam proved to be spatially modulated (just like the pump rays, it amounted to the second harmonic of a Nd:YAG laser with self-synchronized modes). Measurement of the decline in intensity of the diffracted probe pulse with time delay allowed them to estimate the lifetime T_1 of the first singlet excited state of the rhodamine 6G molecule, as well as the time τ of orientational relaxation of the excited molecules (Table V).

[18)] The authors of Refs. 31 and 107 call this method "induced temperature Rayleigh scattering."

TABLE V. Experimental results for the lifetime T_1 of the first singlet excited state of the rhodamine 6G molecule and the orientational relaxation time τ[157].

Solvent	Rhodamine 6G concentration, mole/l	τ, ps	T_1, ps
Methanol	$2\cdot10^{-4}$	140±30	1.7—2.0
Ethanol	$1\cdot10^{-4}$	300±50	3.7±0.5
1-Propanol	$1\cdot10^{-4}$	500±100	3.8±0.5

10. Active spectroscopy of light scattering by dipole-allowed transitions

a) Generation of coherent elementary excitations upon absorption of light. Although we have been speaking thus far of excitation of coherent states in molecules in crystals by two-frequency pumping, it is quite clear that one can also get an analogous effect with one beam, whenever its frequency ω_{ir} coincides with the frequency of a corresponding dipole-allowed transition in the medium.

Again, such states can be probed, by using coherent anti-Stokes scattering according to the scheme $\omega_a = \omega + \omega_{ir}$. Here the frequency of the probe ray can be conveniently chosen in the visible. As always, this process will be most efficient in the synchronization direction $\mathbf{k}_a = \mathbf{k} + \mathbf{q}$, where $\mathbf{q}$ is the wave vector of a polariton of frequency $\Omega_q \approx \omega_{ir}$. Naturally, the stated resonance transition need not obey the alternate selection rule, i.e., it can be manifested simultaneously both in infrared absorption and in Raman scattering.

The symmetry of the medium imposes substantial restrictions on the course of such a process: in centrosymmetric media we have all the $\chi^{(2)} = 0$. Thus the interference of the different elements of this medium will cause the macroscopic polarization at the frequency $\omega_a = \omega + \omega_{ir}$ to be absent.

Yet the described process can be fully manifested in noncentrosymmetric crystals and in media having artificial anisotropy. An analogous process has been observed in n-type CdS[159]; they observed intense Stokes and anti-Stokes satellites formed by the direct UHF excitation of "spin-flip" transitions in the spectrum of the optical radiation scattered in the crystal.

b) Detection of nonequilibrium infrared-active excitations by using light scattering. The equations for the amplitude Q of a normal mode of an element of the medium at the frequency Ω and for the nonlinear polarization $P^{(2)}(\omega_a)$ are derived from (2.10) and (2.9) with the Hamiltonian of (2.8), in which we should keep only several terms; in particular, for a piezoelectric crystal we get

$$\ddot{Q} + 2\Gamma\dot{Q} + \Omega^2 Q = \frac{1}{M}\left(\frac{\partial \mu_i}{\partial Q}\right)_0 \mathscr{E}_i^{(ir)}, \tag{10.1}$$

$$P_i^{(2)}(\omega_a) = \left(\frac{\partial \alpha_{ij}}{\partial Q}\right)_0 Q\mathscr{E}_j + \beta_{ijk}^E \mathscr{E}_j \mathscr{E}_k^{(ir)}; \tag{10.2}$$

Here $\mathscr{E}$ and $\mathscr{E}^{(ir)}$ are, respectively, the amplitudes of the probe and the resonance infrared fields. We can derive from this an explicit expression for the macroscopic polarizability $\chi^{(2)}$ that describes this nonlinear optical effect:

$$P_i^{(2)}(\omega_a) = 2\chi_{ijk}^{(2)}(\omega_a;\ \omega,\ \omega_{ir})\, E_j E_k^{(ir)}, \tag{10.3}$$

$$\chi_{ijk}^{(2)}(\omega_a;\ \omega,\ \omega_{ir}) = \chi_{ijk}^{(2)E}(\omega_a;\ \omega,\ \omega_{ir}) + \chi_{ijk}^{(2)R}(\omega_a;\ \omega,\ \omega_{ir}), \tag{10.4}$$

$$\chi_{ijk}^{(2)E}(\omega_a;\ \omega,\ \omega_{ir}) = NL^3\beta_{ijk}^E, \tag{10.5}$$

where

$$\chi_{ijk}^{(2)R}(\omega_a;\ \omega,\ \omega_{ir}) = \frac{NL^3}{8M\Omega\Gamma}\cdot\frac{1}{2}\left[\frac{(\partial\alpha_{ij}/\partial Q)_0\,(\partial\mu_k/\partial Q)_0}{-i-(\omega_{ir}-\Omega)\,\Gamma^{-1}} + \frac{(\partial\alpha_{ik}/\partial Q)_0\,(\partial\mu_j/\partial Q)_0}{-i-(\omega-\Omega)\,\Gamma^{-1}}\right], \tag{10.6}$$

and L is a correction factor for the internal field. Since here, as in ordinary ARS, one is studying the variation of $I^{(a)} \sim |E^{(a)}|^2$ upon scanning ω_{ir} about Ω, the measured spectrum here also reflects the dispersion of the modulus of the nonlinear susceptibility $|\chi^{(2)}|^2$:

$$|\chi^{(2)}(\omega_a;\ \omega,\ \omega_{ir})|^2 = (\chi^{(2)E})^2\left[1 - \frac{2\,(\bar{\chi}^{(2)R}/\chi^{(2)E})}{1+\tilde{\Delta}^2}\tilde{\Delta} + \frac{\bar{\chi}^{(2)R}/\chi^{2(E)}}{1+\tilde{\Delta}^2}\right], \tag{10.7}$$

where

$$\bar{\chi}^{(2)R} = \frac{1}{2}\frac{NL^3}{8M\Omega\Gamma}\left(\frac{\partial\alpha}{\partial Q}\right)_0\left(\frac{\partial\mu}{\partial Q}\right)_0, \quad \tilde{\Delta} = \frac{\omega_{ir}-\Omega}{\Gamma}$$

(we have omitted the indices in order to abbreviate the notation). We see from (10.7) that the dispersion curve of $|\chi^{(2)}|^2$ possesses the same features as the $|\chi^{(3)}|^2$ measured in ARS. In particular, it bears the imprint of the interference of the electronic ($\chi^{(2)E}$) and ionic ($\chi^{(2)R}$) contributions, etc. However, the extraction from the experimental spectra $I^{(a)}$ ($\omega_a = \omega + \omega_{ir}$) of information on the dispersion curve of $|\chi^{(2)}(\omega_a;\ \omega,\ \omega_{ir})|^2$ should be accompanied by normalization of the experimentally measured $I^{(a)}$ (ω_a) curve to the square of the coherent-interaction length l_{coh} (ω_{ir}), which also undergoes dispersion near the infrared absorption line:

$$l_{coh}(\omega_{ir}) = \frac{1}{\pi}\Big/\sqrt{[\Delta k(\omega_{ir})]^2 + \left[\frac{1}{2}\alpha(\omega_{ir})\right]^2}, \tag{10.8}$$

Here $\Delta\mathbf{k}(\omega_{ir}) = \mathbf{k}_a - \mathbf{k}_{ir}(\omega_{ir}) - \mathbf{k}$ is the phase mismatch, where $\mathbf{k}_a$, $\mathbf{k}_{ir}$, and $\mathbf{k}$ are the wave vectors of the corresponding waves, and α (ω_{ir}) is the absorption coefficient of the infrared field.

Thus, here one must have exhaustive information on

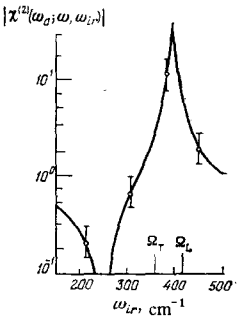

FIG. 26. Result of an experiment to measure the dispersion of the modulus of the quadratic susceptibility $|\chi^{(2)}(\omega_a;\ \omega,\ \omega_{ir})|$ of a GaP crystal for several values of the frequency ω_{ir} near the lattice resonance.[158] The solid line shows the result of calculating by Eq. (10.7) for $\Omega_q/2\pi c = 365$ cm^{-1}, $\Gamma = 10^{-2}\,\Omega$, $\chi^{(2)R}/\chi^{(2)E} = 53 \pm 3$.

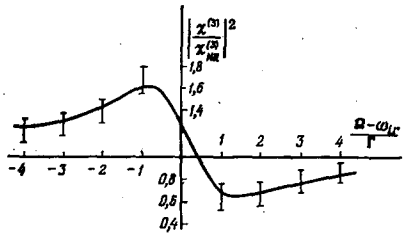

FIG. 27. Dispersion of the cubic susceptibility $|\chi^{(3)}(\omega_c; \omega, \omega, -\omega_{1r})|^2$ of liquid chloroform near the frequency of the first overtone of the C–H stretching vibration ($\Omega/2\pi c = 5828$ cm^{-1}) as measured by using a parametric light generator.[161]

the linear dispersion of the crystal in the infrared in order to get the dispersion curve of the nonlinear susceptibility. However, this information is not always easily attainable.

Figure 26 shows the result of the first experiment of the described type[158]: the spectrum of $|\chi^{(2)}|^2$ of a GaP crystal in the region of the lattice resonance at the frequency $\Omega_q/2\pi c = 365$ cm^{-1}. It was calculated from five experimental points measured upon mixing five discrete lines of an infrared laser with the line $\lambda = 6328$ Å of an He-Ne laser.

c) Active spectroscopy of hyper-Raman scattering of light. In addition to ordinary Raman scattering, direct infrared excitation of molecular or lattice vibrations can also stimulate a nonlinear Raman scattering that has also been called hyper-Raman scattering (HRS). Its spectrum is formed of lines that are shifted from the doubled frequency of the exciting light by the frequency of the corresponding optical modes: $\omega_{c,a} = 2\omega \pm \Omega$.[160] Spontaneous hyper-Raman scattering is described by a third-order tensor $(\partial\beta_{ijk}/\partial Q)_0$ (see (2.8)). In particular, it differs from zero for all vibrations that are manifested in the infrared absorption spectrum.[63] The corresponding coherent nonlinear-optical process proves to be a four-wave process and it is described by a third-order nonlinear susceptibility of the form $\chi^{(3)}(\omega_c; \omega, \omega, -\omega_{1r})$. One can conveniently measure it in a centrosymmetric medium, in which a contribution from the second-order nonlinear susceptibility is ruled out.[162] By using Eqs. (2.8)–(2.10), one can easily derive the following expression for $\chi^{(3)}$ under the assumption that the tensor $(\partial\beta_{ijk}/\partial Q)_0$ is symmetric with respect to the last two indices:

$$\chi^{(3)}_{ijkl}(\omega_c; \omega, \omega, -\omega_{1r}) = \chi^{(3)E}_{ijkl}(\omega_c; \omega, \omega, -\omega_{1r}) + \chi^{(3)R}_{ijkl}(\omega_c; \omega, \omega, -\omega_{1r}), \tag{10.9}$$

where

$$\chi^{(3)E}_{ijkl}(\omega_c; \omega, \omega, -\omega_{1r}) = NL^4\langle\gamma^E_{ijkl}\rangle, \tag{10.10}$$

$$\chi^{(3)R}_{ijkl}(\omega_c; \omega, \omega_1-\omega_{1r}) = \frac{NL^4}{8M\Omega\Gamma}\cdot\frac{1}{3}\left[\frac{\langle(\partial\beta_{ijk}/\partial Q)_0(\partial\mu_l/\partial Q)_0\rangle}{i-(\omega_{1r}-\Omega)\Gamma^{-1}}\right.$$
$$\left.+\frac{\langle(\partial\beta_{ilk}/\partial Q)_0(\partial\mu_j/\partial Q)_0\rangle}{i-(\omega-\Omega)\Gamma^{-1}}+\frac{\langle(\partial\beta_{ijl}/\partial Q)_0(\partial\mu_k/\partial Q)_0\rangle}{i-(\omega-\Omega)\Gamma^{-1}}\right]. \tag{10.11}$$

Here again, just as in ordinary ARS, the hyper-Raman lines have a pedestal that arises from the existence of a non-resonance electronic susceptibility. Thus, although here the line intensities can be very large, in contrast to spontaneous hyper-Raman scattering, yet the degree of suitability of the "active" spectra for measuring the hyper-Raman scattering tensor is again determined by the value of the "contrast" of the dispersion curve of $|\chi^{(3)}(\omega_c; \omega, \omega, -\omega_{1r})|^2$, which can often be too small. The first successful experiment on active spectroscopy of hyper-Raman scattering of the overtone of the C–H vibration in chloroform ($\Omega/2\pi c = 5828$ cm^{-1}) has been reported in Ref. 161 (see Fig. 27). The tunable line was furnished by the radiation of a parametric generator excited by the second harmonic of a Nd : YAG frequency laser, while the fundamental pump line (ω) was represented by the line $\lambda = 1.06$ μm of the same laser.

The value of $\bar{\chi}^{(3)R}_{1111}/\chi^{(3)E}_{1111}$ could be estimated from the curve shown in Fig. 27. It proved to be

$$\frac{\bar{\chi}^{(3)R}_{1111}}{\chi^{(3)E}_{1111}} = -0.5,$$

where

$$\bar{\chi}^{(3)R}_{1111} = \frac{1}{3}\cdot\frac{1}{8M\Omega\Gamma}\left\langle\left(\frac{\partial\beta_{111}}{\partial Q}\right)_0\left(\frac{\partial\mu_1}{\partial Q}\right)_0\right\rangle.$$

The experimental variation of $I^{(c)}$ ($\omega_c = 2\omega - \omega_{1r}$) had to be normalized to the square of the coherent line (see (10.8)), which underwent dispersion along with $|\chi^{(3)}|^2$.

The latter circumstance apparently restricts the application of this variant of active spectroscopy to studying well marked, isolated infrared absorption lines, since one can estimate the dispersion of l_{coh} accurately enough only for them.

We can easily see from (10.11) that the averaging over the orientations of the molecules causes the contribution to the value of $\chi^{(3)R}$ measured experimentally to give only the invariant of the vector part of the tensor $(\partial\beta_{ijk}/\partial Q)_0$. One can show this directly by expanding the corresponding nonlinear polarization into irreducible sets. sets.[163]

11. Active spectroscopy of anharmonic vibrations of molecules

a) Manifestation of mechanical and electrooptical anharmonicity of molecular vibrations in ARS. The electrooptical anharmonicity, which is manifested in the nonlinear parametric dependence of the polarizability α_{ij} of the molecule on the vibrational coordinates ($\partial^2\alpha_{ij}/\partial Q_\sigma \partial Q_{\sigma'} \neq 0$ (see (2.8)), is determined in the second-order spontaneous Raman spectra mainly by the intensity of the overtones and mixed tones.[62,63] Correspondingly, in ARS this same parameter, along with the line width, determines the peak value of $\chi^{(3)R}$ of the Raman susceptibility upon tuning $\omega_1 - \omega_2$ to the overtone frequency $\Omega^{(2)}$. However, the weakness of the overtones in second-order Raman spectra causes their contribution to the entire nonlinearity $\chi^{(3)}$ of the whole medium to be generally small. Therefore one cannot experimentally measure the dispersion of $|\chi^{(3)}|^2$ arising from the contribution of even the most intense overtones, such as the second-order line in the diamond crystal at the frequency $\Omega^{(2)}/2\pi c = 2666$ cm^{-1}.[60]

Some exceptions are the overtones whose intensities are anomalously large owing to the existence of Fermi resonance with first-order lines of the same symmetry. A strong dispersion of $|\chi^{(3)}|^2$ has been observed[164] in carbon dioxide near the first overtone of the vibration Π_u (02^00 line), which is the low-frequency component of a Fermi doublet. This same experiment also measured the weaker second-order vibrational transition (01^10)–(03^00).

One can considerably increase the contrast of the dispersion curves of $|\chi^{(3)}|^2$ near second-order lines by using one of the methods of removing the nondispersing pedestal of active spectra that were described in Secs. 3*b*, *d* and 4*b*. This opens up for coherent ARS a new broad and interesting set of spectroscopic applications. Electrooptical and mechanical anharmonicity of molecules is manifested in the scheme of active spectroscopy also in new physical effects that have no analog in spontaneous scattering, such as generation of harmonics of fundamental molecular vibrations upon intense "pumping" of vibrations at the fundamental frequency and parametric resonances in complicated molecules.

b) Generation of harmonics of dipole-forbidden molecular vibrations by using two-frequency pumping. Anharmonicity will cause the coherent response of a molecule to a resonance two-frequency exposure ($\omega_1 - \omega_2 = \Omega$, where ω_1 and ω_2 are the frequencies of the pump light waves, and Ω is the frequency of a fundamental Raman-active vibration) to contain spectral components at multiple frequencies $n(\omega_1 - \omega_2)$ ($n = 2, 3, \ldots$), as well as the fundamental harmonic. In particular, the polarizability at the frequency of the second harmonic $2(\omega_1 - \omega_2)$ of a molecule with the Hamiltonian of (2.8) can be expressed by the following formula[165] that was derived by solving the Liouville equation for the density matrix:

$$\alpha(2(\omega_1-\omega_2)) = \frac{[x(\partial\alpha/\partial Q)_0]^2[4x(\partial\alpha/\partial Q)_0(\beta x^3/\hbar\Omega) + x^2(\partial^2\alpha/\partial Q^2)_0]}{6\Omega(\beta^2x^6/\hbar\Omega) - 12\gamma x^4} G(\omega_1-\omega_2)(E^{(1)})^2(E^{(2)*})^2 = \gamma^{(5)R}(\omega_a;\ \omega_1, \omega_1, -\omega_2, \omega_1, -\omega_2)(E^{(1)})^2(E^{(2)*}); \tag{11.1}$$

here

$$\gamma = \left(\frac{\partial^4\Phi}{\partial Q^4}\right)_0, \quad G(\omega_1-\omega_2) = \int \frac{g(\omega_{10})\,d\omega_{10}}{\omega_1-\omega_2-\omega_{10}+i\Gamma_{10}}, \quad x = \sqrt{\frac{\hbar}{2M\Omega}}, \quad \beta = \left(\frac{\partial^3\Phi}{\partial Q^3}\right)_0.$$

$G(\omega_1 - \omega_2)$ is the distribution function of the vibrational frequencies ω_{10}; and $\gamma_R^{(5)}(\omega_a; \omega_1, \omega_1, -\omega_2, \omega_1, -\omega_2)$ is the fifth-order resonance Raman hyperpolarizability that describes the direct nonlinear process that follows the scheme $\omega_a = \omega_1 + 2(\omega_1 - \omega_2)$, which is used for detecting the coherent molecular response at the frequency of the second harmonic. The experiment was performed with compressed hydrogen. The given effect was discriminated from the competing repeated scattering by the fundamental molecular harmonic via the differing dependence of the intensities of the "direct" and "cascade" anti-Stokes signals on the gas pressure: $I^{(a)} \sim p^2$, while in the cascade process $I^{(a)} \sim p^4$. Thus the former process should dominate at low pressures. Unfortunately, the signal level here was so low (at the level of one photoelectron per 20 laser pulses) that it was impossible to perform reliable measurements giving information on the nonlinear response of the H_2 molecule.

Another experimental scheme seems more promising for recording the harmonics of molecular vibrations.

c) Direct excitation of anharmonic molecular vibrations that do not obey the alternative selection rule. One can use the following scheme to get information on the anharmonicity parameters of fundamental vibrations: the resonance infrared field

$$E^{(ir)} = \frac{1}{2}(E^{(ir)}e^{-i\omega_{ir}t} + \text{c.c.}) \tag{11.2}$$

excites coherent molecular vibrations at the frequency Ω, while their overtones are recorded in the visible according to the scheme $\omega_a = \omega + 2\omega_{ir}$, where ω is the frequency of the probe laser. (A centrosymmetric medium lacks the competing process of repeated scattering at the fundamental vibration frequency.) Again this process is described by the cubic nonlinear susceptibility

$$\chi^{(3)}(\omega_a;\ \omega,\ \omega_{ir},\ \omega_{ir}).$$

One can write the following expression for the resonance component of the nonlinear source $P^{(3)}(\omega_a)$ by using (2.8) and (2.9), while neglecting for simplicity the tensor properties of the quantities that enter into it:

$$P_R^{(3)}(\omega_a) = N\left[\left(\frac{\partial\alpha}{\partial Q}\right)_0 Q^{(2)}\mathscr{E} + \frac{1}{2}\left(\frac{\partial^2\alpha}{\partial Q^2}\right)_0 [Q^{(1)}]^2\mathscr{E}\right]; \tag{11.3}$$

Here $Q^{(1)}$ is the fundamental tone of the forced vibration and $Q^{(2)}$ is its first overtone.

Let us solve the Liouville equation for the density matrix with the Hamiltonian

$$\hat{\mathscr{H}} = \frac{P^2}{2m} + \frac{M\Omega^2Q^2}{2} + \frac{M\beta}{3}Q^3 + \gamma Q^4 \tag{11.4}$$

and the perturbation

$$\hat{V} = -\frac{1}{2}\left(\frac{\partial\mu}{\partial Q}\right)_0 Q\mathscr{E}$$

(β and γ are defined in (11.2)). Then we can easily derive an expression for the amplitude of the first overtone and then calculate the resonance hyperpolarizability of a single molecule (with account only for mechanical anharmonicity):

$$\gamma^{(3)R}(\omega_a;\ \omega,\ \omega_{ir},\ \omega_{ir}) = \frac{1}{4}\left(\frac{\partial\alpha}{\partial Q}\right)_0\left(\frac{\partial\mu}{\partial Q}\right)_0^2 \frac{M\beta x^6}{12\hbar^3\Omega}(\omega_{ir}-\Omega+i\Gamma_{10})^{-1}(2\omega_{ir}-\Omega^{(2)}+i\Gamma_{20})^{-1}; \tag{11.5}$$

Here

$$\Omega^{(2)} = 2\Omega - \left(\frac{20}{3}\frac{M^2\beta^2x^6}{\hbar^2\Omega} - \frac{12\gamma}{\hbar}x^4\right).$$

A characteristic feature of the hyperpolarizability of (11.5) is that it possesses two resonances, which are manifested upon tuning ω_{ir}.

One can also understand the fundamental features of

the studied mechanism in a purely classical description.[166]

The relationship of the amplitude of the overtone $Q^{(2)}$ to the anharmonicity parameter is not monotonic: when $|2\Omega - \Omega^{(2)}| < \Gamma_{10}, \Gamma_{20}$, then $Q^{(2)} \sim \beta$, while when $|2\Omega - \Omega^{(2)}| \geq \Gamma_{10}, \Gamma_{20}$, then $Q^{(2)} \sim 1/\beta$: The amplitude of the overtone is maximal when the value of β_0 satisfies the condition

$$2\Omega - \Omega^{(2)} \approx \frac{20}{3} \frac{M^2\beta_0^2 x^6}{\hbar^2\Omega} = \Gamma_{20}. \qquad (11.6)$$

Estimates show[166] that the anharmonicity is large ($2\Omega - \Omega^{(2)} \gg \Gamma_{20}$) in the CH_4 molecule for the fundamental vibration $\nu = 3020$ cm^{-1}, which is manifested simultaneously in both the infrared and the Raman spectra. Here we have $M\beta = 4\times10^{12}$ cm^{-3} erg, and

$$\bar{\gamma}^{(3)R}(\omega_a;\ \omega,\ \omega_{ir},\ \omega_{ir}) \approx 1\cdot10^{-37}\ \text{cm}^6/\text{erg},$$

whereas, according to Ref. 127,

$$\gamma^{(3)E}(\omega_a;\ \omega_{ir},\ \omega_{ir}) = 1\cdot10^{-37}\ \text{cm}^6/\text{erg}.$$

Thus the contributions of the discussed resonance process and of the electronic subsystem are comparable. In order to elevate the "contrast" of the dispersion curve of $|\chi^{(3)}(\omega_a;\ \omega,\ \omega_{ir},\ \omega_{ir})|^2$, one can employ one of the methods for removing the nondispersing pedestal that were discussed in Secs. 3*b*, *d* and 4*b*.

d) Parametric excitation of molecular vibrations. This process has been discussed[167] in connection with the threshold nature of laser chemical reactions. Yet direct experiments in which this process has been detected are still lacking. Moreover, experiments on nonsteady-state ARS have demonstrated[130] that the parametric instability processes that have been predicted[45] are not manifested in condensed media, even at very high levels of excitation of coherent optical photons obtained by stimulated Raman scattering of high-power picosecond pulses. Thus the lifetime of the coherent elementary excitations does not differ from that of spontaneous excitations.

Nevertheless, classical calculations of the coherent parametric excitation thresholds in triatomic atoms[49] show that the threshold intensities are lower than the saturation intensity in molecular beams and in a low-pressure gas.

One can detect parametrically excited molecules by the methods of coherent and incoherent ARS.

12. Active spectroscopy of elementary excitations in noncentrosymmetric crystals (effects that are cubic in the field

a) Coherent ARS *of bulk polaritons. Spectroscopy in* **k***-space.* Thus far we have been considering only centrosymmetric media in speaking of the spectroscopy of the cubic susceptibilities. The dispersion of the susceptibility $\chi^{(3)}_{ijkl}(\omega_a;\ \omega,\ \omega_1,\ -\omega_2)$ is more complicated in nature in noncentrosymmetric crystals. It is governed not only by the phonon modes having $\mathbf{q} = 0$, but also by the polariton modes, which amount to propagating dipole-active states of mixed nature. In particular, we shall treat in the infrared. As before, we can use the microscopic model introduced in Sec. 2*c* in calculating the corresponding third-order susceptibilities. However, one can understand the fundamental features of the described process also in a phenomenological description.[168]

The distinctive nature of the active spectroscopy of polaritons arises from the fact that the intrinsic frequencies of these states depend on the wave vector $\Omega = \Omega(\mathbf{q})$, owing to strong coupling with the transverse infrared field, and also from the fact that an additional channel for generation of anti-Stokes radiation exists in noncentrosymmetric crystals: here a two-cascade process involving the quadratic nonlinearity also exists in addition to the direct four-photon process $\omega_a = \omega + \omega_1 - \omega_2$. In the first stage, a wave at the difference frequency $\omega' = \omega_1 - \omega_2$ is excited. Frequency mixing according to the scheme $\omega_a = \omega + \omega'$ occurs in the second stage. In other words, interference processes occur that involve nonlinear susceptibilities of different orders. Whenever the wave at the difference frequency falls in the polariton region, i.e., when $\omega_1 - \omega_2 \approx \Omega(\mathbf{q})$, $\mathbf{k}_1 - \mathbf{k}_2 \approx \mathbf{q}$, the efficiency of the cascade process rises sharply. Thus the ARS signal here depends not only on the frequency difference of the pump waves, but also on the difference of their wave vectors $\mathbf{k}'$, which allows us to speak of spectroscopy in $\mathbf{k}$-space.[24] In describing polariton effects, one must allow for the retardation of the Coulombic interaction forces between the ions arising from the finite velocity of light.[169,170]

The detailed calculation of the effective cubic susceptibility $\chi^{(3)}_{eff}(\omega_a;\ \omega_1,\ \omega_1,\ -\omega_2)$ is highly cumbersome even for very simple crystals of cubic symmetry,[171] and we shall not present it. We shall only point out that one can represent $\chi^{(3)}_{eff}$ in the form

$$\chi^{(3)\,\text{eff}}_{ijkl}(\omega_a;\ \omega_1,\ \omega_1,\ -\omega_2)$$

$$= \chi^{(3)}_{ijkl}(\omega_a;\ \omega_1,\ \omega_1,\ -\omega_2) + \chi^{(3)\,\text{casc}}_{ijkl}(\omega_a;\ \omega_1,\ \omega_1,\ -\omega_2),$$

Here $\chi^{(3)}_{ijkl}$ describes the "direct" four-photon process, while $\chi^{(3)\text{casc}}_{ijkl}$ describes the two-cascade process that involves the quadratic nonlinearity.[171]

In contrast to the "direct" susceptibility $\chi^{(3)}_{ijkl}$, the susceptibility $\chi^{(3)\text{casc}}_{ijkl}$ of the "cascade" process depends on $\mathbf{k}_1$ and $\mathbf{k}_2$. That is, it undergoes spatial dispersion.

Observation in ARS of "transverse" phonon-like resonances can happen if the wave vectors $\mathbf{k}_1$ and $\mathbf{k}_2$ lie in the xy plane ($\Delta\mathbf{k}_z = 0$), and the synchronization condition $(c\Delta k/\Delta\omega)^2 = \varepsilon(\Delta\omega)$ holds for the polaritons.

This is just the situation in which F. DeMartini *et al.*[24] and J. Wynne[34] have experimentally observed a strong dispersion of the anti-Stokes signal $I^{(a)}(\omega_a = 2\omega_1 - \omega_2)$ (Fig. 28). In addition to the dispersion law for the polaritons, ARS permits one also to determine their damping from the width of the resonance.[24,174]

Whenever the frequencies $2\omega_1$ and $\omega_1 - \omega_2$ are far

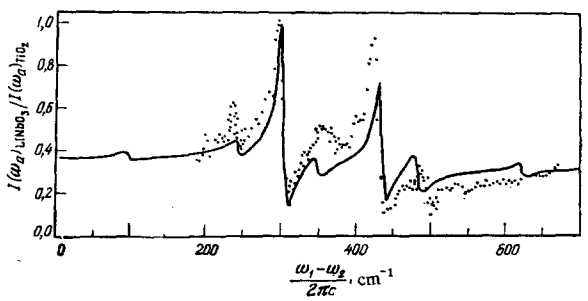

FIG. 28. Dispersion of the anti-Stokes signal from an $LiNbO_3$ crystal upon tuning the pump frequency difference $\omega_1-\omega_2$ in the polariton region (dots).[34] The ARS signal is normalized to the nondispersing signal obtained with a control specimen of rutile (TiO_2). Solid line—calculation, dots—experiment.

from resonances, observation of interference of the "direct" and "cascade" processes in generation of the anti-Stokes frequency $\omega_a=2\omega_1-\omega_2$ can be used for exact determination of the absolute magnitude and sign of the susceptibility $\chi^{(3)E}$ by comparing it with the value of $|\chi^{(3)E}|^2$ measured in independent experiments[172,173] (see also Refs. 194 and 195).

b) Coherent ARS of surface states. The high intensity of the scattered signal in a coherent ARS scheme allows us to pose the question of using this method for studying such weak processes as light scattering by surface states—in particular by surface polaritons or plasmons.[175,176]

Study of surface states gives valuable information on the state of the surface of semiconductors or metals, and also of layers of oxides or other compounds covering them.[177]

Calculations show[178–180] that the use of coherent excitation of surface polaritons by employing a biharmonic pump and observing the scattering of the probe wave by them in the synchronization direction can give an increase in the scattering efficiency by several orders of magnitude as compared with spontaneous Raman scattering.

Just as in the case of bulk polaritons, coherent surface polaritons are efficiently excited by the biharmonic pump (ω_1, $\mathbf{k}_1$), (ω_2, $\mathbf{k}_2$) when the wave at the difference frequency that is generated by the quadratic nonlinear polarization falls in the dispersion region of the surface polaritons, $\omega_1-\omega_2\approx\Omega_q$, $k_{1x}-k_{2x}\approx q_x'$, where Ω_q and $q_x=q_x'+iq_x''$ are the frequency and the complex wave vector of the free polaritons, which are interrelated by the dispersion relation

$$q_x^2=\left(\frac{\Omega_q}{c}\right)^2\frac{\varepsilon(\Omega_q)}{1+\varepsilon(\Omega_q)},$$

where ε is the complex dielectric constant of the nonlinear crystal. We assume that the crystal borders on a linear optical medium that has $\varepsilon_0\approx1$; the x axis lies along the phase-boundary plane. One can calculate the amplitude of the stimulated surface wave by using the Maxwell equations (in which one must take the ordinary bulk polarization $P_i^{(2)}(\omega_1-\omega_2,\ \mathbf{k}_1-\mathbf{k}_2)=2\chi_{ijk}^{(2)}(\omega_1-\omega_2)E_j^{(1)}E_k^{(2)*}\exp[i(\omega_1-\omega_2)t+i(\mathbf{k}_1-\mathbf{k}_2)\cdot\mathbf{r}$ as the nonlinear source). Here one uses the commonly adopted boundary conditions in nonlinear optics in treating the effects at the phase bounadry.[180] The result contains the linear and quadratic susceptibilities of the crystal. As a function of $\Delta k_x=(k_{1x}-k_{2x})-q_x'$, it has a Lorentzian shape with the half-width of $(\Delta k_x)_{1/2}=2q_x''$.[180]

One can detect coherent surface polaritons according to the following scattering scheme of the probe ray: $\omega_{c,a}=\omega\mp(\omega_1-\omega_2)$, where ω is the frequency of the probe light. As usual, the scattering reaches a maximum in the synchronization direction. However, in contrast to the ARS of bulk polaritons, one requires here agreement of only the tangential components of the wave vactors, $(k_{c,a})_x=k_x\mp(k_{1x}-k_{2x})$.[180] The intensity of the component of the probe wave scattered in the synchronization direction upon tuning the difference of the wave vectors Δk_x (with a fixed frequency difference $\Delta\omega=\omega_1-\omega_2$) again has a Lorentzian shape with a maximum at $\Delta k_x=0$ and a half-width $(\Delta k_x)_{1/2}=2q_x''$. This makes it possible to study not only the dispersion curve of the surface polaritons, but also their damping. Figure 29 shows the results of the first experiment of DeMartini *et al.*[181] on coherent ARS of surface polaritons in GaP. The measured level of the scattered component ($P_a=0.1$ μW for $P_{1,2}=50$ kW) agrees with the calculations.[180] It is important to note that in these experiments the level of the nondispersing signal caused by the competing direct four-photon process involving the electronic nonlinearity proved to be considerably lower than the resonance signal from scattering by the coherent surface polaritons, owing to the difference in the synchronization conditions for the useful and the competing effects.

A recent study[182] reports the successful application of the stated technique for exciting and detecting surface excitonic polaritons in ZnO.

c) Active exciton spectroscopy. Interference of exciton and phonon resonances. One can also apply the nonlinear optical process that employs the frequency shift according to the scheme $\omega_a=\omega+\omega_1-\omega_2$ for probing high-frequency resonances (electronic and excitonic), if, suppose, the frequency combination $\omega+\omega_1$

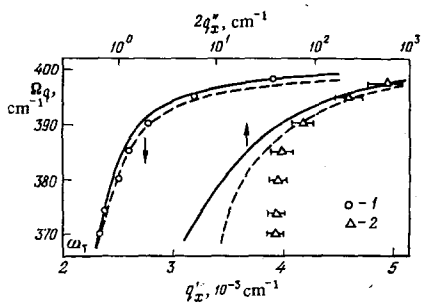

FIG. 29. Dispersion characteristics of surface polaritons in GaP. 1—q_x' as a function of Ω_q, 2—$2q_x''$ as a function of Ω_q, as measured by using an ARS system.[181] Solid line—calculation taking account of the contribution solely from one lattice mode; dotted line—the same for a multioscollator model.

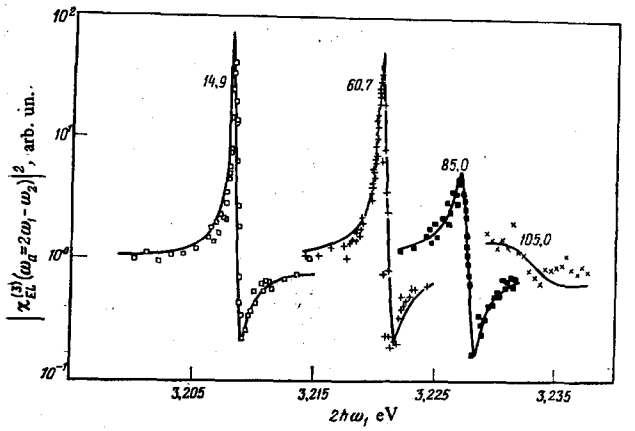

FIG. 30. Dispersion of $|\chi^{(3)}_{EL}(\omega_a; \omega_1, \omega_1, -\omega_2)|^2$ of a CuCl crystal upon tuning $2\omega_1$ about the resonance with a longitudinal exciton for various crystal temperatures[42,184] (in kelvins).

is scanned about the frequency of the appropriate transition. The main merit of using the frequency shift typical of ARS in this case consists in the idea that the entire field that participates in probing can have frequencies in a region of transparency of the medium. Thus we exclude the effect of dispersion of the linear optical parameters on the spectra to be measured.[42,184] In particular, measurement of the dispersion of the effective third-order nonlinear susceptibility $|\chi^{(3)}_{eff}(\omega_a; \omega_1, \omega_1, -\omega_2)|^2$ of the CuCl crystal allowed Bloembergen and his associates[42] to perform a complete spectroscopic study of the nonlinear characteristics of a Z_3-type excitonic polariton and its damping, including the temperature-dependence over a broad range (cf. also[185-189]).

Strictly speaking, the semiclassical formalism presented in Sec. 2 no longer suffices for describing the dispersion of the cubic susceptibility in the exciton region, nor the interference of the exciton and phonon resonances. However, as analysis of the pertinent theories shows,[171] one can describe the state of the excitonic subsystem by using the exciton "coordinates" $Q^{(e)}_\sigma$ in the immediate vicinity of isolated exciton resonances lying below the frequencies of the interband transitions, while one can describe its response to an external agent by using a Hamiltonian coinciding with (2.8) in form. Here the quantities α^E_{ij}, β^E_{ijk}, γ^E_{ijkl}, ... must be replaced by $\alpha^{E'}_{ij}$, $\beta^{E'}_{ijk}$, $\gamma^{E'}_{ijkl}$, ..., respectively, which contain contributions only from the interband transitions, whereas the excitonic contributions must be accounted for by using an equation of motion in the form of (1.7). Evidently the excitonic and non-resonance electronic parameters generally depend on the displacements of the ions from their equilibrium positions. In the case where these displacements are small, they can be expanded in a power series in the phonon coordinates. In particular, this implies that interference can occur between the exciton and phonon oscillators. Since a full analogy exists between the equations that describe the exciton and phonon subsystems, we may omit the distinctions between the indices σ, σ', and σ'' that refer to any given subsystem. We must only bear in mind that the resonance effect exerted by the field on the phonons occurs when $\omega_1 - \omega_2 \approx \Omega_\sigma$, while it happens for excitons at $2\omega_1 \approx \Omega^{(e)}_\sigma$. One should correspondingly change the resonance denominators in the formulas that describe the phonon dispersion of the nonlinear susceptibilities.

Figure 30 shows as an example the dispersion curves of $|\chi^{(3)}(\omega_a; \omega_1, \omega_1, -\omega_2)|^2$ of a CuCl crystal that were obtained[42] upon scanning $2\omega_1$ near the frequency of a Z_3-type "longitudinal" exciton. The different curves pertain to different crystal temperatures that are indicated by the numbers (in °K) beside the corresponding curves. We can distinctly see the displacement of the exciton frequency and the broadening of the resonance curve that corresponds to the increased exciton decay with increasing temperature.

As it turned out,[184] the experimental temperature-dependence of the exciton decay constant is well described by the formula

$$\Gamma = \Gamma_0 + \bar{B}|e^{\hbar\Omega_R/kT} - 1|^3, \qquad (12.1)$$

where Ω_R is the frequency of the longitudinal optical phonon that participates in the decay of the exciton, k is the Boltzmann constant, T is the temperature, and B characterizes the exciton-phonon coupling. This relationship corresponds to the decay of a Z_3-type into a Z_2-type exciton, which has an energy 0.07 eV lower, and into three longitudinal phonons of energy $\hbar\Omega_R \approx 0.025$ eV. This experimental result sharply contradicts Toyozawa's[190] theoretical predictions.

Whenever the frequency $2\omega_1$ is close to the exciton frequency $\Omega^{(e)}$, while $\omega_1 - \omega_2 = \Omega_R$ is a phonon frequency, the spectrum of $|\chi^{(3)}(\omega_a; \omega_1, \omega_1, -\omega_2)|^2$ can manifest interference effects analogous to those discussed in Sec. 4 in connection with the interaction of vibrational and one-quantum electronic resonances in a molecule. Figure 8 shows the deformation of the contour of $|\chi^{(3)}(\omega_a; \omega_1, \omega_1, -\omega_2)|^2$ of a CuCl crystal in the region of resonance with a longitudinal phonon: $\omega_1 - \omega_2 = \Omega_L$, with $\Omega_L/2\pi c \approx 280$ cm^{-1}, as $2\omega_1$ is scanned about the exciton resonance $\hbar\Omega^e \approx 3.208$ eV. Just as in the case of isolated molecules, the observation of interference here allows us to compare the quantities pertaining to the one type of resonance with the corresponding quantities that characterize the other resonance. In particular, the authors of Ref. 42 were able to determine from the known data on the Z_3-type excitonic transition to determine the spontaneous Raman cross-section of a longitudinal phonon. The latter turned out to be smaller by a factor of six than that estimated in Ref. 191 on the basis of absolute measurements. Perhaps this difference stems from the large errors that are unavoidable in the absolute measurements.

IV. CONCLUSION. THE CURRENT STATE OF FOUR-PHOTON NONLINEAR SPECTROSCOPY

The material that we have presented in this review indicates that active spectroscopy of light scattering near phonon, exciton, and electronic resonances has become

one of the fundamental universal methods of nonlinear spectroscopy in studying gases, liquids, and solids, owing to the intensive development during the past 4–5 years.

Just as in the other methods of nonlinear spectroscopy,[116] the information obtained in active spectroscopy has a double nature. On the one hand, one can get the same information by the method of active spectroscopy with greater sensitivity, accuracy, and better spectral resolution than by the methods of traditional linear spectroscopy. From this standpoint the polarization and resonance variants of active spectroscopy are of especial interest. The great possibilities of active spectroscopy in analytical applications have already been clearly elucidated, and they substantially surpass at a number of points the analogous possibilities of the traditional methods of spectroscopy.

On the other hand, as is natural, active spectroscopy also allows one to measure an entire set of parameters that are beyond the reach of linear spectroscopy. Of special interest here are the possibilities of shaping the contour of the line of a resonance transition, of measuring the signs and relative phases of the different contributions to the nonlinear susceptibility, of observing interference of different effects (which often occur even in different molecules), of directly measuring relaxation times and establishing the channels of dissipation of the energy of excited states, of performing spectroscopy in **k**-space, etc.

If we approach from the standpoint of phenomenological interpretation of nonlinear spectroscopy based on measuring the cubic optical susceptibilities $\chi^{(3)}$, then the variants of active spectroscopy discussed here amount to different special cases of four-photon nonlinear spectroscopy. From the standpoint of such a phenomenological classification, we should say that in many cases we should classify with four-photon spectroscopy also saturation spectroscopy and two-photon absorption (TPA) spectroscopy. In particular, this is just why one can measure the two-photon absorption cross-section by the methods of ASRS. Yet we should note that the methods of ASRS and two-photon absorption have developed independently to a considerable degree. Hence it has been only in very recent time that the methods developed in one of these methods have begun to be transferred to the other.

For example, in TPA spectroscopy, detection was effected for a long time by measuring either the direct absorption or the luminescence that accompanies it. And only very recently have studies appeared in which the coherent response of a two-photon transition was detected (e.g., Refs. 140 and 141).

The methods of active spectroscopy of Raman and hyper-Raman light scattering are very closely interrelated. In fact the methods can be fully transferred from ARS to active spectroscopy of hyper-Raman scattering.

An interesting variant of four-photon spectroscopy has been developed in recent years.[192,193,210] This refers to four-photon spectroscopy within a spectral line in which all of the applied frequencies lie within the contour of a single resonance, while all the frequency differences do not exceed the overall width of the absorption line. Here one can trace the analogy with one- and two-photon spectroscopy within an inhomogeneously broadened line.

Very recently the spectroscopic information that is obtained upon measuring the higher nonlinearities has been discussed ever more widely. In certain sections of the review, we have already touched upon this problem from the standpoint of studying the dispersion of the fifth-order nonlinearity $\chi^{(5)}$ (see also Ref. 194).

Finally, as we have pointed out, one of the interesting aspects of active spectroscopy is the study of strongly excited atomic and molecular systems, especially under conditions of selective excitation by a laser beam. The discovery of the phenomenon of collisionless dissociation of molecules in a strong infrared field[144] has made the spectroscopic study of molecules in highly excited vibrational states very topical. The methods of active spectroscopy can be used for separate measurement of the coherent and incoherent components of the excitation.

[1]G. S. Landsberg and L. I. Mandel'shtam, Naturwissenschaften **16**, 557 (1928); Prikl. Fiz. **6**, 155 (1929); see also: L. I. Mandel'shtam, Trudy (Works), Vol. 1, Izd-vo AN SSSR, M.-L., 1948, p. 318.
[2]E. Woodbury and W. K. Ng, Proc. IRE **50**, 2347 (1962).
[3]G. Eckardt, R. W. Hellwarth, F. J. McClung, S. E. Schwartz, D. Weiner, and E. Woodbury, Phys. Rev. Lett. **9**, 455 (1962).
[4]R. W. Hellwarth, Phys. Rev. **130**, 1850 (1963).
[5]V. T. Paltonenko and R. V. Khokhlov, Zh. Eksp. Teor. Fiz. **46**, 555, 2126 (1964) [Sov. Phys. JETP **19**, 378, 1435 (1964)].
[6]E. Garmire, E. Pandarese, and C. Townes, Phys. Rev. Lett. **11**, 160 (1963).
[7]S. A. Akhmanov and R. V. Khokhlov, Problemy nelineĭnoĭ optiki (Problems of Nonlinear Optics), Izd. VINITI, M., 1964 (Engl. Transl., Gordon & Breach, N. Y., 1972).
[8]N. Bloembergen, Nonlinear Optics, Benjamin, N. Y., 1965 (Russ. Transl., Mir, M., 1965).
[9]G. Placzek, Rayleigh Scattering and the Raman Effect, in Handbuch der Radiologie, Ed. E. Marx, Vol. 6, Pt. 2, Akademische Verlagsgesellschaft, Leipzig, 1934 (Engl. Transl., Lawrence Radiation Laboratory, Univ. of California, Livermore, 1959; Russ. Transl., ONTIU, Kiev–Kharkov, 1934).
[10]N. Bloembergen, Am. J. Phys. **35**, 989 (1967).
[11]V. S. Starunov and I. L. Fabelinskiĭ, Usp. Fiz. Nauk **98**, 441 (1969) [Sov. Phys. Usp. **12**, 463 (1970)].
[12]B. Ya. Zel'dovich and I. I. Sobel'man, Usp. Fiz. Nauk **101**, 3 (1970) [Sov. Phys. Usp. **13**, 307 (1970)].
[13]W. Kaiser and M. Maier, in: Laser Handbook, Ed. F. T. Arecchi and E. O. Schulz-Dubois, v. 2, Amsterdam, North-Holland, 1972, p. 1077.
[14]M. Maier, Appl. Phys. **11**, 209 (1976).
[15]N. Bloembergen, G. Bret, P. Lallemand, A. Pine, and P. Simova, IEEE J. Quantum Electron. **QE-3**, 197 (1967).
[16]S. R. Brueck and A. Mooradian, Opt. Comm. **8**, 263 (1973).
[17]I. Reinhold and M. Maier, *ibid.* **5**, 31 (1972).
[18]H. Görner, M. Maier, and W. Kaiser, J. Raman Spectroscop. **2**, 363 (1974).
[19]P. A. Apansevich and V. A. Orlovich, Ispol'zovanie VKR

dlya izmereniya sechenii kombinatsionnogo rasseyaniya (Use of Stimulated Raman Scattering for Measuring Raman Cross-Sections), in All-Union Conference on Raman Scattering of Light, Kiev, 1975 (abstracts).
[20]P. Maker and R. Terhune, Phys. Rev. **A137**, 801 (1965).
[21]S. A. Akhmanov, A. I. Kovrigin, N. K. Kulakova, A. K. Romanyuk, M. M. Strukov, and R. V. Khokhlov, Zh. Eksp. Teor. Fiz. **48**, 1202 (1965)[Sov. Phys. JETP **21**, 801 (1965)].
[22]J. A. Giordmaine and W. Kaiser, Phys. Rev. **144**, 676 (1966).
[23]G. Chartier and S. Biraud-Laval, Phys. Rev. Lett. **21**, 1641 (1968).
[24]J. P. Coffinet and F. De Martini, *ibid.* **22**, 60 (1969).
[25]J. J. Wynne, Phys. Rev. **188**, 1211 (1969).
[26]E. Yablonovitch, N. Bloembergen, and J. J. Wynne, *ibid.* **B3**, 2060 (1971).
[27]J. J. Wynne, *ibid.* **B6**, 534 (1972).
[28]J. P. Woerdeman and B. Bolger, Phys. Lett. **A30**, 164 (1969).
[29]A. A. Borshch, M. S. Brodin, V. V. Ovchar, S. G. Odulov, and M. S. Soskin, Pis'ma Zh. Eksp. Teor. Fiz. **18**, 679 (1973) [JETP Lett. **18**, 397 (1973)].
[30]A. S. Rubanov and E. V. Ivakin, Dokl. Akad. Nauk B SSR **14**, 506 (1970).
[31]D. W. Pohl, S. E. Schwarz, and V. Irniger, Phys. Rev. Lett. **31**, 32 (1973).
[32]F. DeMartini and J. Ducuing, *ibid.* **17**, 117 (1966).
[33]S. A. Akhmanov, V. G. Dmitriev, A. I. Kovrigin, N. I. Koroteev, V. G. Tunkin, and A. I. Kholodnykh, Pis'ma Zh. Eksp. Teor. Fiz. **15**, 600 (1972) [JETP Lett. **16**, 425 (1972)]; Rept. at 7th Intern. Quantum Electronics Conference, Montreal, Canada, 1973; IEEE J. Quantum Electron. **QE-10**, 680 (1972).
[34]J. J. Wynne, Phys. Rev. Lett. **29**, 650 (1972); Rept. at 7th Intern. Quantum Electron. Conference, Montreal, Canada, 1972.
[35]M. D. Levenson, C. Flytzanis, and N. Bloembergen, Phys. Rev. **B6**, 3962 (1972).
[36]S. A. Akhmanov and N. I. Koroteev, Zh. Eksp. Teor. Fiz. **67**, 1306 (1974) [Sov. Phys. JETP **40**, 650 (1975)].
[37]Won B. Roh, P. W. Schreiber, and J. P. E. Taran, Appl. Phys. Lett. **29**, 174 (1976).
[38]S. A. Akhmanov, N. I. Koroteev, and A. I. Kholodnykh, J. Raman Spectroscopy **2**, 209 (1974).
[39]A. Lewis, Spex Speaker **21** (2), 1 (1976).
[40]A. F. Bunkin, S. G. Ivanov, and N. I. Koroteev, Pis'ma Zh. Tekh. Fiz. **3**, 450 (1977) [Sov. Tech. Phys. Lett. **3**, 182 (1977)].
[41]A. F. Bunkin, S. G. Ivanov, and N. I. Koroteev, Pis'ma Zh. Eksp. Teor. Fiz. **24**, 468 (1976) [JETP Lett. **24**, 429 (1976)].
[42]S. D. Kramer and N. Bloembergen, Phys. Rev. **B14**, 4654 (1976).
[43]D. W. Pohl and V. Irniger, Phys. Rev. Lett. **36**, 480 (1976).
[44]R. W. Hellwarth, Appl. Phys. **11**, 147 (1976).
[45]R. Orbach, IEEE Trans. Sonics and Ultrasonics **SU-14**, 140 (1967).
[46]D. von der Linde, A. Lauberau, and W. Kaiser, Phys. Rev. Lett. **27**, 802 (1971).
[47]I. B. Levinson, Fiz. Tekh. Poluprovodn. **9**, 1673 (1973)[sic].
[48]Fizika fononov bol'shikh energii (Physics of High-Energy Phonons), Mir, M., 1976.
[49]S. A. Akhmanov, A. A. Vigasin, and V. N. Seminogov, in Teoreticheskaya spektroskopiya (Theoretical Spectroscopy) (Proceedings of the 18th All-Union Congress on Spectroscopy), Gor'kii, June 1977.
[50]V. S. Letokhov, Usp. Fiz. Nauk **118**, 199 (1976) [Sov. Phys. Usp. **19**, 109 (1976)].
[51]Y. R. Shen, Rev. Mod. Phys. **48**, 1 (1976).
[52]W. Kaiser, Kvantovaya Elektron., No. 1, "Sov. Radio", M., 1973, p. 2500: see also in Spectroscopia Nonlineare. Rendiconti della Scuola Intern. di Fisica "Enrico Fermi" LXIV Corso a cura di N. Bloembergen, Amsterdam-New York-Oxford, North-Holland, 1977, p. 404.
[53]I. L. Fabelinskii and M. S. Pesin, Usp. Fiz. Nauk **120**, 273 (1973) [Sov. Phys. Usp. **19**, 844 (1976)].
[54]R. L. Byer, R. F. Begley, and A. B. Harvey, Appl. Phys. Lett. **25**, 387 (1974).
[55]F. DeMartini, G. P. Giuliani, and E. Santamoto, Opt. Comm. 5, 126 (1972); **9**, 176 (1973).
[56]C. Flytzanis, in: Quantum Electronics: A Treatise, Ed. by H. Rabin and C. L. Tang, v. 1A, N.Y., Academic Press, 1975, p. III.
[57]P. Butcher, Nonlinear Optical Phenomena, Ohio State University, Ohio, USA, 1966.
[58]J. Schubert and B. Wilhelmi, Introduction to Nonlinear Optics (Russ. transl.) Mir, M., 1973.
[59]D. A. Kleinman, Phys. Rev. **126**, 1977 (1962).
[60]M. D. Levenson and N. Bloembergen, *ibid.* **B10**, 4447 (1974).
[61]R. T. Lynch Jr., M. D. Levenson, and N. Bloembergen, Phys. Lett. **A50**, 61 (1974).
[62]M. M. Sushchinskii, Spektry kombinatsionnogo rasseyaniya molekul i kristallov (Raman Spectra of Molecules and Crystals), Nauka, M., 1969 (Engl. Transl., Israel Program for Scientific Translations, N.Y., 1972).
[63]J. A. Koningstein, Introduction to the Theory of the Raman Effect, Reidel, Dordrecht, 1972 (Russ Transl., Mir, M., 1975).
[64]H. A. Szymanski, Raman Spectroscopy, ed. 1, 2, N.Y., Plenum Press, 1967, 1970.
[65]M. Born and E. Wolf, Principles of Optics, 4th Edn., Pergamon Press, Oxford, N.Y. 1969 (Russ. Transl., Nauka, M., 1970).
[66]A. F. Bunkin, S. G. Ivanov, and N. I. Koroteev, Dokl. Akad. Nauk SSSR 233, 82 (1977).
[67]M. A. Yuratich and D. C. Hanna, Opt. Comm. **18**, 134 (1976).
[68]I. V. Aleksandrov, Ya. S. Bobovich, N. M. Belyavskaya, A. V. Bortkevich, and V. G. Maslov, Zh. Eksp. Teor. Fiz. **68**, 1274 (1975) [Sov. Phys. JETP **41**, 632 (1975)].
[69]N. I. Koroteev, Paper given at the 4th Vavilov Conference on Nonlinear Optics, Novosibirsk, 1975; Kvantovaya Elektron. (Moscow) **3**, 755 (1976) [Sov. J. Quantum Electron. **6**, 411 (1976)].
[70]S. A. Akhmanov, Lecture given at the E. Fermi International School of Physics, Varenna, Italy, 1975; see Ref. 52, p. 217.
[71]J. J. Song, G. L. Eesley, and M. D. Levenson, Appl. Phys. Lett. **29**, 567 (1976).
[72]D. Heiman, R. W. Hellwarth, M. D. Levenson, and G. Martin, Phys. Rev. Lett. **36**, 189 (1976).
[73]L. M. Sverdlov, M. A. Kovner, and E. P. Krainov, Kolebatel'nye spektry mnogoatomnykh molekul (Vibrational Spectra of Polyatomic Molecules), "Nauka", M., 1970.
[74]A. Lau, Paper given at the 4th Vavilov Conference on Nonlinear (Moscow) **3**, 739 (1976) [Sov. J. Quantum Electron. **6**, 402 (1976)].
[75]J. F. Nye, Physical Properties of Crystals, Clarendon Pres Press, Oxford, 1957 (Russ. Transl., Mir, M., 1967).
[76]R. Loudon, Adv. Phys. **13**, 423 (1964).
[77]J. Midwinter, and J. Warner, Brit. J. Appl. Phys. **16**, 1667 (1965).
[78]W. Wernke, J. Klein, A. Lau, K. Lenz, and G. Hunsalz, Opt. Comm. **11**, 159 (1974).
[79]M. D. Levenson, J. J. Song, R. W. Hellwarth, and D. Heiman, *ibid.* **18**, 133 (1976).
[80]A. Owyoung, App. Phys. Lett. **26**, 168 (1975).
[81]S. A Akhmanov, A. P. Sukhorukov, and R. V. Khokhlov, Usp. Fiz. Nauk **93**, 19 (1967) [Sov. Phys. Usp. **10**, 609 (1968)].
[82]A. Owyoung, Opt. Comm. **16**, 266 (1976).
[83]J. J. Barrett, Appl. Phys. Lett. **29**, 722 (1976).
[84]S. A. Akhmanov, A. F. Bunkin, S. G. Ivanov, N. I. Koroteev, A. I. Kovigin, and I. L. Shumai, in: Tunable Lasers and Applications, Ed. A. Mooradian, and S. Stokseth, T. Jaeger, Berline–Heidelberg-New York, Springer–Verlag, 1976,

p. 389.
[85]M. D. Levenson, and N. Bloembergen, J. Chem. Phys. **60**, 1323 (1974).
[86]R. T. Lynch and H. Lotem, *ibid.* **66**, 1905 (1977).
[87]R. T. Lynch and H. Lotem, Phys. Rev. Lett. **37**, 323 (1976).
[88]V. A. Bredikhin, M. D. Galanin, and V. N. Genkin, Usp. Fiz. Nauk **110**, 3 (1973) [Sov. Phys. Usp. **16**, 299 (1973)].
[89]J. G. Skinner and W. G. Nilsen, J. Opt. Soc. Am. **58**, 113 (1968).
[90]V. S. Gorelik and M. M. Sushchinskiĭ, Fiz. Tverd. Tela (Leningrad) **12**, 1475 (1970) [Sov. Phys. Solid State **12**, 1157 (1970)].
[91]R. K. Chang and D. G. Fouche, Appl. Phys. Lett. **20**, 256 (1972).
[92]S. A. Akhmanov, S. M. Saltiel, V. G. Tunkin, and S. N. Parinov, Zh. Eksp. Teor. Fiz. (1977).
[93]R. T. Lynch, S. D. Kramer, H. Lotem, and N. Bloembergen, Opt. Comm. **16**, 372 (1976).
[94]H. Lotem, R. T. Lynch, and N. Bloembergen, Phys. Rev. **A14**, 1748 (1976).
[95]P. R. Regnier and J. P. E. Taran, Appl. Phys. Lett. **23**, 240 (1973). P. R. Regnier and F. Moya, J. P. E. Taran, AIAA J. **12**, 826 (1974).
[96]J. E. Moore and L. M., Fraas, Anal. Chem. **45**, 2009 (1973).
[97]M. D. Levenson, IEEE J. Quantum Electron. **QE-10**, 110 (1974).
[98]S. A. Akhmanov, K. N. Drabovich, A. P. Sukhorukov, and A. S. Chirkin, Zh. Eksp. Teor. Fiz. **59**, 485 (1970) [Sov. Phys. JETP **32**, 266 (1971)]; S. A. Akhmanov, Mater. Res. Bull. **4**, 455 (1969).
[99]R. L. Carman, F. Shimizu, C. S. Wang, and N. Bloembergen, Phys. Rev. **A2**, 60 (1970).
[100]T. M. Makhviladze, M. E. Sarychev, and L. A. Shelepin, Zh. Eksp. Teor. Fiz. **69**, 499 (1975) [Sov. Phys. JETP **42**, 255 (1975)].
[101]T. M. Makhviladze and M. E. Sarychev, *ibid.* **71**, 896 (1976) [Sov. Phys. JETP **44**, 471 (1976)].
[102]G. I. Kashen and W. Lowdermilk, Phys. Rev. **A14**, 1472 (1976).
[103]R. G. Brewer, see Ref. 52, p. 87.
[104]S. L. McCall and E. L. Hahn, Phys. Rev. **183**, 457 (1969).
[105]G. A. Massey and I. M. Yarborough, Appl. Phys. Lett. **18**, 576 (1971).
[106]I. Itzkan and D. A. Leonard, *ibid.* **26**, 106 (1975).
[107]J. W. Nibler, J. R. McDonald, and A. B. Harvey, Opt. Comm. **18**, 134, 371 (1976).
[108]I. Chabay, G. Klauminzer, and B. Hudson, Appl. Phys. Lett. **28**, 27 (1976).
[109]N. N. Badalyan, G. A. Vartanyan, N. I. Koroteev, and Yu. S. Chilingaryan, Kvantovaya Elektron. (Moscow) **3**, 1850 (1976) [Sov. J. Quantum Electron. **6**, 1015 (1976)].
[110]J. J. Barett and R. F. Begley, Appl. Phys. Lett. **27**, 129 (1975).
[111]S. A. Akhmanov, N. I. Koroteev, R. Yu. Orlov, and I. L. Shumai, Pis'ma Zh. Eksp. Teor. Fiz. **23**, 276 (1976) [JETP Lett. **23**, 249 (1976)].
[112]M. A. Henesian, L. Kulevskii, R. L. Byer, and R. L. Herbst, Opt. Comm. **18**, 225 (1976).
[113]M. A. Henesian, L. Kulevskii, and R. L. Byer, J. Chem. Phys. **65**, 5530 (1976).
[114]A. Hirth and K. Vollrath, Opt. Comm. **18**, 213 (1976).
[115]R. L. Barger, J. B. West, and T. C. English, Appl. Phys. Lett. 27, 31 (1975).
[116]V. S. Letokhov and V. P. Chebotaev, Printsipy nelineĭnoĭ lazernoĭ spektroskopii (Principles of Nonlinear Laser Spectroscopy), Nauka, M., 1975 (Engl. Transl., Nonlinear Laser Spectroscopy, Springer-Verlag, Berlin, N.Y., 1977).
[117]A. I. Pyndyk, Podobedov, and Kh. E. Sterin, in Vynuzhdennoe kombinatsionnoe rasseyanie (Stimulated Raman Scattering), "Znanie," Kiev, Ukr. SSR 1975, p. 24.
[118]A. P. Sukhorukov and I. V. Tomov, Zh. Eksp. Teor. Fiz. **58**, 1626 (1970). [Sov. Phys. JETP **31**, 872 (1970)].
[119]J. F. Ward and G. H. C. New, Phys. Rev. **185**, 57 (1969).
[120]G. Bjorklund, IEEE J. Quantum Electron. **QE-11** (1975).
[121]N. I. Koroteev and I. L. Shumaĭ, Kvantovaya Elektron. (Moscow) **1**, 2489 (1974)[Sov. J. Quantum Electron. **4**, 1386 (1975)].
[122]C. V. Shank and E. Ippen, in: Lazery na krasitelyakh (Dye Lasers), Ed. F. P. Shefer, Mir, M., 1976, p. 146.
[123]K. P. Burneĭka, M. V. Ignatavichus, V. I. Kabelka, A. S. Piskarskas, and A. Yu. Stabinis, Pis'ma Zh. Eksp. Teor. Fiz. **16**, 365 (1972) [JETP Lett. **16**, 257 (1972)].
[124]A. Laubereau, D. Greiter, and W. Kaiser, Appl. Phys. Lett. **25**, 87 (1974).
[125]C. V. Shank and E. Ippen, in: Ultrashort Light Pulses, Ed. S. L. Shapiro, New York-Heidelberg-Berlin, Springer-Verlag, 1977, p. 200.
[126]A. S. Piskarskas and V. G. Tunkin, Paper given at the 5th Vavilov Conference on Nonlinear Optics, Novosibirsk, June 1977.
[127]W. G. Rado, Appl. Phys. Lett. **11**, 123 (1967).
[128]M. M. Audibert, G. Joffrin, and J. Ducuing, Chem. Phys. Lett. **19**, 26 (1973).
[129]G. M. Gale, C. Delalande, and J. Ducuing, Opt. Comm. **18**, 192 (1976).
[130]D. von der Linde, A. Lauberau, and W. Kaiser, Phys. Rev. Lett **26**, 954; **27**, 802 (1971).
[131]A. Laubereau, D. von der Linde, and W. Kaiser, *ibid.* **28**, 1162 (1972).
[132]R. R. Alfano and S. L. Shapiro, Phys. Rev. **26**, 1247 (1971).
[133]J. E. Griffith, M. Clerc, and P. M. Rentzepis, J. Chem. Phys. **60**, 3824 (1974).
[134]W. F. Calaway and G. E. Ewing, Chem. Phys. Lett. **30**, 485 (1975).
[135]A. Laubereau, G. Kehl, and W. Kaiser, Opt. Comm. **11**, 74 (1974); Chem. Phys. Lett. **27**, 600 (1974).
[136]S. R. J. Brueck and R. M. Osgood, Jr., *ibid.* **39**, 568 (1976).
[137]A. Laubereau, G. Wochner, and W. Kaiser, Opt. Commun. **17**, 91 (1976); Phys. Rev. A13, 2212 (1976).
[138]E. B. Aleksandrov, Opt. Spektrosk. **17**, 957 (1964). S. Haroche, J. A. Paisner, and A. L. Shawlow, Phys. Rev. Lett. **30**, 948 (1973).
[139]T. Yajima, J. Phys. Soc. Japan **19**, 2343 (1964).
[140]M. Matsuoka, N. Nakatsuka, and J. Okada, Phys. Rev. **A12**, 1062 (1975).
[141]T. R. Royt, Chi H. Lee, and W. L. Faust, Opt. Comm. **18**, 108 (1976).
[142]R. R. Alfano and S. L. Shapiro, Phys. Rev. Lett. **29**, 1655 (1972).
[143]A. Laubereau, L. Kirshner, and W. Kaiser, Opt. Comm. **9**, 182 (1973); **14**, 75 (1975).
[144]R. V. Ambartsumyan, Yu. A. Gorokhov, V. S. Letokhov, and G. N. Makarov, Zh. Eksp. Teor. Fiz. **69**, 1956 (1975) [Sov. Phys. JETP **42**, 993 (1975)]; R. V. Ambartsumyan, V. S. Letokhov, E. A. Ryabov and N. V. Chekalin, Pis'ma Zh. Eksp. Teor. Fiz. **20**, 597 (1974) [JETP Lett. **20**, 273 (1974)].
[145]F. Moya, S. Druet, and J. P. E. Taran, Opt. Comm. **13**, 169 (1975).
[146]Laser Raman Gas Diagnostics, Ed. M. Lapp and C. M. Penney, New York-London, Plenum Press, 1974.
[147]P. R. Monson, L. Patumtevapibal, K. J. Kaufman, and R. W. Robinson, Chem. Phys. Lett. **28**, 312 (1974).
[148]G. Beadry and J. Martineau, Phys. Lett. **A43**, 331 (1973).
[149]K. A. Brueckner and S. Jorna, Rev. Mod. Phys. **46**, 325 (1974).
[150]N. M. Kroll, A. Ron and N. Rostoker, Phys. Rev. Lett. **13**, 83 (1964).
[151]H. Kogelnik and C. V. Shank, J. Appl. Phys. **43**, 2327 (1972).
[152]S. A. Akhmanov and G. A. Lyakhov, Zh. Eksp. Teor. Fiz. **66**, 96 (1974) [Sov. Phys. JETP **39**, 43 (1974)].

[153]Yu. Vaĭtkus and K. Yarashyunas, Lit. Fiz. Sb. **14**, 345 (1974); Phys. Stat. Sol. **A23**, K19 (1974).
[154]L. D. Landau and E. M. Lifshits, Élektrodinamika sploshnykh sred (Electrodynamics of Continuous Media), Fizmatgiz, M., 1959 (Engl. Transl., Pergamon Press, Oxford, N.Y., 1960).
[155]D. W. Pohl and V. Irniger, Opt. Comm. **18**, 149 (1976).
[156]H. E. Jakson and C. T. Walker, Phys. Rev. **B3**, 1428 (1971)
[157]D. W. Phillion, D. J. Kuizenga, and A. E. Siegman, Appl. Phys. Lett. **27**, 85 (1975).
[158]W. L. Faust and C. H. Henry, Phys. Rev. Lett. **17**, 1265 (1966).
[159]R. Romestain, S. Geschwind, G. E. Devlin, and P. A. Wolff, *ibid.* **33**, 10 (1974).
[160]R. W. Terhune, P. D. Maker, and C. M. Savage, *ibid.* **14**, 681 (1965).
[161]S. A. Akhmanov, A. I. Kovrigin, B. V. Zhdanov, V. I. Kuznetsov, S. M. Pershin, and A. I. Kholodnykh, Kvantovaya Elektron (Moscow) **4**, 1500 (1977) [sic!].
[162]S. A. Akhmanov, Kvantovaya Elektron (Moscow) **3**, 1846 [Sov. J. Quantum Electron. **6**, 1012 (1976)].
[163]Yu. A. Il'inskii and V. D. Taranukhin, Zh. Eksp. Teor. Fiz. **69**, 833 (1975) [Sov. Phys. JETP **42**, 425 (1975)].
[164]G. V. Azizbekyan, N. N. Badalyan, N. I. Koroteev, K. A. Nersisyan, M. A. Khurshudyan, and Yu. S. Chilingaryan, Kvantovaya Elektron (Moscow) **4**, 1150 (1977) [sic!].
[165]J. Lukasik and J. Ducuing, Phys. Rev. Lett. **28**, 1155 (1972)
[166]V. F. Kamalov and N. I. Koroteev, Kvantovaya Elektron. (Moscow) **4**, 2460 (1977) [sic].
[167]N. G. Basov, A. N. Oraevskiĭ and A. V. Pankratov, *ibid.* **3**, 814 (1976) [Sov. J. Quantum Electron. **6**, 443 (1976)].
[168]D. N. Klyshko, *ibid.* **2**, 265 (1975) [Sov. J. Quantum Electron. **5**, 149 (1975)].
[169]M. Born and Kun Huang, Dynamical Theory of Crystal Lattices, Clarendon Press, Oxford, 1954 (Russ. Transl. IL, M., 1958).
[170]J. Hopfield, Phys. Rev. **112**, 1555 (1958).
[171]Ch. Flytzanis and N. Bloembergen, in: Progress of Quantum Electronics, Ed. J. H. Sanders, and S. Stenholm, v. 4, pt. 3, N.Y., Pergamon Press, 1976, p. 271.
[172]E. Yablonovitch, C. Flytzanis, and N. Bloembergen, Phys. Rev. Lett. **29**, 865 (1972).
[173]S. M. Saltiel, Abstract of Candidate's Dissertation, Moscow State University, M., 1976.
[174]V. L. Strizhevskii and Yu. N. Yashkir, Kvantovaya Elektron. (Moscow) **2**, 995 (1975) [Sov. J. Quantum Electron. **5**, 541 (1975)].
[175]V. M. Agranovich and V. L. Ginzburg, Zh. Eksp. Teor. Fiz. **61**, 1243 (1972) [Sov. Phys. JETP **34**, 662 (1972)].
[176]D. J. Evans, S. Ushioda, and J. D. McMullen, Phys. Rev. Lett. **31**, 369 (1973). J. Y. Prieur and S. Ushioda, *ibid.* **34**, 1012 (1975). Y. J. Chen, E. Burstein and D. L. Milles, *ibid.*, p. 1516.
[177]E. Burstein, Bull. Am. Phys. Soc. **21**, 427 (1976).
[178]N. I. Likholit, V. L. Strizhevskiĭ, and Yu. N. Yashkir, Kvantovaya Elektron (Moscow) **3**, 457 (1976) [Sov. J. Quantum Electron. **6**, 250 (1976)].
[179]N. I. Akhmediev, Opt. Spektrosk. **41**, 820 (1976) [Opt. Spectrosc. (USSR) **41**, 820 (1976) [Opt. Spectrosc. (USSR) **41**, 484 (1976)].
[180]F. DeMartini and Y. R. Shen, Phys. Rev. Lett. **36**, 216 (1976).
[181]F. DeMartini, G. Guiliani, P. Mataloni, E. Palange, and Y. R. Shen, *ibid.* **37**, 440.
[182]M. Collocci, F. DeMartini, S. Kohn, and Y. R. Shen, Phys. Rev. Lett. **38**, 1223 (1977).
[183]S. D. Kramer, F. G. Parsons, and N. Bloembergen, Phys. Rev. **B9**, 1853 (1974).
[184]S. D. Kramer and N. Bloembergen, in: Optical Properties of Highly Transparent Solids, Ed. S. S. Mitra and B. Bendow, N.Y., Plenum Press, 1975, p. 365.
[185]M. Cardona, Phys. Rev. **129**, 69 (1963).
[186]D. Fröhlich, B. Staginnus, and E. Shönherr, Phys. Lett. **19**, 1032 (1967). A. Bivas, C. Marange, J. B. Grun, and C. Schwab, Opt. Comm. **6**, 142 (1972).
[187]D. C. Haueisen and H. Mahr, Phys. Rev. Lett. **26**, 838 (1971).
[188]D. Boggett and R. Loudon, *ibid.* **28**, 1051 (1972).
[189]D. N. Klyshko and B. F. Polkovnikov, Zh. Eksp. Teor. Fiz. **64**, 297 (1973) [Sov. Phys. JETP **37**, 154 (1973)].
[190]Y. Toyozawa, Progr. Theor. Phys. **20**, 53 (1958).
[191]I. P. Kaminow and E. H. Turner, Phys. Rev. **B5**, 1564 (1972).
[192]T. Yajima, Opt. Comm. **14**, 378 (1975) **A18**, 150 (1976).
[193]Im Tkhek-de, O. P. Podavalova, A. K. Popov, and G. Kh. Tartakovskii, Pis'ma Zh. Eksp. Teor. Fiz. **21**, 427 (1975). [JETP Lett. **21**, 195 (1975)].
[194]S. A. Akhmanov, A. N. Dubovik, S. M. Saltiel, I. V. Tomov, and V. G. Tunkin, *ibid.* **20**, 264 (1974) [JETP Lett. **20**, 117 (1974)]; S. A. Akhmanov, L. B. Meĭsner, S. M. Saltiel, and V. G. Tunkin, *ibid.* **22**, 143 (1975) [JETP Lett. **22**, 65 (1975)].
[195]Yu. N. Polivanov and A. T. Sukhodol'skiĭ, *ibid.* **25**, 240 (1977) [JETP Lett. **25**, 221 (1977)].
[196]S. A. Akhmanov, A. F. Bunkin, S. G. Ivanov, and N. I. Koroteev, Pis'ma Zh. Eksp. Teor. Fiz. **25**, 244 (1977) [JETP Lett. **25**, 225 (1977)].
[197]A. Owyoung and P. S. Peercy, J. Appl. Phys. **48**, 674 (1977).
[198]T. Carreira, T. C. Maguire, and T. B. Malloy, Jr., J. Chem. Phys. **66**, 2621 (1977); L. A. Carreira, L. P. Goss, and T. B. Malloy, Jr., *ibid.*, p. 2762.
[199]B. Hudson, W. Hetherington, S. Cramer, I. Chabay, and G. Klauminzer, Proc. Nat. Acad. Sci. USA **73**, 3798 (1976).
[200]J. Nestor, T. G. Spiro, and G. Klauminzer, *ibid.*, p. 3329.
[201]J. Berghman, K. Kneipp, and H. Ponath, Phys. Stat. Sol. **80**, K55 (1977).
[202]A. Owyoung, Post-deadline paper, presented at Conference on Laser Engineering and Applications, Washington, May 1977.
[203]N. I. Koroteev, Paper given at the 5th Vavilov Conference on Nonlinear Optics, Novosibirsk, June 1977.
[204]J. P. -E. Taran, see Ref. 84, p. 381.
[205]S. A. Akhmanov and N. I. Koroteev, in: Theory of Light Scattering in Condensed Matter, Eds. J. Birman, B. Bendow and V. M. Agranovitch, N.Y.—L., Plenum Press, 1976, p. 243.
[206]A. F. Bunkin, S. G. Ivanov, N. I. Koroteev, A. V. Rezov, and M. L. Sybeva, Vestn. Mosk. Univ., Ser. "Fizika", No. 5, 120 (1977).
[207]V. I. Fabelinskiĭ, B. B. Krynetskiĭ, L. A. Kulevskiĭ, V.A. Mishin, A. M. Prokhorov, A. D. Savel'ev, and V. V. Smirnov, Opt. Comm. **20**, 389 (1977).
[208]B. B. Krynetskiĭ, L. A. Kulevskiĭ, V. A. Mishin, A. M. Prokhorov, A. D. Savel'ev, and V. V. Smirnov, *ibid.* **21**, 225 (1977).
[209]R. L. Byer, Paper given at the 5th Vavilov Conference on Nonlinear Optics, Novosibirsk, June 1977.
[210]A. Siegman, Appl. Phys. Lett. **30**, 21 (1977).
[211]R. H. Stolen, J. E. Bjorkholm, and A. Ashkin, *ibid.* **24**, 308 (1974).
[212]R. B. Miles, G. Laufer, and G. Bjorklund, *ibid.* **30**, 417 (1977).

Translated by M. V. King